MASTER'S THESIS

Quantum Chaos and Quantum Speed Limits

Author:
Pablo MARTÍNEZ AZCONA

Supervisor:
Dr. Aurélia CHENU

A thesis submitted in fulfillment of the requirements
for the degree of M. Sc. on Quantum Science and Technology

September 7, 2021

"Physics is not just concerning the Nature of Things, but concerning the Interconnectedness of all the Natures of Things"

Charles Frank

This project has many numerical results obtained with *Python* and some analytical results obtained with *Wolfram Mathematica*. All of the codes can be found in a GitHub repository `https://github.com/fame64/QChaosQSpeedLimits`. To make it easier for the interested reader, we introduce links to the specific code in each figure or calculation.

UNIVERSIDAD DEL PAÍS VASCO / EUSKAL HERRIKO UNIBERTSITATEA

Abstract

Facultad de Ciencia y Tecnología / Zientzia eta Teknologia Fakultatea

M. Sc. on Quantum Science and Technology

Quantum Chaos and Quantum Speed Limits

by Pablo MARTÍNEZ AZCONA

Quantum chaos is a young research field that merges two of the scientific triumphs of the 20th century: nonlinear dynamics and quantum mechanics. Classically, chaos is diagnosed from the exponential separation in time of initially neighboring trajectories, characterized by a positive Lyapunov exponent. In turn, quantum mechanical criteria to distinguish between different quantum dynamics are found in the statistics of energy eigenvalues and eigenvectors, or in the temporal evolution of suitable expectation values. Quantum chaotic systems are adequate to study complex quantum systems: their behavior is much richer than simple Hamiltonian systems while still being analytically or numerically tractable, thus reducing the complexity of most many-body quantum systems.

The Heisenberg uncertainty in quantum mechanics sets a bound on the speed of evolution of a system. This phenomenon, known as quantum speed limits, applies to any system, be it isolated or interacting with an environment (open). Further, it is not purely of quantum nature and also holds for classical dynamics. By the characterization of quantum speed limits in chaotic systems, this project aims to answer whether the fundamental bound on a system evolution limits the development of chaos. We shall start with unitary dynamics, considering the evolution of pure and mixed states, to see if the bound on chaos, conjectured by Maldacena for large thermal states, can be formally derived from quantum speed limits.

The work is structured as follows: we first study the Kicked Top to develop further intuition on the connection between the classical and quantum evolution. We compute the classical and quantum Lyapunov exponents and find the Quantum Speed Limits for this system. We then use Random Matrix Theory to study complex many-body chaotic systems, in which we find an interesting behavior on the Spectral Form Factor and explain the role played by different correlations. We also find that it can be fitted to a decaying exponential, which exponent, surprisingly, saturates Maldacena's bound. We also study Quantum Speed Limits in the context of Random Matrix ensembles and compare them with Maldacena's bound. One of our main results suggests that the bound inferred by Maldacena on Quantum Chaos might also hold to different dynamical quantities in non-chaotic systems.

Acknowledgements

I would like to express my deepest gratitude to my supervisor Dr. Aurélia Chenu for her unconditional support during this project, for her clear and sharp guidance, and for the great opportunity of visiting the *University of Luxembourg* during the realization of this project. Her approach to physics, trying to understand each step carefully, deeply inspires me and has made this project much better.

I am also very grateful to Prof. Adolfo del Campo for his great expertise and insightful discussions, which pointed out possible ways forward and ended up contributing greatly to this project.

Many thanks also to my mates and friends Mar Ferri, Léonce Dupays, Nicoletta Carabba, Apollonas Matsoukas, Dr. Fernando J. Gomez-Ruiz, Mahdi Kourehpaz and Dr. Jing Yang for the great discussions and the great times spent in Luxembourg.

I must also thank the University of Luxembourg for hospitality, economic and human support during my stay in Luxembourg.

Lastly, my family and all my friends in Monzón, Zaragoza, Bilbao, and Luxembourg deserve endless gratitude for all of their love and for making this path much easier.

Contents

List of Figures

List of Abbreviations

OTOC	**O**ut of **T**ime **O**rder **C**orrelator
RMT	**R**andom **M**atrix **T**heory
GOE	**G**aussian **O**rthogonal **E**nsemble
GUE	**G**aussian **U**nitary **E**nsemble
QSL	**Q**uantum **S**peed **L**imit
MT	**M**andelstam-**T**amm
ML	**M**argolus-**L**evitin
QKT	**Q**uantum **K**icked **T**op
SFF	**S**pectral **F**orm **F**actor
DoF	**D**egrees **o**f **F**reedom
TFD	**T**hermo-**F**ield **D**ouble
BCH	**B**aker **C**ampbell **H**aussdorf

List of Symbols

λ	Lyapunov exponent
Ω	Phase Space
$\nu(A)$	Measure over the phase space
$T^t(A)$	Time evolution rule over A
λ_Q	Quantum Lyapunov exponent
i	Imaginary unit
$\hbar$	Reduced Plank's constant
$\hbar_{\text{eff}}$	Effective Planck' constant
$g(\beta, t)$	Spectral Form Factor
$g_c(\beta, t)$	Connected part of the Spectral Form Factor
$Z(\beta)$	Partition Function
$Z(\beta + it)$	Analytically continued Partition Function
$\|\Psi_0\rangle$	Initial Coherent Thermal State
$\|\Psi_t\rangle$	Coherent Thermal State at time t
$\hat{H}$	Hamiltonian
H_{mn}	Element (m, n) of the Hamiltonian
E_n	Energies (eigenvalues of $\hat{H}$)
$\|n\rangle$	Eigenvectors of $\hat{H}$
$\mathscr{H}$	Hilbert space
N	Dimension of the Hilbert Space
β	Inverse temperature
T	Temperature
t	Time
τ	Imaginary part of the complex time $t + i\tau$
$[\ ,\ ]$	Commutator between operators
$\{\ ,\ \}$	Poisson bracket between classical quantities
$\{\{\ ,\ \}\}$	Moyal bracket between Wigner functions
$C(t),\ \tilde{C}(t)$	Out of Time Order Correlators (OTOCs)
$\hat{A}(t),\ \hat{B}(t)$	General operators in Heisenberg picture
t_E	Ehrenfest time
t_d	Dissipation time
$\delta\phi$	Strength of some small perturbation
$\|\text{TFD}\rangle$	Thermo-Field Double State
$\hat{\rho}$	Density matrix of the system
$\varkappa$	Surface gravity of a Black Hole
$\mathcal{S}$	Entropy
$f(t + i\tau)$	General function of a complex variable
$\mathcal{P}(\hat{H})$	Probability density over an ensemble of Random Hamiltonians
$p_{mn}(H_{mn})$	Probability density over one of the matrix elements of $\hat{H}$
O	General Orthogonal transformation
$\hat{T}$	Time Reversal Symmetry operator
U	General Unitary transformation

$A,\ B,\ C$	Parameters of the Probability density of Random Hamiltonians
θ	Angle characterizing a orthogonal transformation (rotation)
$\delta\mathcal{P}$	Variation of the Probability density of Hamiltonians
s_n	Nearest neighbour level spacing
$\mathcal{P}(s)$	Level Spacing distribution
$\tilde{p}$	Brody Parameter
$\Gamma(x)$	Euler's Gamma Function
$\mathcal{P}_B(\tilde{p}, s)$	Brody distribution
$E_\pm$	Energies of a 2×2 Hamiltonian
J	Jacobian of a Transformation
ϕ	Second parameter characterizing a Unitary transformation
$\tilde{\beta}$	Parameter characterizing the level repulsion of a RMT ensemble
$P_{N\tilde{\beta}}(E_1, \ldots, E_N)$	Probability density of a Random Hamiltonian
$\varrho(E)$	Density of States of RMT (Semicircle Law)
$V(x_1, \ldots, x_N)$	Potential energy of the Coulomb gas
$P(x_1, \ldots, x_N)$	Probability distribution of the positions in a Coulomb gas
$V[\varrho(x)]$	Functional characterizing the potential energy
μ	Lagrange multiplier
$\frac{\delta}{\delta\varrho(x)}$	Functional differentiation
$\mathscr{P}\int$	Principal value of an integral
R	Radius of the Semicircle Law
$\Theta(x)$	Heaviside step function
$\mathcal{N}(E)$	Integrated Density of States
$\tilde{\mathcal{N}}(E)$	Smoothed Integrated Density of States
e_n	Unfolded energies
$\Delta\hat{A}$	Standard deviation of a general operator
τ_{QSL}	Quantum Speed Limit
$\tau_{\text{QSL}}^{\text{MT}}$	Mandelstam-Tamm Quantum Speed Limit
$\tau_{\text{QSL}}^{\text{ML}}$	Margolus-Levitin Quantum Speed Limit
E_0	Ground state energy
$S(t)$	Overlap between two quantum states
$F(t)$	Fidelity between two quantum states
$\mathcal{L}(\rho_0, \rho_t)$	Bures angle
S	Spin of our system
$\hat{S}_{x,y,z}$	Spin operators
$\hat{S}_\pm$	Spin ladder operators
ϵ_{ijk}	Levi-Civita symbol
τ_p	Period between kicks in the Kicked Top
$\delta(x)$	Dirac's delta function
p	Parameter characterizing the free evolution of the Kicked Top
k	Strength of the kicks in the Kiced Top
$\mathcal{T}$	Time-ordering operator
$\hat{\mathcal{U}}$	Floquet operator over one period
$\hat{\mathcal{U}}_t$	Time evolution operator from time 0 to time t
$\lvert\theta, \phi\rangle$	Coherent SU(2) state
$\hat{S}^n_{x,y,z,\pm}$	Spin operator at time $t = n\tau_p$
h.c.	Hermitian conjugate
$\tilde{S}_{x,y,z,\pm}$	Auxiliary spin operators
X, Y, Z	Coordinates of the Classical Kicked Top, also called R_i
$Q(\theta, \phi)$	Husimi Q function of a Quantum State $\hat{\rho}$

λ_{bound}	Upper bound on the Lyapunov exponent for the Kicked Top
λ_{saddle}	Lower bound on λ_Q for the QKT
$p_{x,y,z}$, $k_{x,y,z}$	Parameters characterizing the Generalized Kicked Top
ϵ_m	Pseudo-energies of our Floquet system
$\|\chi_m\rangle$	Floquet eigenbasis
n_{QSL}	Quantum Speed Limit for a Floquet system
$g_{k_x,k_z}(\beta,t)$	Spectral Form Factor for a generalized Kicked Top
$\langle g(\beta,t)\rangle$	Average Spectral Form Factor for a generalized Kicked Top
N_{av}	Number of elements to average
$\langle \rho_c^{(2)}(E,E')\rangle$	Connected 2-level correlation function
$\varphi_j(E)$	Eigenfunctions of the Harmonic Oscillator
$\mathcal{H}_j(E)$	Hermite polynomial
$L_n(x)$	Laguerre polynomial
$L_n^{\alpha}(x)$	Generalized Laguerre polynomial
σ	Analytically continued inverse temeperature $\beta + it$
η	Decay exponent of the SFF
$S(\beta,t)$	Survival probability
$B_\beta(t)$	2-point correlator
z	Mapping from the half-strip to the unit circle
t_0	Reference time in Maldacena's derivation
γ	Parameter characterizing the general regularized OTOC
$C_\gamma(t)$	One parameter family of differently regularized OTOCs
$\mathcal{I}_n(\sigma), \mathcal{I}_{mn}(\sigma)$	Integrals over Hermite polynomials

Chapter 1

Introduction

1.1 Background and motivation

The concept of *Quantum Speed Limits* has been largely developed in recent years. It shows that there is a minimum time, or maximum speed, at which a quantum state can evolve. [1–5]. These bounds on the speed of quantum evolution exist for any system, regardless whether it exhibits regular or chaotic motion.

Furthermore, recently a bound on chaos was conjectured by Maldacena [6]. The main idea is that the quantum version of the Lyapunov exponent is bounded for any thermal state. The Quantum Lyapunov exponent gives a measure of how fast a chaotic system can explore its phase space. The authors conjectured that its maximum possible value is related to the temperature of the system.

The two bounds, on the evolution of a quantum system and on the rate at which a quantum chaotic system explores its phase space, while derived in different contexts, seem similar in essence. In this project, our goal is to try to relate both limits and understand what are their similarities.

Beyond the conceptual understanding such a relation could be relevant to deepen our understanding of chaos in both the quantum and classical realms. Indeed, speed limits were shown to also exist in the classical world [7, 8] so maybe we can also extend this universal bound to the classical world.

1.1.1 Structure of the work

The structure of this report is as follows. In Chapter 1 we introduce most of the concepts that we will deal with. We begin this chapter with a brief introduction to Classical Chaos §1.2.1, after which we introduce some key quantities on Quantum Chaos, namely, the Spectral Form Factor and the OTOC §1.2.2. Once we are familiar with the OTOC we can understand Maldacena's bound, discussed in §1.2.3 and derived in App. A. Random Matrix Theory, which is a very useful framework is introduced in §1.3 in which some of the key analytical results are illustrated explicitly for small systems. To end this chapter we introduce Quantum Speed Limits §1.4, the last key ingredient to our work. This section is complemented by a derivation of Quantum Speed Limits in phase space in App. B which are used to find Speed Limits on the fidelity of the system.

In Chapter 2 we introduce a model in which most of the chaotic features of quantum systems can be understood easily, the *Quantum Kicked Top*. We begin the chapter computing the quantum §2.1.1 and classical §2.1.2 equations of motion for this

system. Then we introduce a phase-space visualization for the system, the $Q(\theta, \phi)$ function, which can give a sense of a quantum trajectory and gives a nice connection between the classical and the quantum versions of the system §2.1.3. Then we compute the classical §2.1.4 and quantum §2.1.5 Lyapunov exponents for the system. One of the great features of Kicked Tops is that they can give a physical model for Random Matrix Theory ensembles, this is introduced in §2.2 and the quantum Lyapunov exponent is computed in §2.2.2. After that we derive Quantum Speed Limits for the Kicked Top in §2.3 and introduce a Spectral Form Factor for this system in §2.4.

In Chapter 3 we study some features of Random Matrix Theory, both numerically and analytically, the analytical results are derived in App. C. We find a relation between the OTOC and the SFF in §3.1.1 and study the relation between the SFF and the Level Spacing Statistics in §3.1.2. We find that the initial decay of the SFF obeys Maldacena's bound in §3.2.1, we then discuss the possible relations with another bound obtained by Bhattacharyya in §3.2.2 and give a possible reason for the saturation in §3.2.3. However this feature is not due to chaos, as we discuss in §3.2.4, this implies that we can saturate Maldacena's bound in non-chaotic systems by properly choosing the dynamical quantity. After this, we compute Quantum Speed Limits in the context of Random Matrix Theory §3.3, argue that Random Matrices do not have a Lyapunov exponent §3.4 and find a relation between Maldacena's bound and Quantum Speed Limits on fidelity in §3.5.

In Chapter 4 we detail the main results of our work §4.1, pointing out some physical many-body models in which one can witness the phenomena discussed in the work §4.2.1 and some directions for future work §4.3.

Chapter 1 is fully introductory, therefore all of the concepts discussed there were already known. We try to present them in the clearest way possible so that the work can be understood and followed properly. The same is true with most of Chapter 2, with the exception of §2.2.2 and §2.3 which we are not aware of any reference where these results have been obtained. Chapter 3 is fully original, maybe with the exception of §3.4 which was already known but is illustrated in a different way.

Before proceeding with the report, let us talk briefly about the units used. We mostly use natural units throughout all the work, this means that we take $k_B = \hbar = 1$. However there are three exceptions, three sections in which for clarity we use $\hbar$. When discussing the semiclassical limit of the OTOC in §1.2.2 we use $\hbar$ since it gives a more clear semiclassical limit, when first introducing Quantum Speed Limits in §1.4 since it gives a more clear connection to Heisenberg's uncertainty principle and when we discuss Bhattacharyya's bound in §3.2.2. Also in §A.2 $\hbar$ is used to give a clearer intuition of Maldacena's bound.

1.2 Quantum Chaos

Classically, the features of nonlinear phenomena are well understood and they are key to many areas of knowledge including fields as diverse as physics, biology, chemistry, epidemiology, or economy [9]. Classical nonlinear systems can show *chaos* in the sense that a very small perturbation on the initial conditions of the system can lead to huge changes after some time. Two neighboring initial conditions in a chaotic system have trajectories that diverge exponentially in time at a rate given

by the **Lyapunov exponent**. This is known as the **Butterfly effect** or, more technically, *exponential sensitivity on initial conditions*.

When trying to translate the classical chaotic behavior into the quantum realm, many of the properties become much harder to formulate since we no longer have a clear concept of trajectories. Moreover the notion of sensitivity on initial conditions does not apply quantum mechanically due to Heisenberg's uncertainty principle. Yet another difficulty arises because Schrödinger's equation is linear, but by the correspondence principle we know that classical nonlinear dynamics has to arise smoothly from its quantum version.

With these difficulties in mind, quantum chaos was thus first developed by studying quantum systems whose classical analog is chaotic [10]. Some of the systems extensively studied include billiards and periodically kicked systems. The study of quantum systems with a classically chaotic limit is sometimes also called "*quantum chaology*" [11]. In recent years also there was a rising interest in chaotic features of many-body systems without any classical analog in what has been called "*Many-body quantum chaos*" [12–18]. For this reason, we will just stick to the term "Quantum Chaos" to refer to the whole field.

In this project, we mostly focus on Hamiltonian chaos, both classically and quantum mechanically. This means that we will not consider dissipation. By Liouville's theorem, the phase space volume of our system is always conserved. Treating dissipative chaos classically is a well-known topic. However, its quantum mechanical treatment is a current area of research, and could be a follow-up project.

1.2.1 Key ideas on Classical (Hamiltonian) Chaos

In a big class of systems, we can study the chaotic or regular behavior of the system looking at the classical limit $\hbar_{\text{eff}} \to 0$. In the classical limit, we can compute quantities that characterize the system's behavior like the orbits in phase space or the Lyapunov exponent.

Let the dynamics of our system be codified in a time-dependent vector $\mathbf{r}(t)$. The dimension of this vector is the dimension of the phase space of the system. For example, for a simple 1-D system, it is $\mathbf{r} = (x, p)$.

Definition 1. *Classical Lyapunov exponent: Let us take the distance between two points as* $\delta(t) = |\mathbf{r}_2(t) - \mathbf{r}_1(t)|$. *If the two points are initially very close,* $\delta(0) \ll 1$, *the Lyapunov exponent is given by*

$$\lambda := \lim_{t\to\infty} \frac{1}{t} \ln \left| \frac{\delta(t)}{\delta(0)} \right|. \tag{1.1}$$

This quantity measures the distance between the two initially neighbouring points that grows exponentially as $\delta(t) = \delta(0)e^{\lambda t}$.

The Lyapunov exponent measures the degree of sensitivity to initial conditions, so a positive Lyapunov exponent implies that the trajectories do separate at an exponential rate. However, only asking for this exponential sensitivity on initial conditions is not enough. For example, one may think of an inverted Harmonic oscillator, or any

other unstable system, that can also present exponential sensitivity on initial conditions being totally integrable. For a system to be chaotic, we also need to ask it to present **mixing**[1].

The concept of mixing is related also to that of **ergodicity**. Following [19] let us introduce both of them mathematically and afterward we will give some physical intuition of them.

Let our dynamical system be characterized by a phase space Ω and some time evolution T^t, which may be continuous or discrete, the only condition is that it is invertible. Let us define a measure ν over that phase space such that it is invariant under time evolution and $\nu(\Omega) = 1$. This means that for any set $A \subseteq \Omega$ we have

$$\nu(T^t(A)) = \nu(A), \quad \nu(A) \leq 1 \; \forall A \in \Omega. \tag{1.2}$$

A T^t invariant set is a set A that obeys $T^t(A) = A$. The physical concept associated with ν is a sort of "volume" associated with every subset A. We ask it to be invariant under time evolution because the volume on phase space is conserved for Hamiltonian systems by Liouville's theorem.

Definition 2. *Ergodicity: A dynamical system is ergodic if for all T^t invariant sets $A \subseteq \Omega$ we either have $\nu(A) = 0$ or $\nu(A) = 1$.*

This definition tells us that the only set with a non-zero measure which is invariant under the time evolution is the whole phase space Ω itself. The physical intuition behind ergodicity is that a single initial state on an ergodic system will explore the whole phase space given a long enough time. This allows us to interchange time averages with ensemble averages and is one of the key concepts underlying statistical mechanics.

Now we will define mixing which is a stronger condition than ergodicity in the sense that if we have mixing we do have ergodicity but the inverse implication is not true.

Definition 3. *Mixing: A dynamical system that preserves the measure is (strongly) mixing if for any two subsets $A, B \subseteq \Omega$ we have*

$$\lim_{t\to\infty} \nu(A \cap T^t(B)) = \nu(A)\nu(B). \tag{1.3}$$

We can physically picture mixing if we assume that we have a cocktail shaker with two different drinks A and B. In the beginning, the two liquids are not yet mixed but after stirring for some time the two drinks are well mixed so any small piece of the volume of the drink that we take will have the same proportion of A and B as the whole shaker. Say that the proportion of one of the drinks is 20% and the other one is 80%. So $\nu(A) = 0.2$ and $\nu(B) = 0.8$. The fraction of A in the region originally occupied by B after an infinite time of stirring is

$$p_A = \frac{\lim_{t\to\infty} \nu(A \cap T^t(B))}{\nu(B)} = \frac{\nu(A)\cancel{\nu(B)}}{\cancel{\nu(B)}}, \tag{1.4}$$

so the proportion in any volume we choose is $\nu(A)$ since the property has to hold for any two subsets $A, B \subseteq \Omega$.

[1] There are other possible definitions that rely on asking for aperiodic motion in the sense that the system does not end up in a fixed point or on a limit cycle. For a more in-depth discussion of this approach see [9]

So a system is chaotic if it has a positive Lyapunov exponent and it presents mixing. The property of mixing of a system can be related to a quantity called the *Kolmogorov-Sinai entropy* (KS) [20–23] such that if the KS entropy is larger than zero, the system presents mixing. Since we know that any system which presents mixing also shows ergodicity chaotic systems are ergodic. The notion of Kolmogorov-Sinai entropy can be related to the sum of Lyapunov exponents of the system in what is known as the Pesin identity [24]. So in a sense what mixing is implying is that the sensitivity on initial conditions is seen over all of the directions of phase space.

1.2.2 Tools to diagnose Quantum Chaos

We here present different measures that are useful to quantify chaos in quantum systems.

Spectral Form Factor(SFF)

Definition 4. *Spectral Form Factor: For a system with eigenenergies* $\{E_n\}$ *the Spectral Form Factor (SFF) at inverse temperature* β *and time* t *is defined as*

$$g(\beta,t) := \sum_{n,m} e^{-(\beta+it)E_n} e^{-(\beta-it)E_m} = Z(\beta+it)Z(\beta-it), \tag{1.5}$$

where $Z(\beta+it)$ is the analytically continued partition function. The SFF can be understood as the survival probability, or fidelity, $|\langle\psi_\beta|\hat{\mathcal{U}}_t|\psi_\beta\rangle|^2$ of the coherent thermal state $|\psi_\beta\rangle = Z^{-1/2}(\beta)\sum_n e^{-\beta E_n/2}|n\rangle$ where $Z(\beta) = \sum_n e^{-\beta E_n}$ is the partition function.

The SFF shows an initial decay and a plateau at long times. The chaotic features of the system manifest in correlations between the energies [25–27]. These correlations generate a **ramp** during a range of times. To compute $g(\beta,t)$ in an ensemble we will need to average ove realizations of different spectra of the ensemble. This is needed when we work with **Random Matrix Theory**, introduced in §1.3. When such average is needed the SFF can be split into three terms

$$g(\beta,t) = \langle Z(\beta+it)Z(\beta-it)\rangle = \langle Z(2\beta)\rangle + \langle Z(\beta+it)\rangle\langle Z(\beta-it)\rangle + g_c(\beta,t), \tag{1.6}$$

where $g_c(\beta,t)$ is the connected part of the SFF which carries the information on the correlations. It is the complex Fourier transform of the connected 2-point correlation function $\langle\rho_c^{(2)}(E,E')\rangle = \langle\rho(E)\rho(E')\rangle - \langle\rho(E)\rangle\langle\rho(E')\rangle$. For one of the Random Matrix Theory ensembles, the Gaussian Unitary Ensemble, all of these terms can be computed exactly [28].

Fig. 1.1 shows the SFF in the GUE and clearly displays the key features of the SFF for chaotic systems. At short times the behavior of the SFF is dictated by the 2nd term in (1.6), i.e. the disconnected part and the connected contribution is constant. The ramp originates from the connected part and at very long times the only term remaining is the constant part.

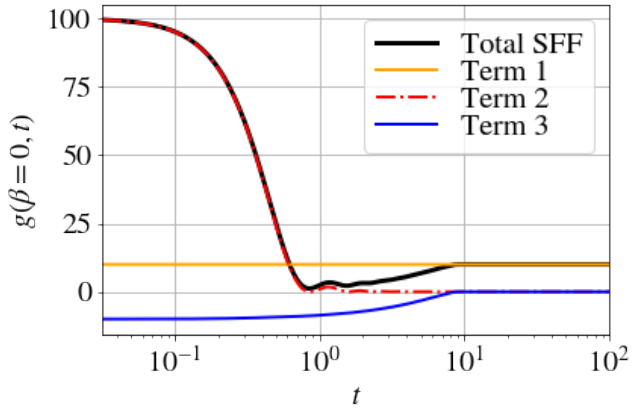

FIGURE 1.1: An exact expression for the SFF for the GUE [28] with parameters $\beta = 0$ and $N = 10$. The explicit expression for the terms can be seen in §3.1. Code here.

Out of Time Ordered Correlator (OTOC)

The definition of a Lyapunov exponent in the quantum realm is not trivial and not even possible for a system without a phase space representation. One of the most used definitions for a quantum Lyapunov exponent relies on the definition of an Out of Time Ordered Correlator (OTOC). This quantity was first proposed in the context of the theory of superconductivity [29], and has now become central to study quantum chaos.

Definition 5. *Infinite Temperature OTOC: The OTOC, at infinite temperature, between two hermitian operators $\hat{A}$ and $\hat{B}$ in a Hilbert space of dimension N is defined as*

$$C(t) := \frac{1}{N}\mathrm{Tr}([\hat{A}(t), \hat{B}(0)]^2). \tag{1.7}$$

Note that the operators are evaluated at different times, therefore we are using Heisenberg's picture. The reason why this quantity is closely related to the Lyapunov exponent can be justified in the semiclassical limit. Let us consider $\hat{A}(t) = \hat{x}(t)$ and $\hat{B} = \hat{p}$. The commutator is known to be related to the Poisson Bracket by

$$[\hat{x}(t), \hat{p}] \to i\hbar\{x(t), p\} = i\hbar \frac{\partial x(t)}{\partial x(0)} \frac{\partial p(0)}{\partial p(0)}^{1} \sim i\hbar e^{\lambda t}, \tag{1.8}$$

then the OTOC becomes

$$C(t) \sim \hbar^2 e^{2\lambda t}, \tag{1.9}$$

and captures the classical notion of exponential divergence of the trajectory. For this reason, the quantum Lyapunov exponent λ_Q is related to 2λ instead of λ directly.

The definition of a Lyapunov exponent quantum mechanically only holds for a certain window of time. Since the Hilbert space is finite-dimensional the OTOC eventually saturates to a value ~ 1. From this argument, we find that the **Ehrenfest time** t_E, defined as the time at which the OTOC saturates, is

$$C(t_E) \sim 1 \to 2\lambda t_E \sim 2\ln\frac{1}{\hbar} \to t_E = \frac{1}{\lambda}\ln\frac{1}{\hbar}. \tag{1.10}$$

Another very important time scale is the **dissipation time** t_d at which the two point functions $B(t) = \langle \hat{A}(t)\hat{B} \rangle$ saturate.

If we expand the commutator squared, we obtain 4 terms which essentially boil down to two different ways to order the operators. One of the ways is of the form $\sim \text{Tr}(\hat{A}(t)\hat{B}\hat{B}\hat{A}(t))$ and the other one is $\sim -\text{Tr}(\hat{A}(t)\hat{B}\hat{A}(t)\hat{B})$. The latter terms are those that contribute to the dynamics of the OTOC since they are the ones really out-of-time ordered. We will refer to the full expression (1.7) and only those terms as OTOC[2].

To understand better the meaning of the OTOC we study the case in which $\hat{B} = |n\rangle \langle n|$, where $|n\rangle$ is an eigenstate of $\hat{H}$. In this case, we find

$$C(t) = \text{Var}(\hat{A}) = \langle n|\hat{A}^2|n\rangle - \langle n|\hat{A}|n\rangle^2, \tag{1.11}$$

so we find that the OTOC is related to the variance of the time-evolving operator. Note that as we selected an eigenstate, the variance does not evolve in time, so we cannot get insight on the dynamics of the system through this procedure. A similar approach in which the dynamics can be understood is through the Fidelity OTOC, defined in the next section.

Now let us focus on the case of finite temperature. In principle an expectation over the thermal is state is obtained from $\langle \circ \rangle_\beta = \text{Tr}(\circ\, e^{-\beta\hat{H}})/Z(\beta)$. However this way of averaging shows some problems in the context of Quantum Field Theory when we work with out-of-time ordered operators [30]. For this reason a regularized version of the OTOC has been introduced. To regularize the OTOC, the thermal factor $e^{-\beta\hat{H}}$ is split into various terms. The way we will mostly use relies on splitting the thermal factor into 4 different terms[6, 31].

Definition 6. *Regularized OTOC: Let $\hat{A}(t)$ and $\hat{B}(0)$ be two Hermitian operators in Heisenberg picture , $\hat{H}$ the Hamiltonian, β the inverse temperature of the system and $Z(\beta) = \text{Tr}(e^{-\beta\hat{H}})$ the partition function. Then the regularized OTOC is defined as*

$$\tilde{C}(\beta, t) := \frac{1}{Z(\beta)}\text{Tr}(\hat{A}(t)e^{-\beta\hat{H}/4}\hat{B}(0)e^{-\beta\hat{H}/4}\hat{A}(t)e^{-\beta\hat{H}/4}\hat{B}(0)e^{-\beta\hat{H}/4}) \tag{1.12}$$

We can gain some intuition on the need to implement some regularization strategy if we imagine a complex time plane $t + i\tau$ such that the real axis corresponds to t and the imaginary axis corresponds to the inverse temperature.

The need for regularization arises from the fact that the path goes back and forth in the same point, as we see in Fig. 1.2. This can cause some divergences in a quantum field theory and for that reason, we need to introduce the regularized version. As we already pointed out before, this regularization is not unique, one can even introduce a family of OTOCs with different regularizations which depend on a parameter γ [32]. This is in fact very useful and the authors were able to prove the Maldacena's bound from a completely different perspective which has some advantages.

[2] We will use a tilde $\tilde{C}(t)$ to refer to $\text{Tr}(\hat{A}(t)\hat{B}\hat{A}(t)\hat{B})$

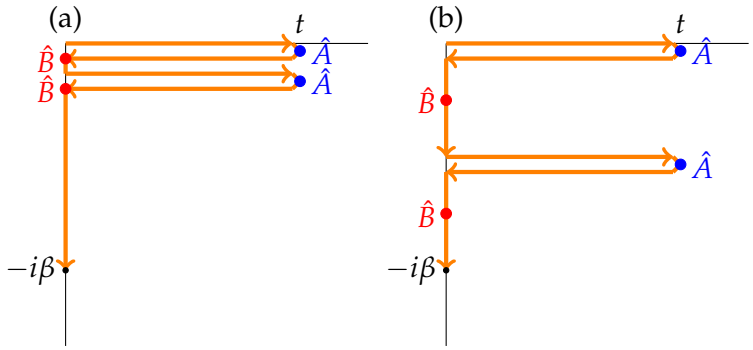

FIGURE 1.2: The path on the complex time plane for (a) non-regularized OTOC and (b) regularized OTOC. For the non-regularized OTOC, the distance between the lines is just there to help visualize it, in reality, the lines go back and forth on top of each other.

In general, the OTOC has some time window in which it shows an exponential behavior. This is known as **Lyapunov regime** and holds between the *dissipation time* t_d and the *Ehrenfest time* t_E, i.e. $t_d \ll t \ll t_E$. So, between these times the OTOC decays as [33]

$$\tilde{C}(\beta, t) = \tilde{C}_d - \epsilon e^{\lambda_Q t}, \tag{1.13}$$

where λ_Q is the Quantum Lyapunov exponent and $\tilde{C}_d$ is the disconnected part of the OTOC

$$\tilde{C}_d = \frac{1}{Z^2}\mathrm{Tr}(e^{-\beta\hat{H}/2}\hat{B}e^{-\beta\hat{H}/2}\hat{B})\mathrm{Tr}(e^{-\beta\hat{H}/2}\hat{A}(t)e^{-\beta\hat{H}/2}\hat{A}(t)). \tag{1.14}$$

Fidelity OTOC

The expression for the decay of the OTOC in the Lyapunov regime (1.13) may seem odd and not very well justified. Actually, there is a special class of OTOC's for which that dependence is much clearer, the **Fidelity OTOC's** [34]. The idea is that we choose one of the operators to be the density matrix of some pure state $|\psi_0\rangle$, $\hat{B} = \hat{\rho} = |\psi_0\rangle\langle\psi_0|$. In analogy with Loschmidt echo experiments [28, 35–41], the time-evolving operator initially is $\hat{A}(0) = e^{i\delta\phi\hat{G}}$, where $\delta\phi \ll 1$ is some small parameter and $\hat{G}$ is Hermitian. If we want our Fidelity OTOC to have dynamics we need $[\hat{H}, \hat{G}] \neq 0$ and $\hat{H}|\psi_0\rangle \not\propto |\psi_0\rangle$, i.e. $|\psi_0\rangle$ should not be an eigenstate of $\hat{H}$. Since the operator $\hat{A}$ is not Hermitian, a more general infinite temperature OTOC is needed

$$\tilde{C}(t) = \frac{1}{N}\mathrm{Tr}(\hat{A}^\dagger(t)\hat{B}^\dagger(0)\hat{A}(t)\hat{B}(0)). \tag{1.15}$$

From the property of the trace $\mathrm{Tr}(\hat{X}|\psi_0\rangle\langle\psi_0|) = \langle\psi_0|\hat{X}|\psi_0\rangle$, it is easy to see that

$$\tilde{C}(t) = |\langle\psi_0|e^{i\hat{H}t}e^{i\delta\phi\hat{G}}e^{-i\hat{H}t}|\psi_0\rangle|^2. \tag{1.16}$$

From this formula, we see that $\tilde{C}$ is a Fidelity between the pure state $e^{-i\hat{H}t}|\psi_0\rangle$ and that evolved with a slight perturbation $e^{i\delta\phi\hat{G}}e^{-i\hat{H}t}|\psi_0\rangle$. Actually, this fidelity is called **Loschmidt echo** since we are comparing two versions of some time-evolved state, one that undergoes the normal evolution and one that undergoes the same evolution but is kicked in the end with the operator $\hat{G}$. This Loschmidt echo was the first quantity used to define a quantum version of the Lyapunov exponent [39] since it

captures sensitivity to a *small* perturbation on the system, small in the sense that $\delta\phi \ll 1$.

The main idea in [39] is that we have two regimes, the *Golden rule regime*, in which the decay of the Loschmidt echo is exponential but the exponent depends on the strength of the perturbation $\delta\phi$, and the *Lyapunov regime*, in which the decay is independent on the strength of the perturbation.

Expanding (1.16) at second order in the perturbation strength yields[3]

$$\tilde{C}(t) = 1 - \delta\phi^2(\langle\psi_0|\hat{G}^2(t)|\psi_0\rangle - \langle\psi_0|\hat{G}(t)|\psi_0\rangle^2) + \mathcal{O}(\delta\phi^3). \tag{1.17}$$

One should note the appearance of the variance of $\hat{G}(t)$ in analogy with what we obtained in (1.11). The Lyapunov regime in this expression happens when the variance of $\hat{G}(t)$ grows like $\mathrm{Var}(\hat{G}(t)) \sim e^{\lambda t}$ with λ being the Quantum Lyapunov exponent. So the Lyapunov regime happens when the strength of the decay of the Loschmidt echo is independent of the strength of the perturbation $\delta\phi$. This approach allows connecting the concepts of fidelity, OTOC and Loschmidt echo and shows that the different definitions of the Quantum Lyapunov exponent are essentially equivalent.

1.2.3 Maldacena's bound on chaos

Maldacena, Shenker, and Stanford [6] recently conjectured a bound on the Quantum Lyapunov exponent λ_Q for a chaotic system at thermal equilibrium, such that

$$\lambda_Q \leq \frac{2\pi}{\beta}. \tag{1.18}$$

Their approach is inspired by quantum gravity, while it is not needed for the demonstration, we introduce a few of the concepts in order to understand their motivation. One of the key concepts is that of **scrambling**. To build some intuition of it we will follow [42]. Let us consider that we have a complex chaotic system with many degrees of freedom N initially prepared on a pure state. One such system eventually thermalizes but its quantum state continues to be pure because of unitary quantum dynamics. What does thermalization mean then? If we take a subsystem of M DoF such that $M \ll N$, after some time, the reduced density matrix of that subsystem will also tend toward thermal equilibrium due to mixing. This means that the entanglement entropy of the subsystem will approach a maximum. When this maximum of entanglement entropy has been reached, the system is considered to be *scrambled* and the time necessary for that is the **scrambling time**. Actually, the subsystem does not need to be very small, any M smaller than $N/2$ will show scrambling [43]. This scrambling time also corresponds to the Ehrenfest time we already discussed in the context of OTOC's.

The connection with Black Hole physics comes because Black Holes should be fast scramblers[42, 44–46] with a scrambling time logarithmic in the number of degrees of freedom $\propto \log N$, this is thought to be the fastest possible scrambling. No other system could have a faster scrambling rate. The relation between black holes and chaos can be understood from [46] since Conformal Field Theories show sensitive

[3] Note that here $\tilde{C}_d = 1$ because $\tilde{C}_d = \mathrm{Tr}(\hat{A}^\dagger(t)\hat{A}(t))\mathrm{Tr}(\hat{B}^\dagger(0)\hat{B}(0))/N = \cancel{\mathrm{Tr}(\mathbb{1})}\,|\langle\psi_0|\psi_0\rangle|^2/\cancel{\mathcal{N}} = 1$.

dependence on initial conditions and perturbing a state slightly can lead to a completely different evolution.

The relation between Black Hole physics and OTOC's is discussed by Kitaev in [33]. We recast below his main argument. Let us consider a Thermo-Field Double state (TFD) defined on a bipartite Hilbert space $\mathscr{H} = \mathscr{H}_R \otimes \mathscr{H}_L$ as

$$|\text{TFD}\rangle := \frac{1}{\sqrt{Z(\beta)}} \sum_n e^{-\beta E_n/2} |n\rangle_L |n\rangle_R . \tag{1.19}$$

This state represents a thermal state once we trace overone of the subspaces, e.g.

$$\rho_L = \text{Tr}_R(|\text{TFD}\rangle \langle \text{TFD}|) = \frac{1}{Z(\beta)} \sum_n e^{-\beta E_n} |n\rangle \langle n| . \tag{1.20}$$

We will consider this state evolving under a Hamiltonian $\hat{H}_D$ of the form

$$\hat{H}_D = \hat{H} \otimes \mathbb{I} - \mathbb{I} \otimes \hat{H}^T. \tag{1.21}$$

The Thermo-Field Double is a fixed point of this Hamiltonian, but if we slightly perturb the system, expectation values will grow exponentially in time. If we reduce the correlators to correlators in a thermal state we find that the operators are not time ordered, thus obtaining the behavior known for the OTOC. It turns out that if we do the same computations for a semiclassical theory of a Black Hole since the Lorentz factor $e^{\varkappa t}$ is exponentially large, $\varkappa$ being the *surface gravity* of the Black Hole, then the OTOC behaves as

$$C(t) \sim \frac{1}{\mathcal{S}} e^{\varkappa t}, \tag{1.22}$$

for times between $\varkappa^{-1} \ll t \ll t_{\text{scr}} = \varkappa^{-1} \ln \mathcal{S}$, with $\mathcal{S}$ the entropy of the Black Hole. The surface gravity of a Black Hole is related to the temperature of the system by

$$\varkappa = \frac{2\pi}{\beta}, \tag{1.23}$$

and this is the motivation behind Maldacena's conjecture from the context of Quantum Gravity and Black Hole Physics. However to prove their conjecture, they rely only on a mathematical result that reads as follows.

Theorem 1. *Maldacena-Shenker-Stanford: Let a function of complex variable $f(t + i\tau)$ have the following two properties:*

1. *$f(t + i\tau)$ is analytic on the half stripe $-\frac{\beta}{4} \leq \tau \leq \frac{\beta}{4}$, $t \geq 0$ (see Fig. 1.3). Furthermore $f(t + i\tau) \in \mathbb{R}$ for $\tau = 0$.*
2. *$|f(t + i\tau)| \leq 1$ in all the half-strip.*

Then it follows that

$$\frac{1}{1 - f} \left| \frac{df}{dt} \right| \leq \frac{2\pi}{\beta} + \mathcal{O}(e^{-4\pi t/\beta}). \tag{1.24}$$

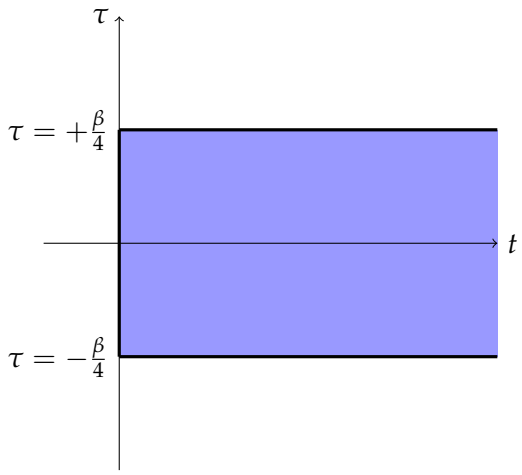

FIGURE 1.3: Half strip in which $f(t + i\tau)$ is analytic.

When considering the OTOC in the Lyapunov regime, $f(t) = 1 - \epsilon e^{\lambda_Q t}$, it trivially follows that

$$\lambda_Q \leq \frac{2\pi}{\beta}. \tag{1.25}$$

The proof of the theorem, along with proving that the OTOC obeys conditions 1 and 2, are presented in §A.1 of Appendix A. An alternative derivation due to Tsuji, Shitara, and Ueda [32] is given in §A.2

1.3 Random Matrix Theory

Random Matrix Theory is a fascinating field that merges beautifully mathematics and physics, with possible exciting fundamental applications in both fields. In Pure Mathematics, for example, it can be related to the study of the *Riemann Hypothesis* [47]. In physics Random Matrix Theory is a useful tool to study quantum chaos. It was first introduced in physics by Wigner [48] to study the properties of heavy nuclei. The main idea behind it is that the system under study is extremely complex, so complex that in a sense it has lost nearly all possible structure. In one such *structureless* system, we can interchange the Hamiltonian of the system by a random Hamiltonian chosen from a suitable ensemble that reflects the symmetry class of the system. In fact, this approach worked very well in heavy nuclei. Afterward, it was realized that classically chaotic systems also show similar properties.

One of the first classically chaotic systems studied were billiards. They were experimentally shown to exhibit the properties of Random Matrices [49]. Following that philosophy, many of the quantum chaotic features are presented from an experimental point of view in [50]. The ensembles with which we will work are called the Gaussian ensembles.

1.3.1 The probability distribution of the Hamiltonian

Definition 7. *Gaussian ensembles: Let us consider the following conditions on the probability distribution of the Hamiltonian*

- *The elements of the matrix are sampled from independent probability distributions. This means that the probability of obtaining a Hamiltonian $\hat{H}$ whose matrix elements are H_{mn} is given by*

$$\mathcal{P}(H) = \prod_n \prod_{m \geq n} p_{mn}(H_{mn}). \tag{1.26}$$

- *The properties should not depend on the basis chosen to represent the Hamiltonian. Here the symmetries dictate the system's ensemble:*

  1. ***Time reversal symmetric systems:**. In these systems, there is an antiunitary time-reversal operator $\hat{T}$ which commutes with the Hamiltonian. For this class of systems, we can choose $\hat{H}$ to be real so that it is symmetric $\hat{H} = \hat{H}^\dagger = \hat{H}^T$. Our probability distribution has to be invariant under any orthogonal transformation $O^{-1} = O^T$.*

  $$[\hat{H}, \hat{T}] = 0, \quad \hat{T}^2 = 1, \quad \text{and} \quad \mathcal{P}(\hat{H}) = \mathcal{P}(O\hat{H}O^T) \; \forall O \text{ s.t. } O^{-1} = O^T. \tag{1.27}$$

  *The ensemble of all operators $\hat{H}$ that obeys these conditions is known as the **Gaussian Orthogonal Ensemble (GOE)**.*

  2. ***Non time reversal symmetric systems:** There is no symmetry so the Hamiltonian is only required to be hermitian $\hat{H} = \hat{H}^\dagger$. The allowed symmetry transformations are unitary $U^{-1} = U^\dagger$.*

  $$[\hat{H}, \hat{T}] \neq 0, \quad \mathcal{P}(\hat{H}) = \mathcal{P}(U\hat{H}U^{-1}) \; \forall U \text{ s.t. } U^{-1} = U^\dagger. \tag{1.28}$$

  *The ensemble of Hamiltonians that obeys these conditions is called the **Gaussian Unitary Ensemble (GUE)**.*

  3. *There is a third possibility, a time-reversal symmetric system which has $\hat{T}^2 = -1$. This defines the Gaussian Symplectic Ensemble [51].*

For the three symmetry classes, the conditions of independence and invariance give

$$\mathcal{P}(\hat{H}) = Ce^{-A\mathrm{Tr}\hat{H}^2}. \tag{1.29}$$

Let us prove explicitly that (1.29) is the true distribution for the GOE with dimension 2×2 [52]. For a more general derivation see [51].

Proof. We will consider the following symmetric matrix

$$\hat{H} = \begin{pmatrix} H_{11} & H_{12} \\ H_{12} & H_{22} \end{pmatrix}. \tag{1.30}$$

By the independence condition (1.26), we can write the probability of finding a Hamiltonian $\hat{H}$ as

$$\mathcal{P}(\hat{H}) = p_{11}(H_{11})p_{12}(H_{12})p_{22}(H_{22}). \tag{1.31}$$

Furthermore, this distribution should be normalized $\int \mathrm{d}H_{11}\mathrm{d}H_{12}\mathrm{d}H_{22}\mathcal{P}(\hat{H}) = 1$, and obey the invariance condition $\mathcal{P}(\hat{H}) = \mathcal{P}(O\hat{H}O^T)$. The most general orthogonal transformation in 2D is a rotation of angle θ

$$O = \begin{pmatrix} \cos\theta & -\sin\theta \\ \sin\theta & \cos\theta \end{pmatrix} = \begin{pmatrix} 1 & -\theta \\ \theta & 1 \end{pmatrix} + \mathcal{O}(\theta^2). \tag{1.32}$$

The variation for a small angle is given by

$$\delta\hat{H} = O\hat{H}O^t - \hat{H} = \begin{pmatrix} -2\theta H_{12} & \theta(H_{11} - H_{22}) \\ \theta(H_{11} - H_{22}) & 2\theta H_{12} \end{pmatrix}. \tag{1.33}$$

We can compute the variation of $\mathcal{P}(\hat{H})$ under a variation of the matrix elements of the Hamiltonian as

$$\delta\mathcal{P} = \frac{dp_{11}}{dH_{11}}\delta H_{11}p_{12}p_{22} + p_{11}\frac{dp_{12}}{dH_{12}}\delta H_{12}p_{22} + p_{11}p_{12}\frac{dp_{22}}{dH_{22}}\delta H_{22}. \tag{1.34}$$

Using the property

$$\frac{1}{p_{mn}}\frac{dp_{mn}}{dH_{mn}} = \frac{d\ln p_{mn}}{dH_{mn}}, \tag{1.35}$$

and the expressions for δH_{mn} obtained in (1.33), we can find

$$\delta\mathcal{P} = \mathcal{P}(\hat{H})\theta\left(-2H_{12}\frac{d\ln p_{11}}{dH_{11}} + (H_{11} - H_{22})\frac{d\ln p_{12}}{dH_{12}} + 2H_{12}\frac{d\ln p_{22}}{dH_{22}}\right). \tag{1.36}$$

For $\mathcal{P}(\hat{H})$ to be invariant for any θ we need, the term in the bracket needs to vanish, which yields to the differential equation for the probability densities

$$\frac{1}{2(H_{11} - H_{22})}\left(\frac{d\ln p_{11}}{dH_{11}} - \frac{d\ln p_{22}}{dH_{22}}\right) = \frac{1}{H_{12}}\frac{d\ln p_{12}}{dH_{12}}, \tag{1.37}$$

which is solved by choosing

$$p_{11}(H_{11}) = e^{-AH_{11}^2 - BH_{11}}, \tag{1.38}$$

$$p_{22}(H_{22}) = e^{-AH_{22}^2 - BH_{22}}, \tag{1.39}$$

$$p_{12}(H_{12}) = e^{-2AH_{12}^2}. \tag{1.40}$$

Substituting these equations in (1.31) after choosing suitably the zero of energy such that $H_{11} + H_{22} = 0$, we arrive at

$$\mathcal{P}(\hat{H}) = Ce^{-A\mathrm{Tr}\hat{H}^2}, \tag{1.41}$$

where C is a constant fixed by normalization and A sets the energy scale. Both of them are fixed by the level spacing distribution obtained in §1.3.2 and they are $C = A = \frac{\pi}{2}$. □

1.3.2 The probability distribution of energies and level spacing

When we have a quantum mechanical system with chaotic properties, the correlations between the energies play a great role. For example, two energy levels will try to not be together and *avoid degeneracies*. The correlations between the energies in chaotic systems are known to obey the description obtained from Random Matrix Theory, this goes back to the Bohigas-Giannoni-Schmit conjecture [53]. Since the conjecture was first proposed in the eighties by now it has been extensively proven in many chaotic systems thus proving the universality of the statement.

We will mostly focus on correlations between neighboring energy levels, however, the correlations between energies do not end up at nearest neighbors but rather extend through all of the spectra of the system. To characterize these *"long-range"* energy correlations one needs to introduce other measures like the *number variance* [51, 52]. However, quantities like the Spectral Form Factor, already introduced in §1.2.2 account for all possible correlations, *long* and *short* range.

To investigate the nearest neighbor energy correlations we introduce the **level spacing** defined as

$$s_n = E_{n+1} - E_n. \tag{1.42}$$

If we look at the probability density of this quantity for a system with uncorrelated energies, the probability density of the difference between two uncorrelated quantities is given by a **Poisson distribution**,

$$\mathcal{P}(s) = e^{-s}. \tag{1.43}$$

In turn, for the Random Matrix Ensembles the behavior is very different, we have the **Wigner-Dyson surmises**, illustrated in Fig. 1.4

$$\mathcal{P}(s) = \frac{\pi}{2} s e^{-\pi s^2/4} \quad \text{for the GOE,} \tag{1.44}$$

$$\mathcal{P}(s) = \frac{32}{\pi^2} s^2 e^{-4s^2/\pi} \quad \text{for the GUE.} \tag{1.45}$$

Both of these distributions vanish at $s = 0$. This indicates level repulsion between the eigenvalues for correlated eigenvalues obtained from RMT.

We can check this behavior numerically, we generate each element of the Hamiltonian from a Gaussian distribution $P(H_{mn}) \propto e^{-H_{mn}^2}$, diagonalize that matrix and obtain the level spacing numerically.

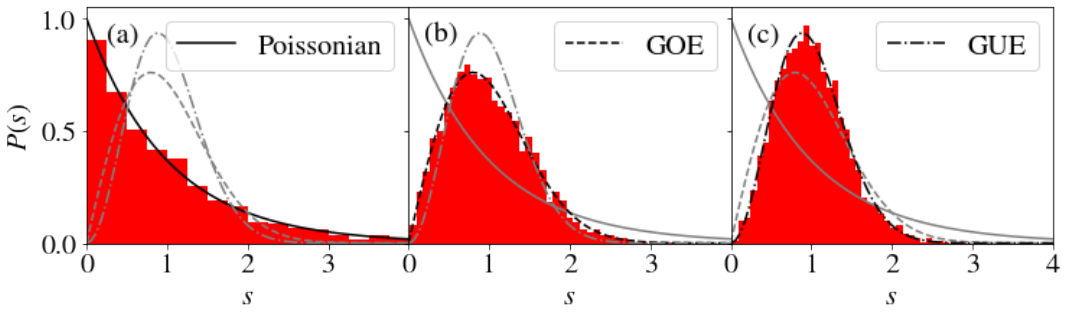

FIGURE 1.4: Level spacing distributions for (a) Poissonian uncorrelated levels, (b) GOE, and (c) GUE. The dimension of the matrix used is $N = 3000$ for all the plots. To obtain a match between the large N numerics and the analytics we need to unfold the energies, as discussed in §1.3.4. Code here.

It will be useful to introduce a distribution that interpolates between the Poissonian and the GOE level spacing. This is known as the **Brody distribution** [54] and is

defined as

$$\mathcal{P}_B(\tilde{p}, s) = (\tilde{p}+1)bs^{\tilde{p}}e^{-bs^{\tilde{p}+1}}, \quad \text{where } b = \left(\Gamma\left(\frac{\tilde{p}+2}{\tilde{p}+1}\right)\right)^{\tilde{p}+1}, \tag{1.46}$$

where $\Gamma(x)$ is Euler's Gamma Function and $\tilde{p}$ is the Brody Parameter. $\tilde{p} = 0$ indicates Poissonian statistics, i.e. integrability, and $\tilde{p} = 1$ indicates GOE statistics, that is to say, quantum chaotic behavior, at least between neighboring levels. Note that any $\tilde{p} > 0$, no matter how small, implies $\mathcal{P}_B(\tilde{p}, 0) = 0$. In other words, for any nonzero Brody parameter, we break exact degeneracy, which is one of the requisites for von Neumann's quantum ergodic theorem [55]. If we want to exactly describe Poissonian, GOE and GUE we need to introduce a generalization of (1.46) [56], however, this requires introducing a second parameter that makes the visualization harder. For this reason, we rely on an approximate method. Fitting the Brody distribution to the Wigner-Dyson GUE surmise gives a Brody parameter of $\tilde{p} \approx 1.55$, we will use that value to characterize GUE level spacing statistics.

Proof. We will now illustrate how to obtain analytically the level spacing distributions for small 2×2 Random Matrices [57]. Again for a more general proof see [51]. We consider the Hamiltonian in (1.30) whose eigenvalues are

$$E_{\pm} = \frac{1}{2}\left(H_{11} + H_{22} + \sqrt{(H_{11} - H_{22})^2 + 4H_{12}^2}\right). \tag{1.47}$$

The Hamiltonian is diagonalized by the orthogonal transformation O which depends on a single parameter θ

$$O = \begin{pmatrix} \cos\theta & -\sin\theta \\ \sin\theta & \cos\theta \end{pmatrix}. \tag{1.48}$$

The Hamiltonian (1.30) then is given by

$$\hat{H} = O \begin{pmatrix} E_+ & 0 \\ 0 & E_- \end{pmatrix} O^t, \tag{1.49}$$

which gives the conditions

$$H_{11} = E_+ \cos^2\theta + E_- \sin^2\theta, \tag{1.50}$$
$$H_{22} = E_+ \sin^2\theta + E_- \cos^2\theta, \tag{1.51}$$
$$H_{12} = (E_+ - E_-)\cos\theta \sin\theta. \tag{1.52}$$

We know that the old and new variables have to obey

$$\mathcal{P}(\hat{H})\mathrm{d}\hat{H} = p(E_+, E_-, \theta)\mathrm{d}E_+\mathrm{d}E_-\mathrm{d}\theta, \tag{1.53}$$

this relation can be re-expressed as

$$p(E_+, E_-, \theta) = \mathcal{P}(\hat{H})\left|\det\left(\frac{\partial(H_{11}, H_{22}, H_{12})}{\partial(E_+, E_-, \theta)}\right)\right|, \tag{1.54}$$

where the determinant is the *Jacobian* of the transformation. Let us compute this Jacobian explicitly

$$
\begin{aligned}
J &= \begin{vmatrix} \cos^2\theta & \sin^2\theta & -2(E_+ - E_-)\cos\theta\sin\theta \\ \sin^2\theta & \cos^2\theta & 2(E_+ - E_-)\cos\theta\sin\theta \\ \cos\theta\sin\theta & -\cos\theta\sin\theta & (E_+ - E_-)(\cos^2\theta - \sin^2\theta) \end{vmatrix} \\
&= -2(E_+ - E_-)\cos^2\theta\sin^2\theta \left(\begin{vmatrix} \sin^2\theta & \cos^2\theta \\ 1 & -1 \end{vmatrix} + \begin{vmatrix} \cos^2\theta & \sin^2\theta \\ 1 & -1 \end{vmatrix} \right) \\
&+ (E_+ - E_-)(\cos^2\theta - \sin^2\theta) \begin{vmatrix} \cos^2\theta & \sin^2\theta \\ \sin^2\theta & \cos^2\theta \end{vmatrix} \\
&= (E_+ - E_-)\left[4\cos^2\theta\sin^2\theta + (\cos^2\theta - \sin^2\theta)(\cos^4 - \sin^4\theta)\right] \\
&= (E_+ - E_-)\left[4\cos^2\theta\sin^2\theta + (\cos^2\theta - \sin^2\theta)(\cos^2\theta - \sin^2\theta)(\cos^2\theta + \sin^2\theta)\right] \\
&= (E_+ - E_-)\left[4\cos^2\theta\sin^2\theta + (\cos^2\theta - \sin^2\theta)^2\right] = (E_+ - E_-)[\cos^2\theta + \sin^2\theta] \\
&= (E_+ - E_-)\cdot 1.
\end{aligned}
$$

Since the trace of a matrix is independent of the basis in which we compute it, we use the eigenvector basis to obtain $\mathrm{Tr}\hat{H}^2 = E_+^2 + E_-^2$. so

$$p(E_+, E_-, \theta) = p(E_+, E_-) = C|E_+ - E_-|e^{-A(E_+^2 + E_-^2)}. \tag{1.55}$$

The variables $s = E_+ - E_-$ and $z = (E_+ + E_-)/2$ can be introduced. In terms of these variables the probability distribution is

$$p(s, z) = Cse^{-A(\frac{s^2}{2} + 2z^2)}. \tag{1.56}$$

As we did before we can set $H_{11} + H_{22} = 0$ and therefore $z = 0$. The constants $A = C = \frac{\pi}{2}$ normalize the spacing distribution.

Now let us look at the case with a unitary symmetry. The most general 2×2 unitary matrix is

$$U = \begin{pmatrix} \cos\theta & -e^{-i\phi}\sin\theta \\ e^{i\phi}\sin\theta & \cos\theta \end{pmatrix}. \tag{1.57}$$

The matrix elements now are

$$H_{11} = E_+\cos^2\theta + E_-\sin^2\theta, \tag{1.58}$$

$$H_{22} = E_-\cos^2\theta + E_+\sin^2\theta, \tag{1.59}$$

$$H_{12} = H_{21}^* = (E_+ - E_-)e^{i\phi}\cos\theta\sin\theta. \tag{1.60}$$

Now the Jacobian is given by

$$J = \det \frac{\partial(H_{11}, H_{22}, \mathrm{Re}[H_{12}], \mathrm{Im}[H_{12}])}{\partial(E_+, E_-, \theta, \phi)} = (E_+ - E_-)^2 \times \tag{1.61}$$

$$\times \begin{vmatrix} \cos^2\theta & \sin^2\theta & -2\cos\theta\sin\theta & 0 \\ \sin^2\theta & \cos^2\theta & 2\cos\theta\sin\theta & 0 \\ \cos\theta\sin\theta\cos\phi & -\cos\theta\sin\theta\cos\phi & \cos\phi(\cos^2\theta - \sin^2\theta) & -\cos\theta\sin\theta\sin\phi \\ \cos\theta\sin\theta\sin\phi & -\cos\theta\sin\theta\sin\phi & \sin\phi(\cos^2\theta - \sin^2\theta) & \cos\theta\sin\theta\cos\phi \end{vmatrix}$$

$$J = (E_+ - E_-)^2 \cos\theta \sin\theta, \tag{1.62}$$

where we compute the Jacobian using *Mathematica*[4]. If we integrate over θ and ϕ we find the eigenvalue distribution

$$P(E_+, E_-) \propto (E_+ - E_-)^2 e^{-A(E_+^2 + E_-^2)}, \tag{1.63}$$

which gives the expected level repulsion (1.45) when introducing the level spacing. □

The general case for any dimension N and any ensemble $\tilde{\beta} = 1, 2, 4$ corresponding, respectively, to GOE, GUE and GSE is obtained in [51] and it is

$$P_{N\tilde{\beta}}(E_1, \ldots, E_N) = C_{N\tilde{\beta}} e^{-\tilde{\beta}\sum_j E_j^2/2} \prod_{j<k} |E_j - E_k|^{\tilde{\beta}}, \tag{1.64}$$

where $C_{N\tilde{\beta}}$ is chosen such that the distribution is normalized and is

$$C_{N\tilde{\beta}}^{-1} = (2\pi)^{N/2} \tilde{\beta}^{-N/2 - \tilde{\beta}N(N-1)/4} \Gamma^{-N}\left(1 + \frac{\tilde{\beta}}{2}\right) \prod_{j=1}^{N} \Gamma\left(1 + \frac{\tilde{\beta} j}{2}\right), \tag{1.65}$$

where $\Gamma(x)$ is Euler's Gamma Function.

1.3.3 Wigner's Semicircle Law

The density of states $\varrho(E)$ for any RMT ensemble in the limit $N \to \infty$ is given by **Wigner's Semicircle law** which states that

$$\varrho(E) = \frac{1}{\pi}\sqrt{2N - E^2}. \tag{1.66}$$

This means that the probability distribution of the eigenvalues of a random matrix, in the limit of large N, is a semicircle of radius $\sqrt{2N}$.

Proof. Let us now reproduce the original argument by Wigner inspired by statistical mechanics to derive this [51, 58]. Consider N point charges in 1-D. They have position $x_1, \ldots x_N$. We can consider that there exists some harmonic oscillator potential in the line and that they are interacting via Coulomb forces on 1-D which are $\propto \ln|x_m - x_n|$. This system is called the *Coulomb gas*. Taking both contributions, we

[4] Code here

find that the potential energy $V(x_1,\ldots,x_N)$ in some suitable units is given by

$$V(x_1,\ldots,x_N)=\frac{1}{2}\sum_n x_n^2-\sum_{m<n}\ln|x_m-x_n|. \tag{1.67}$$

From Statistical Mechanics, we know that the distribution of the system in equilibrium at temperature T is

$$P(x_1,\ldots,x_N)=\frac{1}{Z}\exp\left(-\frac{1}{k_BT}V(x_1,\ldots,x_N)\right), \tag{1.68}$$

where Z is the partition function of the system and k_B is Boltzmann's constant. Actually the probability for the Coulomb gas (1.68) is the same expression as the probability density for the eigenvalues of Random Matrices (1.64) if we relate the degree of level repulsion of the ensemble $\tilde{\beta}$ with the inverse temperature of the system $\tilde{\beta}=\frac{1}{k_BT}$. Interestingly enough the partition function for the Coulomb gas is (1.65). The density of states $\varrho(E)$ is obtained as

$$\varrho(E)=N\int_{-\infty}^{\infty}\mathrm{d}E_2\cdots\int_{-\infty}^{\infty}\mathrm{d}E_N P_{N\tilde{\beta}}(E,E_2,\ldots,E_N). \tag{1.69}$$

This integral may be computed exactly [51] however here we are interested in the large N limit. In analogy with the Coulomb gas, we may assume that the description in terms of a macroscopic continuous density of states works well. This assumption gives:

1. The potential energy V can be represented by the functional

$$V[\varrho(x)]=\frac{1}{2}\int_{-\infty}^{\infty}\mathrm{d}x x^2\varrho(x)-\frac{1}{2}\int_{-\infty}^{\infty}\mathrm{d}x\mathrm{d}y\varrho(x)\varrho(y)\ln|x-y|. \tag{1.70}$$

2. The density of states $\varrho(x)$ minimizes the expression (1.70) following the conditions

$$\int_{-\infty}^{\infty}\mathrm{d}x\varrho(x)=N,\quad\text{and}\quad\varrho(x)\geq 0\ \ \forall x. \tag{1.71}$$

In (1.70) the first term represents the sum when $N\to\infty$. The second term is not exact since it neglects 2-level correlations between the eigenvalues. However, we expect that in the limit of $N\to\infty$ the effect of these 2-level correlations vanishes, and therefore (1.70) is a good approximation. The factor $1/2$ in the second term comes from the condition $m<n$ in the sum. To obtain the equilibrium distribution $\varrho(x)$ we apply the Lagrange multiplier method so we have to find the minimum of the functional $\mathcal{V}[\varrho]$

$$\mathcal{V}[\varrho]=\frac{1}{2}\int_{-\infty}^{\infty}\mathrm{d}x x^2\varrho(x)-\frac{1}{2}\int_{-\infty}^{\infty}\mathrm{d}x\mathrm{d}y\varrho(x)\varrho(y)\ln|x-y|+\mu\Big(\int_{-\infty}^{\infty}\mathrm{d}x\varrho(x)-N\Big),$$

where μ is the Lagrange multiplier.

Functional differentiation with respect to ϱ gives

$$\frac{\delta\mathcal{V}[\varrho]}{\delta\varrho}=0\Rightarrow-\frac{1}{2}x^2+\int_{-\infty}^{\infty}\mathrm{d}y\varrho(y)\ln|x-y|=\mu. \tag{1.72}$$

If we differentiate again with respect to x, we find[5]

$$\mathscr{P}\int_{-\infty}^{\infty}\frac{\varrho(y)}{x-y}\mathrm{d}y = x, \tag{1.73}$$

where $\mathscr{P}$ represents the principal value of the integral. This integral equation can be solved and gives $\varrho(y)$, but let us consider an ansatz and substitute it. We will try

$$\varrho(y) = c\sqrt{R^2-y^2} \text{ for } |y|<R, \quad \varrho(y) = 0 \text{ for } |y|>R. \tag{1.74}$$

We do this integral with *Mathematica*[6] and find

$$\mathscr{P}\int_{-R}^{R}\frac{c\sqrt{A^2-y^2}}{x-y}\mathrm{d}y = c\pi x. \tag{1.75}$$

Therefore, if we want to obey (1.73) we need to take $c=\frac{1}{\pi}$. Now setting the normalization condition we can find a value for R which is

$$\frac{1}{\pi}\int_{-R}^{R}\sqrt{R^2-x^2}\mathrm{d}x = \frac{R^2}{2} = N \to R = \sqrt{2N}. \tag{1.76}$$

Which completes the proof of (1.66). □

Fig. 1.5 illustrates this law numerically and how large N needs to be for its validity.

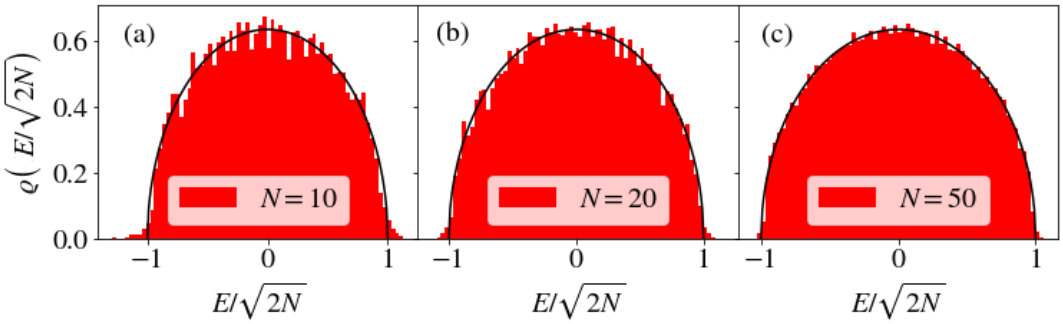

FIGURE 1.5: The density of states for the GUE for different system sizes. All plots were obtained averaging over $N_{\text{av}} = 1000$ matrices of dimension (a) $N = 10$, (b) $N = 20$ and (c) $N = 50$. Note that the x-axis has been rescaled to lay between $(-1, 1)$. The histogram and the semicircle law (1.66) are normalized to unity. Code here.

Thus we see that for $N = 10$ the behavior is far away from the semicircle, for $N = 20$ it starts getting close except the tails of the distribution, and for $N = 50$ the fit to the semicircle law is pretty clear.

[5] To be precise one first needs to split the integral in two terms $\lim_{\varepsilon\to 0}\left(\int_{-\infty}^{x-\varepsilon}+\int_{x+\varepsilon}^{\infty}\right)$ but the terms arising from differentiating the limits cancel out and we can just write the derivative of $\ln|x-y|$.

[6] Code here.

1.3.4 Unfolding the spectra

When studying spectral properties of Quantum Chaotic systems, we will be typically more interested in universal properties of the level statistics rather than on properties that depend on the specific chosen system. To get rid of this system-dependent part and leave only the information of *local fluctuations*, one introduces a procedure called *unfolding of the spectrum* [52]. The procedure is:

1. Order the energies from lowest to highest as $E_0 \leq E_1 \leq \cdots \leq E_N$.
2. Compute the integrated density of states or *staircase function*

$$\mathcal{N}(E) = \int_{-\infty}^{E} \varrho(E')\mathrm{d}E' = \sum_{n, E \geq E_n} \Theta(E - E_n), \tag{1.77}$$

   where $\Theta(x)$ is the Heaviside step function. The main idea is that when we find one level we add one to $\mathcal{N}$. Remember that the density of states is $\varrho(E) = \sum_n \delta(E - E_n)$.
3. From $\mathcal{N}(E)$ compute a smoothed version $\bar{\mathcal{N}}(E)$ by interpolating between the jumps[7]. Then the unfolded energies e_n can be computed as[8] $e_n = \bar{\mathcal{N}}(E_n)$. The density of states for the unfolded levels then has only universal information and has no system-dependent contribution.

We will use unfolding because the level spacing distributions in (1.44) and (1.45) has been chosen such that

$$\int_0^\infty \mathcal{P}(s)\mathrm{d}s = 1, \quad \int_0^\infty s\mathcal{P}(s)\mathrm{d}s = 1, \tag{1.78}$$

and we need the unfolded spectrum in order to obey both of these conditions. However, the unfolding procedure is not very stable, in many cases, it has flaws and does not give the desired outcome. For this reason, other procedures were introduced, apart from the nearest-neighbor level spacing, which sometimes do not need unfolding. The most used one is the consecutive level spacing ratio $r_i = \frac{s_i}{s_{i-1}}$ [59, 60] in which by taking the ratio between consecutive level spacings, one eliminates the dependence on the Local Density of States, thus removing the need for unfolding.

1.4 Quantum Speed Limits

After we have introduced some key concepts on Quantum Chaos and Random Matrix Theory we have to introduce the second key ingredient for our work, this is **Quantum Speed Limits** (QSL). Since the dawn of Quantum Mechanics, the Heisenberg time-energy uncertainty relation is known

$$\Delta E \Delta t \gtrsim \hbar. \tag{1.79}$$

[7] We use a high order polynomial to interpolate this, say of order 10 or 15.

[8] Once we unfold the energies the levels very close to the border of the spectrum have a deviation from a flat distribution so we take them off. This accounts for around 5% of the levels.

However, we know that this uncertainty relation cannot be expressed as a particular case of the uncertainty relation between two non-commuting observables

$$\Delta\hat{A}\Delta\hat{B} \geq \frac{1}{2}|\langle[\hat{A},\hat{B}]\rangle|, \tag{1.80}$$

because time in Quantum Mechanics cannot be expressed correctly as an observable [61]. To put this uncertainty relation in a firmer ground, Mandelstam and Tamm came up with the first Quantum Speed Limit [1]. Many years after them it was known that their limit had some problems and Margolus and Levitin derived yet another Quantum Speed Limit [2].

The main idea behind QSL's is the interpretation that we give to the inequality (1.79). Instead of thinking of it as a statement about simultaneous measurements, one has to think about it as a statement about the *intrinsic time scale* of quantum dynamics $\Delta t \gtrsim \hbar/\Delta E$. This shift of perspective gives a sense of the minimum time in which one can evolve between any two quantum states. Let us, for now, consider the initial and final quantum states to be orthogonal $\langle\psi_0|\psi_f\rangle = 0$, the minimum time to go between the two according to Mandelstam and Tamm is

$$\tau_{\text{QSL}}^{\text{MT}} = \frac{\pi}{2}\frac{\hbar}{\Delta\hat{H}}, \tag{1.81}$$

where $\Delta\hat{H} = \sqrt{\langle\hat{H}^2\rangle - \langle\hat{H}\rangle^2}$ is the standard deviation of the Hamiltonian. Margolus-Levitin bound relies on the average value of the Hamiltonian instead

$$\tau_{\text{QSL}}^{\text{ML}} = \frac{\pi}{2}\frac{\hbar}{\langle\hat{H}\rangle - E_0}, \tag{1.82}$$

where E_0 is the ground state energy of the system.

Actually, it was shown years later [62] that the unified bound is tight in the sense that the minimum time is given by the maximum of both bounds

$$\tau_{\text{QSL}} = \frac{\pi}{2}\max\left(\frac{\hbar}{\Delta\hat{H}}, \frac{\hbar}{\langle\hat{H}\rangle - E_0}\right). \tag{1.83}$$

QSL's then give the minimum time scale under some quantum dynamics. This has many applications all over quantum mechanics and quantum information, e.g. limiting the dynamics of the Spectral Form Factor [63]. The importance of this concept grew a lot after its generalization to open dynamics [4, 5]. For a review in the whole field of study, we refer the reader to [3]. Also recently it was shown that Quantum Speed Limits are not necessarily quantum in nature and that we also have them in Classical Systems [7, 8]. Now we will derive both the MT and ML QSL's following the approach in [3].

1.4.1 Mandelstam-Tamm Bound

Let us consider a general observable $\hat{A}$ which evolves under the Liouville-von-Neumann equation in the Heisenberg picture

$$-i\hbar\partial_t\hat{A} = [\hat{H},\hat{A}]. \tag{1.84}$$

So using the general uncertainty relation (1.80) we find

$$\Delta\hat{H}\Delta\hat{A} \geq \frac{\hbar}{2}\left|\langle\partial_t\hat{A}\rangle\right|. \tag{1.85}$$

Now let us choose $\hat{A}$ to be a projector on the initial state $\hat{A} = |\psi_0\rangle\langle\psi_0|$ so that we can write the standard deviation of $\hat{A}$ as

$$\Delta\hat{A} = \sqrt{\langle\hat{A}^2\rangle - \langle\hat{A}\rangle^2} = \sqrt{\langle\hat{A}\rangle - \langle\hat{A}\rangle^2}, \tag{1.86}$$

and furthermore set $\langle\hat{A}\rangle_{t=0} = 1$. Substituting this in (1.85) and integrating over time, we find

$$\int_0^t \frac{\Delta\hat{H}\mathrm{d}t'}{\hbar} \geq \frac{1}{2}\left|\int_1^{\langle\hat{A}\rangle_t} \frac{\mathrm{d}\langle\hat{A}\rangle_{t'}}{\sqrt{\langle\hat{A}\rangle_{t'} - \langle\hat{A}\rangle_{t'}^2}}\right| \tag{1.87}$$

$$u = \sqrt{\langle\hat{A}\rangle_{t'}} \rightarrow = \frac{1}{2}\left|\int_1^{\sqrt{\langle\hat{A}\rangle_t}} 2\frac{\cancel{u}\mathrm{d}u}{\cancel{u}\sqrt{1-u^2}}\right| \tag{1.88}$$

$$y = \arccos u \rightarrow = \left|\int_0^{\arccos\sqrt{\langle\hat{A}\rangle_t}} -\frac{\cancel{\sin y}\mathrm{d}y}{\cancel{\sin y}}\right| = \arccos\sqrt{\langle\hat{A}\rangle_t}. \tag{1.89}$$

Making use of the identity $\arccos\sqrt{x} = \frac{\pi}{2} - \arcsin\sqrt{x}$ we find

$$t \geq \frac{\hbar}{\Delta\hat{H}}\left(\frac{\pi}{2} - \arcsin\sqrt{\langle\hat{A}\rangle_t}\right). \tag{1.90}$$

Now if we consider that the state at time t and the initial state are orthogonal, $\langle\hat{A}\rangle_t = 0$, we find the Mandelstam-Tamm bound

$$t \geq \tau_{\mathrm{QSL}}^{\mathrm{MT}} = \frac{\pi}{2}\frac{\hbar}{\Delta\hat{H}}. \tag{1.91}$$

Note that the factor $\frac{\pi}{2}$ in this bound comes from considering orthogonal states. A generalized bound for non-orthogonal states is introduced in §1.4.3.

1.4.2 Margolus-Levitin Bound

In [64] the authors discuss how the standard deviation of the energy may not always be a good quantity to use. For example, sometimes it may diverge, like in the Breit-Wigner state, even when the average energy is finite. This lead Margolus and Levitin [2] to derive a new Quantum Speed Limit, now depending on the expectation value of the Hamiltonian.

To derive their bound we start by expanding the initial state on the eigenvector basis $|\psi_0\rangle = \sum_n c_n|n\rangle$, which readily gives the time evolved state

$$|\psi_t\rangle = \sum_n c_n e^{-iE_nt/\hbar}|n\rangle. \tag{1.92}$$

The overlap between the states at times $t = 0$ and t is

$$S_t = \langle \psi_0 | \psi_t \rangle = \sum_n |c_n|^2 e^{-iE_n t/\hbar}. \tag{1.93}$$

Let us compute the real part of this quantity

$$\mathrm{Re}(S_t) = \sum_n |c_n|^2 \cos \frac{E_n t}{\hbar} \geq \sum_n |c_n|^2 \left(1 - \frac{2}{\pi}\left(\frac{E_n t}{\hbar} + \sin \frac{E_n t}{\hbar}\right)\right), \tag{1.94}$$

where we used the inequality $\cos x \geq 1 - \frac{2}{\pi}(x + \sin x)$, true for $x \geq 0$. The term with the sine is related to the imaginary part of S so we find

$$\mathrm{Re}(S_t) \geq 1 - \frac{2}{\pi}\frac{\langle \hat{H} \rangle}{\hbar} t + \frac{2}{\pi}\mathrm{Im}(S_t). \tag{1.95}$$

If we now consider two orthogonal states, we find the Margolus-Levitin bound assuming $E_0 = 0$

$$t \geq \tau_{\mathrm{QSL}}^{\mathrm{ML}} = \frac{\pi}{2}\frac{\hbar}{\langle \hat{H} \rangle}. \tag{1.96}$$

Again note the $\frac{\pi}{2}$ factor being the angle between the orthogonal states. One should note that implicitly we are taking the origin of energy at E_0, for this reason we sometimes write $\langle \hat{H} \rangle - E_0$ instead of $\langle \hat{H} \rangle$.

1.4.3 Speed limits for arbitrary angles

To find bounds for arbitrary angles, we rely on a measure of the distance between states, the fidelity. The **Fidelity** between a initial pure quantum state $|\psi_0\rangle$ and the time-evolved quantum state $|\psi_t\rangle = e^{-i\hat{H}t/\hbar}|\psi_0\rangle$ is

$$F(t) = |\langle \psi_0 | \psi_t \rangle|^2 \tag{1.97}$$

For mixed quantum states, the simple generalization in terms of density matrices, $\mathrm{Tr}(\rho_0 \rho_t)$, does not hold. Uhlmann [65] showed that the correct generalization is given by

$$F(t) = \left(\mathrm{Tr}\sqrt{\sqrt{\rho_0}\rho_t\sqrt{\rho_0}}\right)^2. \tag{1.98}$$

For any two pure quantum states, $|\psi_0\rangle$, $|\psi_t\rangle$ one can define a *distance* between the states, i.e. a *metric* on the Hilbert space. This distance is the angle between the rays spanned by each of the states [66]

$$\mathcal{L}(|\psi_0\rangle, |\psi_t\rangle) = \arccos |\langle \psi_0 | \psi_t \rangle|. \tag{1.99}$$

This quantity is known as the **Bures angle** and its generalization to any quantum state, regardless it being pure or mixed is

$$\mathcal{L}(\rho_0, \rho_t) = \arccos \sqrt{F(t)}. \tag{1.100}$$

Note that it measures the distance, as easily seen from $F(t) = 1 - \sin^2 \mathcal{L}(t)$. If we look at the RHS of (1.89) it is exactly the Bures angle since $\langle \hat{A} \rangle_t = F(t)$ due to the selection of $\hat{A}$ as a projector. So the generalization of the QSL to any two quantum states, not necessarily orthogonal is

$$t \geq \tau_{\text{QSL}} = \hbar \mathcal{L}(\rho_0, \rho_t) \max \left(\frac{1}{\Delta \hat{H}}, \frac{1}{\langle \hat{H} \rangle - E_0} \right). \tag{1.101}$$

1.4.4 Speed Limits on the Fidelity

In [7] a bound on the derivative of the Fidelity is found. This bound can be rewritten as

$$|\dot{F}(t)| \leq \frac{1 - F(t)}{\tau_{\text{QSL}}}. \tag{1.102}$$

This bound is originally found in the context of Wigner's formulation of quantum mechanics in phase space [7]

$$|\dot{F}(t)| \leq \nu_\Gamma = \sqrt{\int \mathrm{d}^2\Gamma \{\{\hat{H}, W_0\}\}^2}, \tag{1.103}$$

where $W_0(x, p)$ is the Wigner function of the initial state and $\{\{\circ, \circ\}\}$ is the *Moyal bracket*, which generalizes the commutator to phase space distributions. The expression for ν_Γ in terms of the Wigner's function is not especially important for our argument. For completeness, it is obtained in Appendix B. The key point of the argument here is that it is bounded by some constant ν_Γ. (1.103) can be integrated on both sides to find

$$-\int_1^{F(t)} \mathrm{d}F = \int_{F(t)}^1 \mathrm{d}F \leq \nu_\Gamma \int_0^t \mathrm{d}t \tag{1.104}$$

$$\frac{1 - F(t)}{\nu_\Gamma} \leq t \Rightarrow \frac{1 - F(t)}{\nu_\Gamma} = \tau_{\text{QSL}}, \tag{1.105}$$

where the fact that $\dot{F}$ is negative at the beginning, since $F(0) = 1$ and $F(t) \leq 1$, was used to interchange the limits in the integral.

So the bound on the derivative of the fidelity can be rewritten in terms of the Quantum Speed Limit time as in (1.102). This new perspective allows for a new visualization of QSL's since they bound the time derivative of the fidelity of the system. This approach will be used in Sections 2.3 and 3.3.

Chapter 2

The Quantum Kicked Top

2.1 Behavior of the Kicked Top

The Quantum Kicked Top[1] is a model that displays many of the features of quantum chaos and serves as a playground for most of the quantum chaotic phenomena [57]. The physical system corresponds to an angular momentum subject to a free precession which is periodically kicked with time. This model was first proposed by Haake in [68]. The relation to other kicked systems was studied in [67]. The relation to the universality symmetry classes was studied in [69, 70]. The classical limit was experimentally demonstrated in [71] and the fully quantum version of the system was studied in [72]. The main features that make this system especially suitable for our studies are the finiteness of its Hilbert space[2] and the fact that we have a well-defined classical limit as the angular momentum of our system $S \to \infty$. Also, we have only one degree of freedom, the strength of the pulses, which allows us to tune the chaoticity of the model going from an integrable to a chaotic phase.

We consider a spin system with spin S, the operators characterizing our system are $\hat{S}_x,\ \hat{S}_y,\ \hat{S}_z$, which of course obey the commutation relations $[\hat{S}_i, \hat{S}_j] = i\epsilon_{ijk}\hat{S}_k$. The Hamiltonian of the system is

$$\hat{H}(t) = \frac{p}{\tau_p}\hat{S}_y + \frac{k}{2S}\hat{S}_z^2 \sum_n \delta(t - n\tau_p). \tag{2.1}$$

One should note that the kicking part of the Hamiltonian points in a different direction to the free evolution and it is non-linear. Also, it is composed of Dirac's delta functions, this means that the kicking is instantaneous. The parameters involved are p which governs the free evolution, k which sets the strength of the nonlinear kick, τ_p which sets the length of the perios and S which sets the spin of the angular momentum. One of the great features of the QKT is that it shows tunability, i.e. when k/p is small the system is regular and when k/p is large the system is chaotic.

In general, time-dependent Hamiltonians can be hard to solve, one has to solve the time-dependent Schrödinger equation or deal with complicated time-ordering operators in the Dyson series. However, for the Kicked Top, we can introduce the **Floquet**

[1] One should be careful not to mistake this model with the Kicked Rotator. The kicked rotator only uses the canonically conjugated variables $\hat{x},\ \hat{p}$. Where the "position" is restricted to lie between $[0,\ 2\pi)$ thus representing an angle. The phase space of the Kicked Rotator is a cylinder, not a sphere. This system can also be understood as a limiting case of the Kicked Top [67].

[2] For other systems with infinite-dimensional Hilbert spaces we sometimes need to truncate $\mathscr{H}$. This truncation can cause that we break some symmetry of the system or introduce a new unwanted symmetry.

representation [73–76] . The main idea is that we introduce the time evolution operator over one period and work with discrete times. This is particularly simple since the kicks are instantaneous.

$$\hat{\mathcal{U}} = \mathcal{T} e^{-i\int_0^{\tau_p} \hat{H}(t)\mathrm{d}t} = e^{-ip\hat{S}_y} e^{-ik\hat{S}_z/2S}, \tag{2.2}$$

where $\mathcal{T}$ is the time-ordering operator. Since the Hamiltonian is written only in terms of spin operators it commutes with $\hat{S}^2$ thus conserving the total spin

$$[\hat{S}^2, \hat{H}(t)] = 0 \;\Rightarrow\; [\hat{S}^2, \hat{\mathcal{U}}] = 0. \tag{2.3}$$

One set of states which will be of major importance in our study of the Kicked Top are the **Coherent SU(2) states** [77, 78].

Definition 8. *Coherent SU(2) States: These are quantum states which point in the direction given by (θ, ϕ) with minimum uncertainty. They can be understood as the action on $|S, S\rangle$ of some unitary operator $U(\theta, \phi)$*

$$|\theta, \phi\rangle = U(\theta, \phi)\,|S, S\rangle = \exp\left[i\theta(\hat{S}_x \sin\phi - \hat{S}_y \cos\phi)\right]|S, S\rangle\,. \tag{2.4}$$

An explicit expression can be found in terms of the complex number $\zeta = -\tan\frac{\theta}{2}e^{-i\phi}$

$$|\theta, \phi\rangle = \sum_{m=-S}^{+S} \sqrt{\frac{(2S)!}{(S+m)!(S-m)!}} \frac{\zeta^{S+m}}{(1+|\zeta|^2)^S}\,|S, m\rangle\,, \tag{2.5}$$

where S is the spin of the system and $|S, m\rangle$ is the usual angular momentum basis composed of simultaneous eigenstates of $\hat{S}^2$ and $\hat{S}_z$.

These states have the properties

$$\langle\theta, \phi|\hat{S}_z|\theta\phi\rangle = S\cos\phi, \quad \langle\theta, \text{ and } \phi|\hat{S}_x \pm i\hat{S}_y|\theta, \phi\rangle = Se^{\pm i\phi}\sin\theta. \tag{2.6}$$

The relative variance of these states is

$$\frac{\langle\theta, \phi|\hat{\mathbf{S}}^2|\theta, \phi\rangle - \langle\theta, \phi|\hat{\mathbf{S}}|\theta, \phi\rangle^2}{S^2} = \frac{1}{S}, \tag{2.7}$$

which is the smallest one allowed by the commutation relations between angular momentum operators. All of these properties allow us to think of $|\theta, \phi\rangle$ as a state pointing in the direction (θ, ϕ) with an uncertainty in the solid angle $\delta\Omega = 1/S$. This relative uncertainty vanishes as we take the classical limit $S \to \infty$.

2.1.1 Quantum equations of motion

The evolution of the system in the Heisenberg picture is given by the recurrence relations $\hat{\mathbf{S}}^{n+1} = \hat{\mathcal{U}}^{\dagger}\hat{\mathbf{S}}^{n}\hat{\mathcal{U}}$ where by n we mean that the time is $t = n\tau_p$. We have

$$\begin{aligned}
\hat{S}_x^{n+1} &= \frac{1}{2}\left(\hat{S}_x^n \cos p + \hat{S}_z^n \sin p + i\hat{S}_y^n\right) e^{ik(\hat{S}_z^n \cos p - \hat{S}_x^n \sin p + \frac{1}{2})/S} + \text{h.c.}, \\
\hat{S}_y^{n+1} &= \frac{1}{2i}\left(\hat{S}_x^n \cos p + \hat{S}_z^n \sin p + i\hat{S}_y^n\right) e^{ik(\hat{S}_z^n \cos p - \hat{S}_x^n \sin p + \frac{1}{2})/S} + \text{h.c.}, \\
\hat{S}_z^{n+1} &= \hat{S}_z^n \cos p - \hat{S}_x^n \sin p.
\end{aligned} \tag{2.8}$$

One should note that the hermitian conjugation changes the order of the exponential and makes it go in front of the brackets.

Proof. Now we will proceed with a derivation of the previous set of equations obtained in [79]. Computing the evolution boils down in the end to computing the product between operators

$$\hat{\mathbf{S}}^{n+1} = e^{ik\hat{S}_z/2S} e^{ip\hat{S}_y} \hat{\mathbf{S}}^n e^{-ip\hat{S}_y} e^{-ik\hat{S}_z/2S}. \tag{2.9}$$

During this proof, we will drop the hats in the notation for operators and the explicit superscript indicating that the spin operators are evaluated at time n. First, we begin by introducing the auxiliary spin operators

$$\tilde{S}_x = e^{ipS_y} S_x e^{-ipS_y} = S_x - i(ip)S_z + \frac{(ip)^2}{2!}S_x - i\frac{(ip)^3}{3!}S_z + \ldots, \tag{2.10}$$

$$= S_x\left(1 - \frac{p^2}{2!} + \ldots\right) + S_z\left(p - \frac{p^3}{3!} + \ldots\right) = S_x \cos p + S_z \sin p, \tag{2.11}$$

where we used the *Baker-Campbell-Haussdorf (BCH) formula*

$$e^X Y e^{-X} = Y + [X, Y] + \frac{1}{2}[X, [X, Y]] + \frac{1}{3!}[X, [X, [X, Y]]] + \ldots \tag{2.12}$$

By a similar argument, we find that

$$\tilde{S}_y = e^{ipS_y} S_y e^{-ipS_y} = S_y, \tag{2.13}$$

$$\tilde{S}_z = e^{ipS_y} S_z e^{-ipS_y} = S_z \cos p - S_x \sin p, \tag{2.14}$$

where the difference in sign arises because $[S_y, S_z] = iS_x$ instead of $[S_y, S_x] = -iS_z$. The remaining term to compute is given by

$$\hat{\mathbf{S}}^{n+1} = \exp\left\{ik\frac{\tilde{S}_z^2}{2S}\right\} \tilde{\mathbf{S}} \exp\left\{-ik\frac{\tilde{S}_z^2}{2S}\right\}, \tag{2.15}$$

note that all of the spin operators appearing in the equation are the auxiliary ones $\tilde{\mathbf{S}}$. For simplicity we introduce the operators $\tilde{S}_{\pm} = \tilde{S}_x \pm i\tilde{S}_y$ that obey the commutation relation

$$[\tilde{S}_+, \tilde{S}_-] = 2\tilde{S}_z, \tag{2.16}$$

expanding $\mathbf{S}^2$ in terms of these operators we find

$$\tilde{\mathbf{S}}^2 = \tilde{S}_+\tilde{S}_- - \frac{1}{2}[\tilde{S}_+, \tilde{S}_-] + \tilde{S}_z^2, \tag{2.17}$$

from which we can obtain a useful expression for $\tilde{S}_z^2$ as

$$\tilde{S}_z^2 = \tilde{\mathbf{S}}^2 - \tilde{S}_+\tilde{S}_- + \tilde{S}_z. \tag{2.18}$$

Now we obtain some commutation relations which will be useful for us

$$[\tilde{S}_z, \tilde{S}_\pm] = [\tilde{S}_z, \tilde{S}_x \pm i\tilde{S}_y] = i\tilde{S}_y \pm i(-i)\tilde{S}_x = \pm\tilde{S}_\pm, \tag{2.19a}$$
$$[\tilde{S}_+\tilde{S}_-, \tilde{S}_z] = 0, \tag{2.19b}$$
$$[\tilde{S}_+\tilde{S}_-, \tilde{S}_+] = \tilde{S}_+[\tilde{S}_-, \tilde{S}_+] = -2\tilde{S}_+\tilde{S}_z, \tag{2.19c}$$
$$[\tilde{S}_+\tilde{S}_-, \tilde{S}_-] = 2\tilde{S}_z\tilde{S}_-. \tag{2.19d}$$

To obtain the equations of motion in the Heisenberg picture we will begin by computing the time evolution of the operators $\tilde{S}_\pm$. The relevant commutators are

$$[\tilde{S}_z^2, \tilde{S}_+] = 2\tilde{S}_+\tilde{S}_z + \tilde{S}_+ = \tilde{S}_+(2\tilde{S}_z + 1), \tag{2.20a}$$
$$[\tilde{S}_z^2, [\tilde{S}_z^2, \tilde{S}_+]] = [\tilde{S}_z^2, \tilde{S}_+](2\tilde{S}_z + 1) = \tilde{S}_+(2\tilde{S}_z + 1)^2, \tag{2.20b}$$
$$[\tilde{S}_z^2, [\tilde{S}_z^2, [\tilde{S}_z^2, \tilde{S}_+]]] = [\tilde{S}_z^2, \tilde{S}_+](2\tilde{S}_z + 1)^2 = \tilde{S}_+(2\tilde{S}_z + 1)^3, \tag{2.20c}$$

and a similar argument applies to $\tilde{S}_-$ with the difference that $[\tilde{S}_z^2, \tilde{S}_-] = -(2\tilde{S}_z + 1)\tilde{S}_-$ therefore applying the BCH formula yields

$$S_+^{n+1} = \tilde{S}_+ \exp\left[i\frac{k}{2S}(2\tilde{S}_z + 1)\right], \quad S_-^{n+1} = \exp\left[-i\frac{k}{2S}(2\tilde{S}_z + 1)\right]\tilde{S}_-. \tag{2.21}$$

Therefore we find that the equations of motion for $\mathbf{S}$ are

$$S_x^{n+1} = \frac{1}{2}\tilde{S}_+ \exp\left[i\frac{k}{2S}(2\tilde{S}_z + 1)\right] + \frac{1}{2}\exp\left[-i\frac{k}{2S}(2\tilde{S}_z + 1)\right]\tilde{S}_-, \tag{2.22}$$
$$S_y^{n+1} = \frac{1}{2i}\tilde{S}_+ \exp\left[i\frac{k}{2S}(2\tilde{S}_z + 1)\right] - \frac{1}{2i}\exp\left[-i\frac{k}{2S}(2\tilde{S}_z + 1)\right]\tilde{S}_-, \tag{2.23}$$
$$S_z^{n+1} = \tilde{S}_z. \tag{2.24}$$

And substituting $\tilde{S}_\pm = S_x\cos p + S_z \sin p \pm iS_y$, $\tilde{S}_z = S_z\cos p - S_x \sin p$ we find the set of equations (2.8) we were looking for. □

2.1.2 Classical evolution

One of the nice properties of the kicked top is the fact that it has a well-defined classical limit. This allows us to study which features the system presents when the classical limit is chaotic. To study the classical dynamics we can introduce the variables $X = \hat{S}_x/S$, $Y = \hat{S}_y/S$, $Z = \hat{S}_z/S$ such that $\mathbf{R} = (X, Y, Z)$. These variables

obey the commutation relations

$$[R_i, R_j] = i\frac{1}{S}\epsilon_{ijk}R_k. \tag{2.25}$$

We see that as we take $S \to \infty$ the commutator vanishes and the R_i become c-numbers. Another way to interpret the classical limit is that as S gets large the allowed values for $m \in [-S, -(S-1), \ldots, S-1, S]$ get to a continuum and so the angular momentum can point in any direction. A nice visualization that indeed the $S \to \infty$ corresponds to the classical limit is using the Husimi Q function. We define it for a spin system with spin S and a state characterized by the density matrix $\hat{\rho}$ as [72]

$$Q(\theta, \phi) = \frac{2S+1}{4\pi} \langle \theta, \phi | \hat{\rho} | \theta, \phi \rangle . \tag{2.26}$$

If we take the initial state to be a pure SU(2) coherent state $\hat{\rho}_0 = |\theta_0, \phi_0\rangle \langle \theta_0, \phi_0|$ we find the plots in Fig. 2.1 which clearly show that the distribution is much more localized for bigger values of the spin. With this, we can visualize that the uncertainty in the solid angle decreases as $1/S$. Note that the maximum value of $Q(\theta, \phi)$ is ≈ 10 times bigger in the lower part of Fig. 2.1.

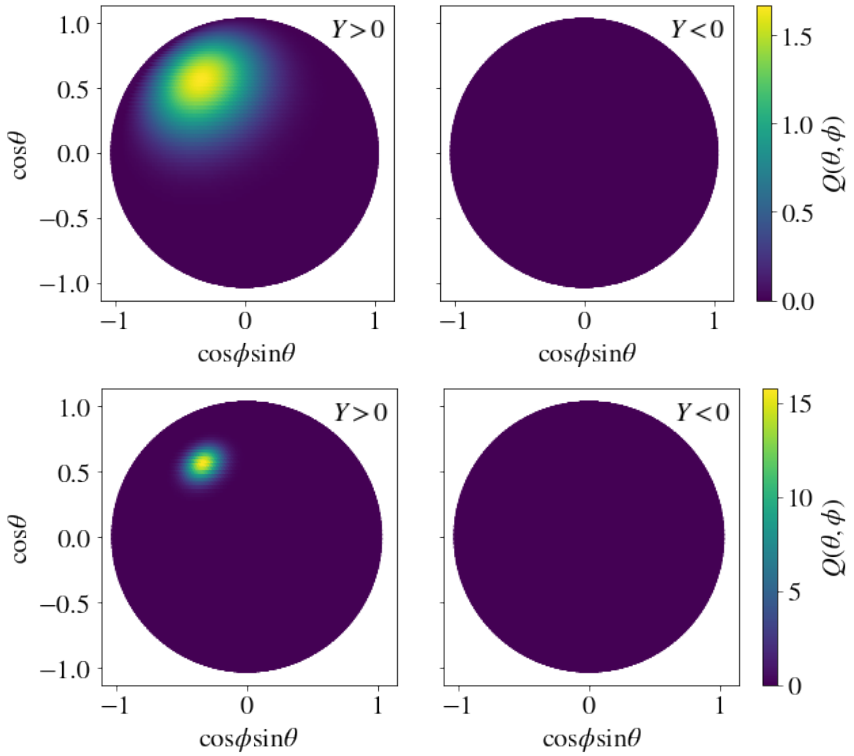

FIGURE 2.1: Q function for an initial coherent SU(2) state for $S = 10$ (upper) and $S = 100$ (lower). Code here.

If we introduce the variables X, Y, Z since they are c-numbers in the limit $S \to \infty$ (2.8) reduce to the **classical map**

$$\begin{aligned} X_{n+1} &= \mathrm{Re}\left\{(X_n \cos p + Z_n \sin p + iY_n)e^{ik(Z_n \cos p - X_n \sin p)}\right\}, \\ Y_{n+1} &= \mathrm{Im}\left\{(X_n \cos p + Z_n \sin p + iY_n)e^{ik(Z_n \cos p - X_n \sin p)}\right\}, \\ Z_{n+1} &= -X_n \sin p + Z_n \cos p. \end{aligned} \tag{2.27}$$

To visualize the classical trajectories we generate many initial points in the phase space of the system and let them evolve with (2.27) we find the plots in Fig. 2.2. As we see for $k = 2$ most of the orbits are periodic and therefore the phase space is mostly regular, a more detailed study of the periodicity of these orbits and the symmetries of the Classical Kicked Top can be found in [68]. As we increase k we see that the area with regular motion shrinks down. At $k = 3$ only 4 islands of regularity remain in a mostly chaotic phase space. Finally, for $k = 6$ no regularity is seen from the trajectory plot, so the phase space is fully chaotic up to some possible zero-measure islands of regularity that cannot be appreciated in the plot.

2.1.3 Quantum Evolution and Fidelity

We can gain some intuition on the quantum evolution by using the Q function defined before. If we sum all of the Q functions at time n $Q_n(\theta, \phi)$ up to some final time $t_f = N_f \tau_p$ we can get a quantum version of the trajectory. Let us call this function the accumulated Q function $\mathcal{Q}_A$

$$\mathcal{Q}_A := \sum_{n=0}^{N_f} Q_n(\theta, \phi). \tag{2.28}$$

We plot this quantity along with its classical counterpart for $S = 50$. When the motion is regular Fig. 2.3 shows a pretty good agreement between the quantum and the classical version of the trajectory.

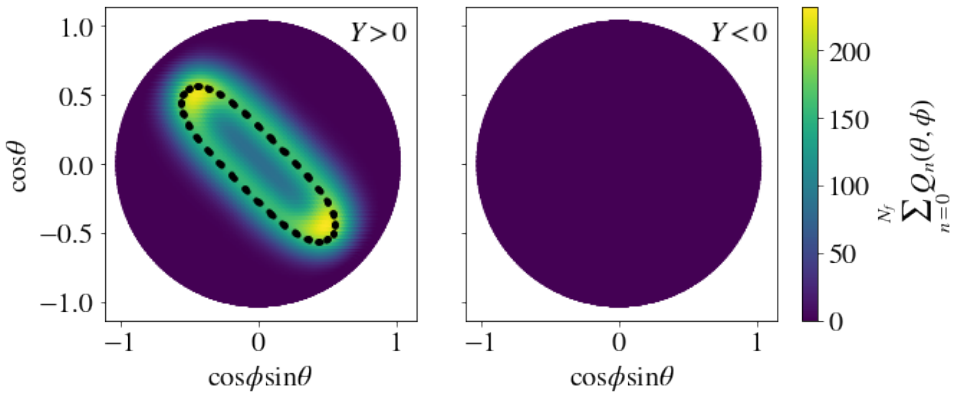

FIGURE 2.3: Accumulated $\mathcal{Q}_A$ function and the classical trajectory (black circles) for the Kicked Top with $S = 50$ in the regular regime $k = 2$, $p = \frac{\pi}{2}$, $N_f = 200$. Code here.

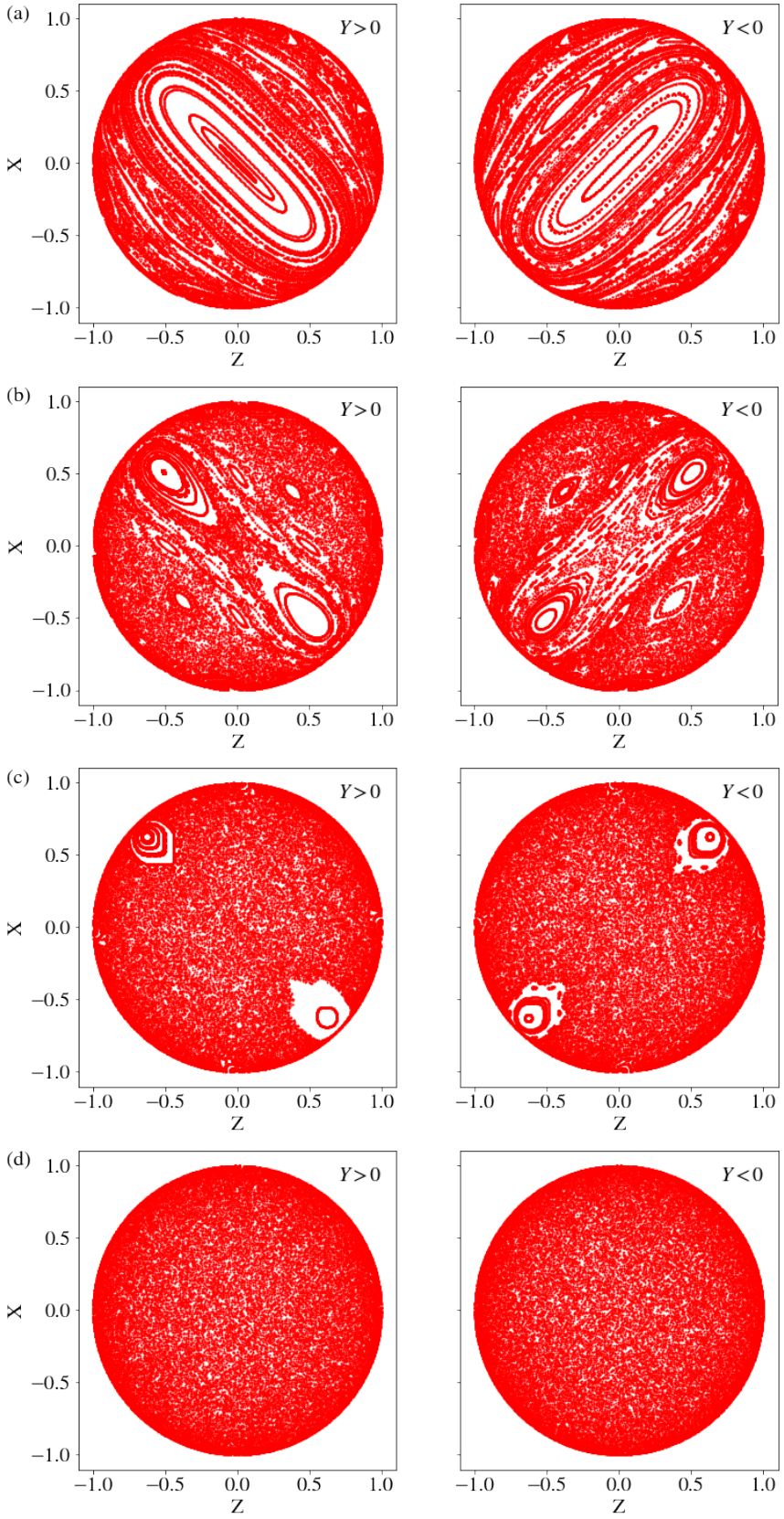

FIGURE 2.2: Classical phase space evolution for $p = \frac{\pi}{2}$ and (a) $k = 2$, (b) $k = 2.5$, (c) $k = 3$ and (d) $k = 6$. The plots with $Y > 0$ represent the northern hemisphere of the phase space while the plots with $Y < 0$ represent the southern hemisphere. Code here.

In the chaotic regime, however, we cannot compare the quantum and classical trajectories so easily. Still we can test ergodicity, which we expect from chaotic systems. Fig. 2.4 shows that nearly all phase space has an accumulated $\mathcal{Q}_A$ function bigger than zero, which implies that the wavepacket went through that region at least once. The structure shown by the plot is expected to vanish as we take the time of the simulation N_f to infinity.

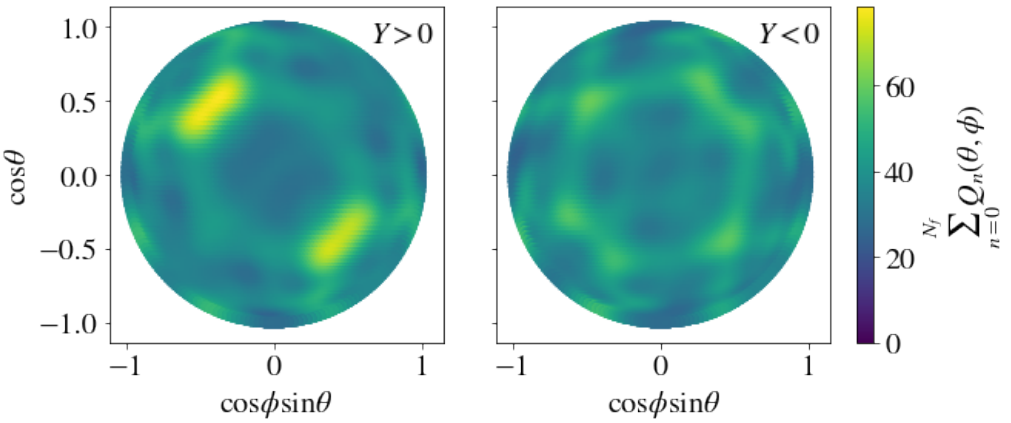

FIGURE 2.4: Accumulated Q function for the Quantum Kicked Top in the chaotic regime. The parameters used are $k = 6$, $p = \frac{\pi}{2}$, $N_f = 200$ and $S = 50$. Code here.

Another way in which we can understand the quantum evolution is by looking at the fidelity, which at time $t = n\tau_p$ is given by

$$F(t) = |\langle\theta,\phi|\hat{\mathcal{U}}^n|\theta,\phi\rangle|^2. \tag{2.29}$$

We plot the Fidelity in Fig. 2.5. We see that for regular motion, and very small values of k we have revivals in the fidelity every 4 periods, this is because every 4 kicks the state comes back to a very similar version to the initial state because $p = \frac{\pi}{2}$. However, in chaotic motion, the Fidelity, at least the one taken between coherent SU(2) states does not give any meaningful information, apart from it being fluctuating around zero.

2.1.4 Classical Lyapunov exponent

We can compute the Lyapunov exponent of the classical map using Def. 1. The way we do this numerically is by computing how the distance between two neighboring points grows with time and fitting that to an exponential $e^{\lambda t}$. Due to the argument in (1.9) we know that if we want to compare classical and quantum Lyapunov exponents we have to use 2λ. We plot this quantity as a function of k in Fig. 2.6

As we see, our numerical results have a similar trend to the analytics, but they do not exactly match at large k the analytical expression. This is because the method we used is different from the approach used in [80]. Our method is as follows:

1. Take many pairs of initial conditions very close together

$$\{(\mathbf{r}_1^j(0), \mathbf{r}_2^j(0)), j \in (1, N_{\text{av}})\} \text{ such that } |\mathbf{r}_1^j(0) - \mathbf{r}_2^j(0)| \lll 1 \ \forall j. \tag{2.30}$$

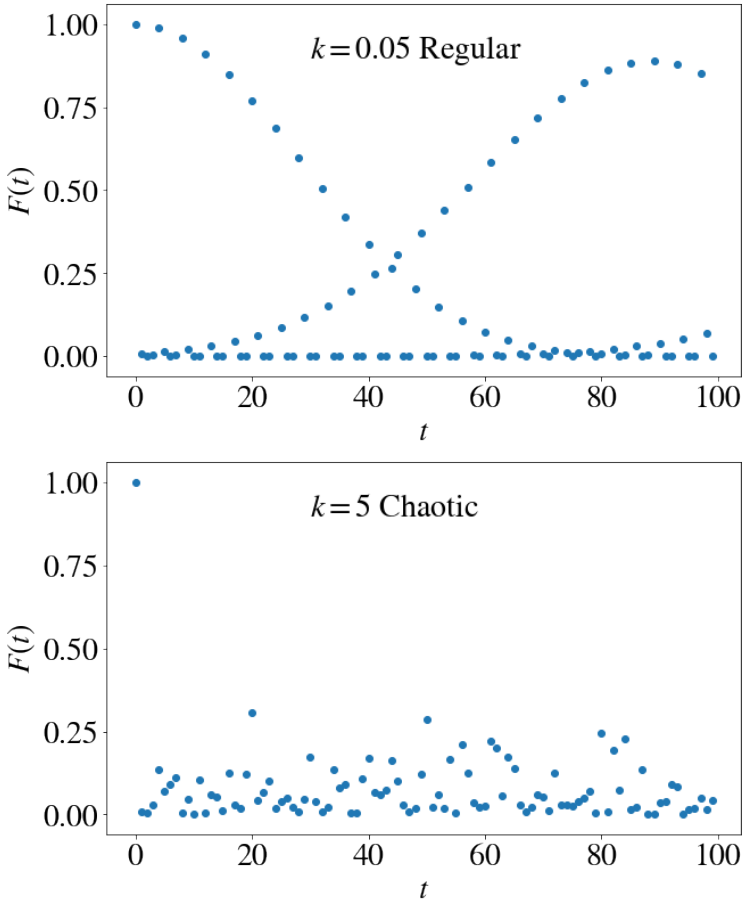

FIGURE 2.5: Fidelity of the Quantum Kicked Top as a function of time for Regular and Chaotic phase spaces. The parameters used are $p = \frac{\pi}{2}$, $S = 9$. Code here.

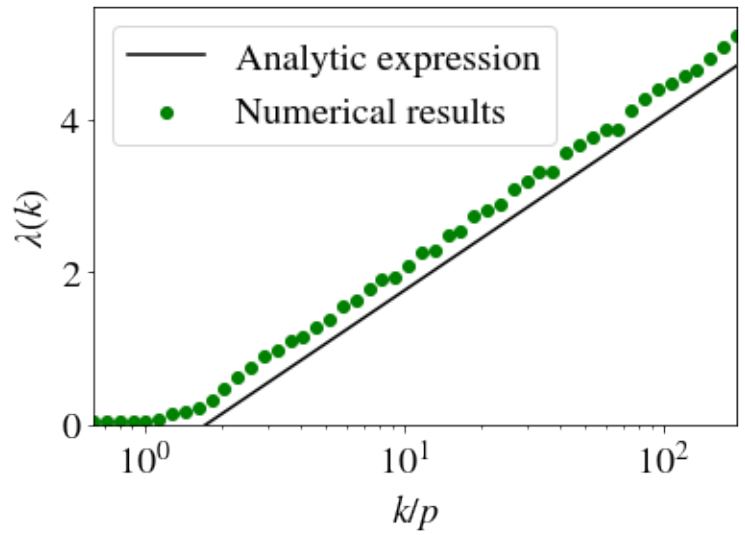

FIGURE 2.6: Classical Lyapunov exponent as a function of the strength of the kicks. The analytic expression $\lambda(k) = \ln(k|\sin p|) - 1$ [80] works in the large k limit. Code here.

2. Compute the distance between the pair of points as a function of time

$$d^j(t) = |\mathbf{r}_1^j(t) - \mathbf{r}_2^j(t)|. \tag{2.31}$$

3. Average the distance over all the pairs of initial conditions

$$d(t) = \frac{1}{N}\sum_j |\mathbf{r}_1^j(t) - \mathbf{r}_2^j(t)|. \tag{2.32}$$

4. Fit an exponential $e^{\lambda t}$ to the distance before it saturates to a value ~ 1. Then λ is the Lyapunov exponent.

The method used in [80] relies on the *tangent map* method. It is based on computing the matrix

$$M(\mathbf{R}_n) = \frac{\partial \mathbf{R}_{n+1}}{\partial \mathbf{R}_n}. \tag{2.33}$$

Then the largest Lyapunov exponent is given by

$$\lambda_+ = \ln\left(\lim_{N\to\infty} |j_+(N)|^{1/N}\right), \tag{2.34}$$

where $j_+(N)$ is the largest eigenvalue of the matrix $\prod_{n=1}^N M(\mathbf{R}_n)$.

2.1.5 Quantum Lyapunov exponent

Following [81] we can define the Quantum Lyapunov exponent for the Kicked Top. The main idea is to compute an infinite temperature OTOC with spin operators. The operator that will evolve in time is $\hat{A}(t)$.

$$C[\hat{A}(t)] = -\frac{1}{2S+1}\sum_{\alpha\in(x,y,z)} \mathrm{Tr}[\hat{S}_\alpha, \hat{A}(t)]^2. \tag{2.35}$$

The exponential growth of this OTOC gives a quantum version of the Lyapunov exponent for the Kicked Top, or in general any spin system. Since this OTOC is only defined at infinite temperature, Maldacena's bound is trivial $\lambda_Q < \infty$ so we cannot obtain a useful bound in this case. However other system-dependent bounds can be obtained. In [81] the authors find an upper and lower bound for the Lyapunov exponent. The upper bound, based on the size of the operator $\hat{A}(t)$ sets

$$\lambda_Q \leq k = \lambda_{\text{bound}}. \tag{2.36}$$

Note that this bound is independent of S. The lower bound is based on semiclassical considerations considering the unstable fixed points of the classical map (2.27). This leads to the bound

$$\lambda_Q \geq \ln\left(\frac{k}{2} + \sqrt{\frac{k^2}{4} - 1}\right) = \lambda_{\text{saddle}}. \tag{2.37}$$

Fig. 2.7 shows these bounds along with the numerical results obtained for the OTOC and the classical Lyapunov exponent. From there we see that λ_Q obeys both bounds.

Also, we see that the quantum Lyapunov Exponent is larger than its classical counterpart. This agrees with the results obtained for the Kicked Rotor in [82], which, we recall is a limiting case of the Kicked Top [67].

One of the problems with the Kicked Top for our purpose of studying Maldacena's bound is the fact that the OTOC we have defined is only defined at infinite temperature. Furthermore, there is not a clear way of defining the Boltzmann factors since the system is periodically kicked, should we use $e^{-\beta \hat{H}(t)}$, $e^{-\beta \epsilon}$ [3]. Does it even make sense to talk about the temperature in a Kicked Top? One possible step in this direction would be to introduce an open version of the Kicked Top in any of the possible formalisms, however this would need tools from *dissipative quantum chaos* [83] and lays outside of the scope of the present work, for this reason we leave it as a direction for further research.

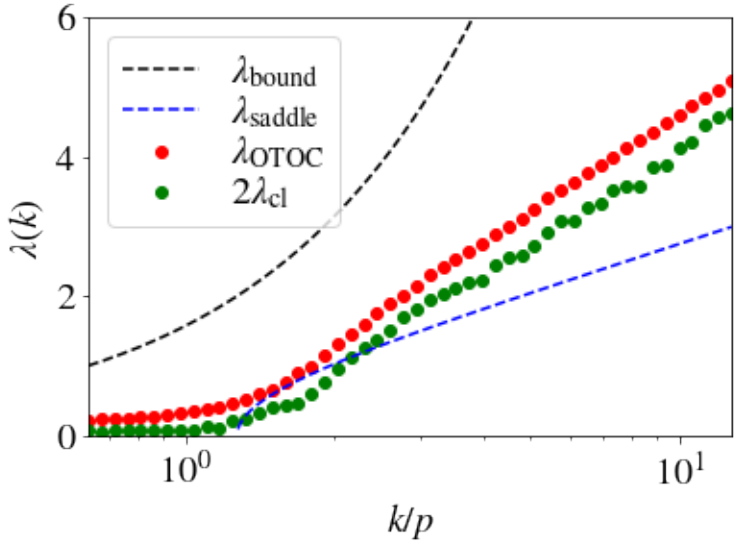

FIGURE 2.7: Lyapunov exponent obtained from the OTOC (red) and the classical map (green). The considered system has $S = 100$ and the operator chosen is $\hat{A}(t) = \hat{S}_x$. Code here.

2.2 Generalized Kicked Tops

2.2.1 Relation to Random Matrix Theory

The great feature about Kicked Top models is that one can obtain a physical model that mimics the level spacing statistics of any of the RMT ensembles [57]. For this let us introduce a Generalized Kicked Top system with both free evolution and kicks in the three directions of space. The Floquet operator for this system reads

$$\hat{\mathcal{U}} = e^{-i(p_z \hat{S}_z + \frac{k_z}{2S+1}\hat{S}_z^2)} e^{-i(p_y \hat{S}_y + \frac{k_y}{2S+1}\hat{S}_y^2)} e^{-i(p_x \hat{S}_x + \frac{k_x}{2S+1}\hat{S}_x^2)}. \tag{2.38}$$

[3] We tried this option with the pseudo-energies and the shape of the Lyapunov curve $\lambda(k)$ did not change at all, for this reason we think we can disregard this option.

The idea then is to obtain the pseudo-energies of the system ϵ_n, compute the (pseudo) level spacing, unfold it and compare it with the Wigner-Dyson surmises. Appropriately choosing the parameters $\mathbf{k} = (k_x, k_y, k_z)$, $\mathbf{p} = (p_x, p_y, p_z)$ we can recover the three universality classes: Poissonian, GOE and GUE [4]. Let us investigate how to obtain these universality classes:

- **Poissonian**: If one chooses $\mathbf{p}$ and $\mathbf{k}$ pointing in the same direction, the system is integrable. Let us consider the case with $\mathbf{p} = (0, 0, 1)$ and $\mathbf{k} = (0, 0, 10)$. This happens because the system has an extra symmetry $[\hat{H}, \hat{S}_z] = 0$.
- **Orthogonal**: If we choose $\mathbf{p}$ and $\mathbf{k}$ such that the system has time-reversal symmetry we will find orthogonal statistics. We can choose[5] for example $\mathbf{p} = (0, 1, 1)$, $\mathbf{k} = (0, 0, 10)$.
- **Unitary**: If we break time-reversal symmetry with the selection of our parameters, we will find unitary statistics. One set of parameters that breaks time-reversal symmetry is for example $\mathbf{p} = (1.1, 1, 1)$, $\mathbf{k} = (4, 0, 10)$.

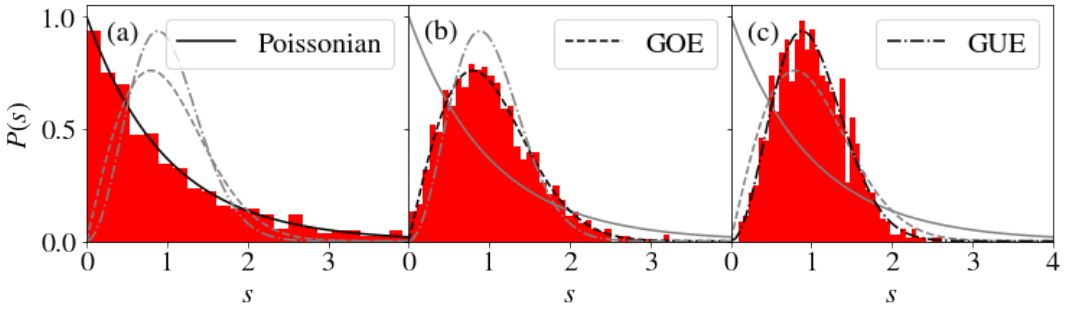

FIGURE 2.8: Level spacing distribution for Kicked Tops with (a) Poissonian, (b) GOE, and (c) GUE nearest neighbors level spacing statistics. The parameters used are those indicated before. The spin of the system is $S = 600$ and only one Floquet operator was considered. Code here.

One should note that obtaining the classical map for the Generalized Kicked Top is much more cumbersome and for that reason, we don't have a classical analog for our quantities.

2.2.2 Lyapunov exponent for the Kicked Top with GUE statistics.

We will be particularly interested throughout this work in the Gaussian Unitary Ensemble, especially in Chapt. 3. For this reason, we want to extend the infinite Temperature Lyapunov exponent obtained for the standard Kicked Top in [81] to the Generalized Kicked Top with GUE statistics. This section is therefore original, indeed from now nearly all the results shown are original. As we already pointed out

[4] Symplectic statistics can also be found under a different selection of the operators in the Floquet operator and for half-integer S. See [84]

[5] In principle the standard Kicked Top with $\mathbf{p} = (0, 1, 0), \mathbf{k} = (0, 0, 10)$ should also show GOE statistics according to [68]. However we do not find this, it shows some degree of level repulsion but does not fit well to the GOE Wigner-Dyson surmise. For this reason and following [84] we will add a free evolution term in the direction of the kick.

any selection of $\mathbf{p}$, $\mathbf{k}$ that breaks time-reversal symmetry will have GUE statistics. To characterize the nearest neighbour level spacing statistics we will use the **Brody parameter** as defined in (1.46). As we did in §2.2.1 we will consider $k_y = 0$ and $p_y = 1$ all the time for simplicity. Then the two parameters that tune chaoticity in our system are k_x, k_z. We have two main ways of breaking down time-reversal symmetry for the GUKT. If we consider $p_x \neq p_z$ the symmetry is broken for any $k_x, k_z > 0$. However if we consider $p_x = p_z$ the symmetry will be broken any time we have $k_x, k_z > 0$ and $k_x \neq k_z$. The way in which we will compute the Lyapunov exponent is with the same OTOC as (2.35). The results obtained for the Lyapunov are plotted in Fig. 2.9. We see that, as we expected, the case with $p_x = p_z$ shows time reversal symmetry, i.e. GOE statistics for $k_x = k_z$. The behavior is in some way similar to the standard Kicked Top in the sense that for small k_j/p_j the system is integrable and as we increase these parameters we get into the chaotic regime. Actually, the limit $k_x = 0$ in Fig. 2.9 (b) is qualitatively similar to Fig. 2.7.

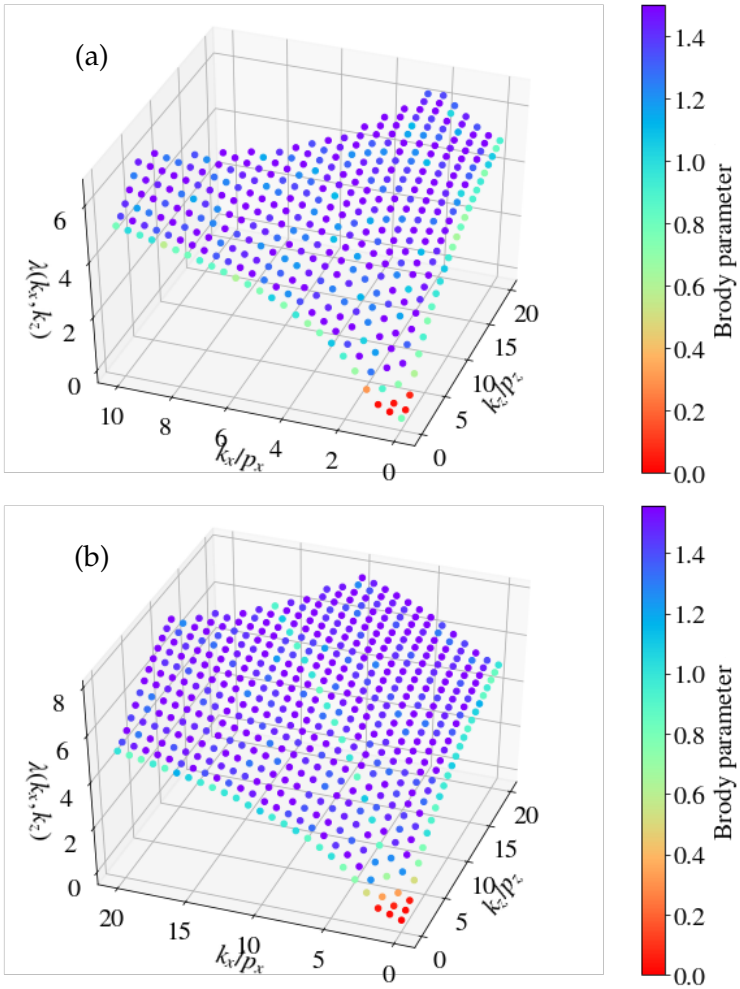

FIGURE 2.9: Infinite temperature Quantum Lyapunov exponent for the GUKT with (a) $p_x \neq p_z$, (b) $p_x = p_z$. A purple color indicates GUE spacing statistics $\tilde{p} \sim 1.55$, a green or blue color indicates GOE statistics $\tilde{p} \sim 1$ and a red color Poissonian statistics $\tilde{p} \sim 0$. In (a) the point at $k_x = k_z = 0$ has a $\mathcal{P}(s)$ with many spikes and for this reason the fit to the Brody parameter gives $\tilde{p} \sim 1$ but it does not have GOE level spacing statistics. Code here.

2.3 Quantum Speed Limits in the Kicked Top

An analogous derivation to the one done for Margolus-Levitin bound holds, we begin by expanding the initial state in the Floquet eigenbasis $\hat{\mathcal{U}} |\chi_n\rangle = e^{-i\epsilon_n} |\chi_n\rangle$, we have

$$|\psi_0\rangle = \sum_m c_m |\chi_m\rangle , \tag{2.39}$$

then the state at time $t = n\tau_p$ is

$$|\psi_t\rangle = \sum_m c_m e^{-i\epsilon_m n} |\chi_m\rangle . \tag{2.40}$$

The overlap between states is just

$$S(t) = \langle\psi_0|\psi_t\rangle = \sum_m |c_m|^2 e^{-i\epsilon_m n}, \tag{2.41}$$

therefore the real part of $S(t)$ is just

$$\mathrm{Re}(S(t)) = \sum_m |c_m|^2 \cos(\epsilon_m n) \geq \sum_m |c_m|^2 \left(1 - \frac{2}{\pi}\left(\epsilon_m n + \sin(\epsilon_m n)\right)\right). \tag{2.42}$$

Then the time evolved state and the initial state to be orthogonal we find

$$0 \geq 1 - \frac{2}{\pi} \langle\epsilon\rangle n, \tag{2.43}$$

where $\langle\epsilon\rangle = \sum_m |c_m|^2 \epsilon_m$, so we find a completely analogous expression for Floquet systems

$$n \geq n_{\mathrm{QSL}} := \frac{\pi}{2\langle\epsilon\rangle}. \tag{2.44}$$

The qualitative difference is that now the QSL gives a minimum number of periods in which one can reach an orthogonal state and the average is taken with respect to the pseudo energy eigenbasis instead of the energy one. The derivation given for the Mandelstam-Tamm bound relies on an integration that cannot be performed in the same way since our system has an intrinsically discrete time. However, based on our Margolus-Levitin argument, we can argue that the roles of energies and pseudo-energies are analogous. For this reason, we will consider the general QSL for any Floquet system to be

$$n_{\mathrm{QSL}} := \mathcal{L}(\rho_0, \rho_t) \max\left(\frac{1}{\Delta\epsilon}, \frac{1}{\langle\epsilon\rangle - \epsilon_0}\right), \tag{2.45}$$

where again the standard deviation of the pseudo-energy is taken with respect to the Floquet eigenbasis $\Delta\epsilon = \sqrt{\sum_m |c_m|^2 \epsilon_m^2 - \left(\sum_m |c_m|^2 \epsilon_m\right)^2}$. Furthermore to extend the bound on the Fidelity (1.102) we will consider the discrete difference instead of the time derivative $\dot{F}(t) \to \Delta F_n/\tau_p = (F_{n+1} - F_n)/\tau_p$. So the analogous expression to (1.102) should be

$$\frac{|\Delta F_n|}{\tau_p} \leq \frac{1 - F_n}{n_{\mathrm{QSL}}}. \tag{2.46}$$

Considering our initial state to be a coherent SU(2) state we find the plots in Fig.

2.10. We see that the difference in the fidelity for the chaotic phase is only big in the first period. For any other time, this difference is very small. While in the regular regime the difference in fidelity shows more structure and more features. We see that the QSL obtained is respected although it is not very tight since the difference in fidelity can never be bigger than 1, considering $\tau_p = 1$. So, even though it is respected it does not give really meaningful information. This may not be the case when considering other states so one could study if there are some states in which the QSL for Floquet systems is meaningful.

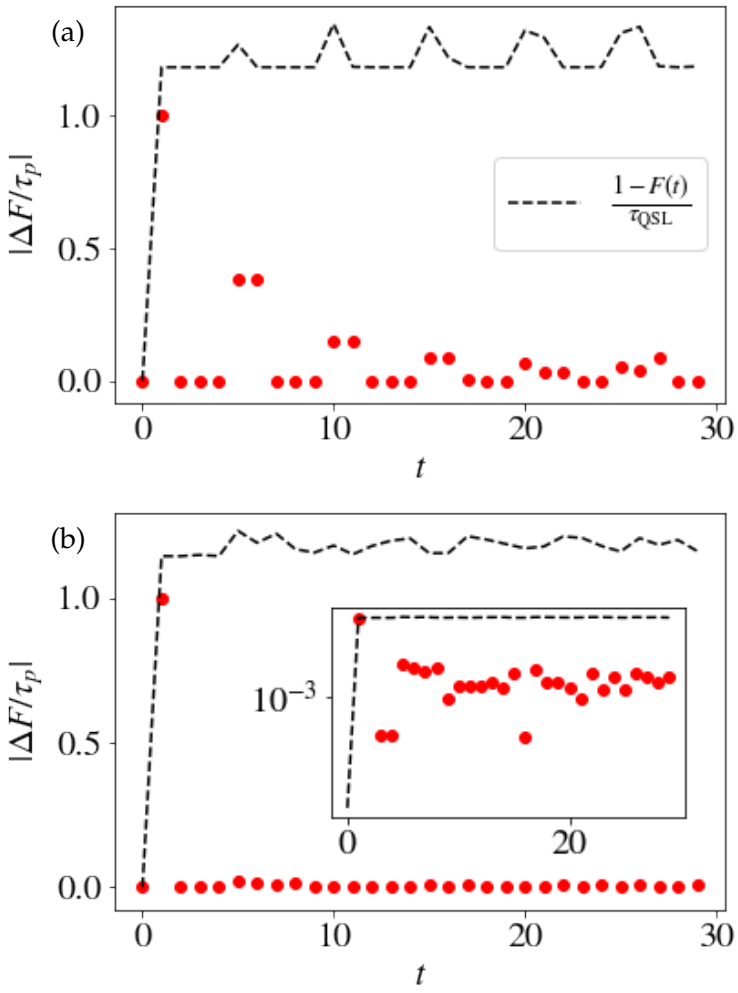

FIGURE 2.10: Quantum Speed Limits on the fidelity $F(n\tau_p) = |\langle\theta,\phi|\hat{\mathcal{U}}^n|\theta,\phi\rangle|^2$ for the Kicked Top. The red dots show the LHS of (2.46) while the dashed black line shows the RHS. In (a) the Kicked Top is in the Regular phase with $p = \frac{\pi}{2}$, $k = 1$ and in (b) it is on the chaotic phase $p = \frac{\pi}{2}$, $k = 6$. The inset of (b) shows the same plot in logartihmic scale since the difference in fidelity is very close to zero for all the times. Both plots have $S = 200$. Code here.

2.4 Spectral Form Factor for Kicked Tops

For Floquet systems [13, 85–87] we can define a (pseudo) Spectral Form Factor at inverse temperature β and time t as

$$g_{k_x,k_z}(\beta,t) := \sum_{m,n} e^{-(\beta+it)\epsilon_n} e^{-(\beta-it)\epsilon_m}, \tag{2.47}$$

where the pseudo-energies ϵ_m have been obtained for the parameters k_x, k_z. Note that now we are not restricting t to be an integer multiple of τ_p. The short-time behavior of this quantity is well behaved, however, the long-time has huge fluctuations. To deal with these we can introduce an averaged SFF over a certain window of parameters, e.g. $(k_z, k_z + \delta k_z)$ as

$$\langle g(\beta,t)\rangle = \frac{1}{N_{av}} \sum_{\kappa\in(k_z,k_z+\delta k_z)} g_{k_x,\kappa}(\beta,t), \tag{2.48}$$

where the values of κ are taken randomly from a uniform distribution. We plot the behavior of this SFF in Fig. 2.11. We see clearly that when we have integrability the SFF initially decays and then saturates to a constant, however when we have quantum chaos we observe the ramp, as the expected signature of chaos. We can also see that the effect of the temperature is to smooth out the initial oscillations in $g(\beta,t)$ and make the ramp shorter. Also, the ramp is shorter in the GOE as compared to the GUE. This happens because the correlations between eigenvalues are more important in the Unitary ensemble and therefore the connected part of the spectral form factor is more important.

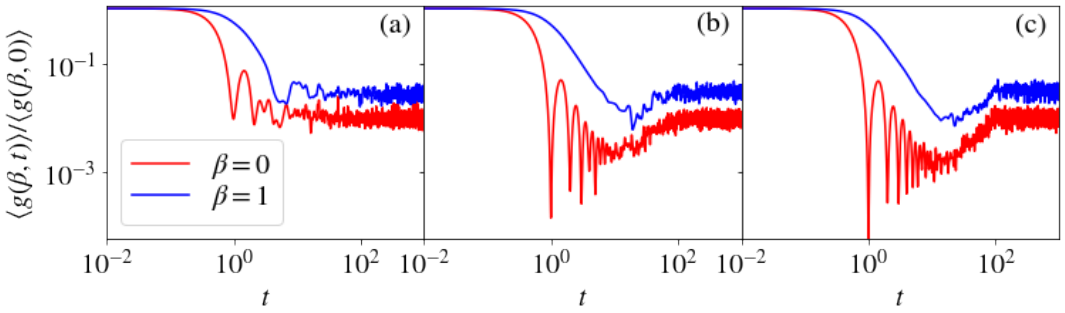

FIGURE 2.11: Averaged Spectral Form Factor for the Generalized Kicked Top with (a) Poissonian level spacing statistics $\mathbf{p} = (0,0,1)$, $\mathbf{k} = (0,0,10)$, (b) GOE level spacing statistics $\mathbf{p} = (0,1,1)$, $\mathbf{k} = (0,0,10)$ and (c) GUE level spacing statistics $\mathbf{p} = (2,1,1)$, $\mathbf{k} = (4,0,10)$. All of the spectral Form Factors are plotted for $\beta = 0$ and $\beta = 1$ computed for $S = 50$ averaging over $N_{av} = 50$ realizations and a window $\delta k_z = 0.1 k_z$. Code here.

Chapter 3

Random Matrix Analysis

Random Matrix Theory was already introduced in §1.3 where we highlighted some of the basic features of it, serving as a playground for many studies on quantum chaos. Some of the features we are interested in studying were not easily studied in the context of the Kicked Top, for this reason we decided to switch to RMT and develop most of our original work in this framework. The work done in this framework is presented in this chapter. First, we study some of the features of the Spectral Form Factor, which is particularly suitable in this framework because there are exact analytical expressions for it [28]. The features of the SFF studied include: The role that different neighbors in energy play in the SFF §3.1.2, an analytical expression for the contribution of nearest neighbors to the SFF §3.1.2 and a surprising result on the initial decay of the SFF, namely, that the exponent saturates Maldacena's bound on chaos §3.2. After this, we study Quantum Speed Limits in the context of Random Matrix Theory §3.3. And we end the chapter by comparing QSL's with Maldacena's bound on chaos §3.5.

3.1 Spectral Form Factor for the GUE

In this chapter some of the features shown by Random Matrix Ensembles will be studied in more detail, the ensemble in which we will focus mainly is the Gaussian Unitary Ensemble (GUE). This is so because analytical expressions can be found for this ensemble [28, 63]. In fact these analytical results are exact in the sense that they do not rely on approximate expressions like Wigner's semicircle law, which would only be valid for large N. This non-perturbative approach is based rather on the exact expression for correlation functions for the GUE [51]. Details on this approach and the derivation of the exact results can be found in App. C. The Spectral Form Factor in the context of Random Matrix Theory may be split into three contributions

$$g(\beta,t) = \langle Z(\beta+it)Z(\beta-it)\rangle = \langle Z(2\beta)\rangle + |\langle Z(\beta+it)\rangle|^2 + g_c(\beta,t), \tag{3.1}$$

which are, respectively, the constant, the disconnected and the connected part, the latter is found as the double complex Fourier transform of the connected correlation function

$$g_c(\beta,t) = \int \mathrm{d}E\mathrm{d}E' \, \langle \rho_c^{(2)}(E,E')\rangle \, e^{-(\beta+it)E-(\beta-it)E'}, \tag{3.2}$$

where $\langle \rho_c^{(2)}(E,E')\rangle = \langle \rho(E)\rho(E')\rangle - \langle \rho(E)\rangle \langle \rho(E')\rangle$ is the connected 2-level correlation function. This quantity measures the correlation between two different energy levels.

For the GUE the density of states for any finite N is given by [51]

$$\langle \rho(E) \rangle = \sum_{j=0}^{N-1} \varphi_j^2(E), \tag{3.3}$$

where $\varphi_j(E) = e^{-E^2/2}\mathcal{H}_j(E)/\sqrt{2^j j!\sqrt{\pi}}$ are the Harmonic Oscillator wavefunctions and $\mathcal{H}_j(E)$ are the Hermite polynomials. The connected 2-level correlation function then is given by [51]

$$\langle \rho_c^{(2)}(E, E') \rangle = -\left(\sum_{j=0}^{N-1} \varphi_j(E)\varphi_j(E') \right)^2. \tag{3.4}$$

Based on these two expressions one can obtain an expression for the average analytically continued partition function [63]

$$\langle Z(\sigma) \rangle = \left\langle \mathrm{Tr}(e^{-\sigma \hat{H}}) \right\rangle_{\hat{H} \in \mathrm{GUE}} = e^{\sigma^2/4} L_{N-1}^1 \left(-\frac{\sigma^2}{2} \right), \tag{3.5}$$

where $\sigma = \beta + it$ and

$$L_n^\alpha(x) = \sum_{j=0}^{n} \binom{n+\alpha}{n-j} \frac{(-x)^j}{j!},$$

is the generalized Laguerre polynomial. The derivation of these results is presented in App. C. This expression opens up the possibility of computing, by simple differentiation, many thermodynamical quantities of the system like $\langle \hat{H} \rangle$ or $\langle \hat{H}^2 \rangle$. For a quantum thermodynamics perspective of these quantities see [28]. There is however one subtlety that needs to be taken care of when taking an average over the ensemble. Imagine that we are interested in computing the average energy

$$\langle \hat{H} \rangle_{\text{n.a.}} = \left\langle \frac{\mathrm{Tr}(\hat{H} e^{-\beta \hat{H}})}{Z(\beta)} \right\rangle. \tag{3.6}$$

Taking the usual statistical mechanics approach, since the partition function is known, the average energy would be given by

$$\langle \hat{H} \rangle = -\frac{1}{Z(\beta)} \frac{\partial Z(\beta)}{\partial \beta}, \tag{3.7}$$

however, since the known quantity is $\langle Z(\beta) \rangle$ we are really computing

$$\langle \hat{H} \rangle_{\text{a}} = -\frac{1}{\langle Z(\beta) \rangle} \frac{\partial \langle Z(\beta) \rangle}{\partial \beta} = \frac{\langle \mathrm{Tr}(\hat{H} e^{-\beta \hat{H}}) \rangle}{\langle Z(\beta) \rangle}, \tag{3.8}$$

which is not always equal to (3.6). The two quantities are approximately equal and the agreement is best for small values of β. The first quantity (3.6) is called the **non-annealed** version and (3.8) is called the **annealed** version. Analytically one can only access the annealed quantities, which is something to keep in mind.

Since the average analytically continued partition function is known the two first

terms in (3.1) can already be computed without any problems, all that is left to compute is the connected SFF, which is [28]

$$g_c(\sigma) = -e^{(\sigma^2+\sigma^{*2})/4} \sum_{n,m=0}^{N-1} \frac{\min(m,n)!}{\max(m,n)!} \left(\frac{|\sigma|^2}{2}\right)^{|n-m|} \left| L^{|n-m|}_{\min(m,n)}\left(-\frac{\sigma^2}{2}\right)\right|^2. \tag{3.9}$$

At infinite temperature and initial time $\sigma = 0$ the only non-zero terms of the sum have $m = n$. Those terms have $|n-m| = 0$ and therefore the Laguerre polynomials are the standard ones that obey $L_m(0) = 1$. Therefore, $g_c(0) = -N$ which cancels out the constant term thus giving $g(0,0) = N^2$. The behavior of these terms can be seen in Fig. 1.1. From there, it is clearly seen that the initial decay of the SFF is governed by the second term, i.e. the *disconnected* part. The connected term is canceling out the constant term for short times. After the initial decay the connected term grows, thus giving rise to the ramp, and eventually it reaches zero leaving only the plateau of the SFF. The details of this derivation clearly point out that the correlations between eigenvalues, encoded in $\langle \rho_c^{(2)}(E,E')\rangle$, are generating the ramp of the SFF. And as was clearly seen in Fig. 2.11 if our system is integrable, these correlations are not present, therefore leaving us with no ramp.

3.1.1 Connection between the OTOC and the Spectral Form Factor

For any two operators $\hat{A}(t)$, $\hat{B}(0)$ the OTOC can be defined as in Def. 6. If the eigenbasis of the Hamiltonian is known $\{|n\rangle\}$ the operators $\hat{A}(t)$, $\hat{B}(0)$ may be chosen as

$$\hat{A}_{nm}(t) = e^{-i(E_n-E_m)t}\,|n\rangle\langle m| = e^{-iE_{nm}t}\,|n\rangle\langle m|\,, \quad \hat{B}_{nm}(0) = |m\rangle\langle n|\,, \tag{3.10}$$

the OTOC arising from them $\tilde{C}_{nm}(t)$ has a particularly nice expression

$$\begin{aligned}\tilde{C}_{nm}(t) &= \frac{\mathrm{Tr}(e^{-\frac{\beta\hat{H}}{4}}|m\rangle\langle n|e^{-\frac{\beta\hat{H}}{4}}e^{-iE_{nm}t}|n\rangle\langle m|e^{-\frac{\beta\hat{H}}{4}}|m\rangle\langle n|e^{-\frac{\beta\hat{H}}{4}}e^{-iE_{nm}t}|n\rangle\langle m|)}{Z(\beta)},\\ &= \frac{1}{Z(\beta)}e^{-\frac{\beta}{2}(E_m+E_n)}e^{-i2(E_n-E_m)t}.\end{aligned} \tag{3.11}$$

This correlator depends both on n and m, for this reason, a sum over the two variables is introduced

$$\tilde{C}(t) = \sum_{n,m}\tilde{C}_{nm}(t) = \frac{1}{Z(\beta)}\sum_{n,m}e^{-(\frac{\beta}{2}+2it)E_n}e^{-(\frac{\beta}{2}+2it)E_m} = \frac{g(\frac{\beta}{2},2t)}{Z(\beta)}. \tag{3.12}$$

Following this argument, in principle, the Spectral Form Factor can be understood as a particular OTOC under a suitable selection of operators. There is, however, one subtlety Def. 6 is valid for Hermitian operators, and the selection in (3.10) is not Hermitian.

3.1.2 Computing the Spectral Form Factor from the Level Spacing statistics

As was already pointed out in §1.3.2 the Spectral Form Factor accounts for all correlations in the system, long and short range[1]. This fact can be better understood rewriting the SFF as

$$g(\beta,t)=\sum_{n,m}e^{it(E_n-E_m)}e^{-\beta(E_n+E_m)}, \tag{3.13}$$

where all possible correlations, E_n-E_m enter the sum. In this section we want to study the role of this correlations, in particular, how much of the chaotic behaviour can be seen in the SFF only taking into account nearest-neighbor level correlations. To study this, we introduce the Fidelity of the Coherent Thermal State[2] $|\psi_\beta\rangle=Z^{-1/2}\sum_n e^{-\beta E_n/2}|n\rangle$ as

$$F_\beta(t)=|\langle\psi_\beta|\hat{\mathcal{U}}_t|\psi_\beta\rangle|^2=\left|\frac{Z(\beta+it)}{Z(\beta)}\right|^2. \tag{3.14}$$

This fidelity may be rewritten as

$$F_\beta(t)=\frac{1}{Z^2(\beta)}\left(Z(2\beta)+\sum_n\sum_{m\neq n}e^{it(E_n-E_m)}e^{-\beta(E_n+E_m)}\right), \tag{3.15}$$

where the first term is time-independent since it accounts for the contribution $n=m$, it is also equal to the long time limit where there is no influence of any neighbor. The **k-th level spacing** $s_n^{(k)}$ can be defined as

$$s_n^{(k)}=E_{n+k}-E_n. \tag{3.16}$$

Introducing $s_n^{(k)}$ in (3.15) we find

$$F_\beta(t)=\frac{1}{Z^2(\beta)}\left(Z(2\beta)+\sum_{k=1}^{N-1}\sum_{n=0}^{N-k}(e^{its_n^{(k)}}e^{-\beta(2E_n+s_n^{(k)})}+e^{-its_n^{(k)}}e^{-\beta(2E_n+s_n^{(k)})})\right), \tag{3.17}$$

$$=\frac{1}{Z^2(\beta)}\left(Z(2\beta)+2\sum_{k=1}^{N-1}\sum_{n=0}^{N-k}\cos(s_n^{(k)}t)e^{-\beta(2E_n+s_n^{(k)})}\right), \tag{3.18}$$

$$=\frac{1}{Z^2(\beta)}\left(Z(2\beta)+\sum_{k=1}^{N-1}F_\beta^{(k)}(t)\right), \tag{3.19}$$

where we have introduced the k-th contribution to the fidelity

$$F_\beta^{(k)}(t)=2\sum_{n=0}^{N-k}\cos(s_n^{(k)}t)e^{-\beta(2E_n+s_n^{(k)})}. \tag{3.20}$$

[1] Here by short range we mean correlations between neighboring levels and by long range correlations between levels very far apart in the spectrum.

[2] When working with this fidelity the annealed version of $F_\beta(t)$ shows a problem. $\langle|Z(\beta+it)|^2\rangle\,/\,\langle Z^2(\beta)\rangle$ is larger than 1 at $t=0$ for $\beta>0$, because the connected term does not fully cancel $\langle Z(2\beta)\rangle$, this causes its interpretation as a fidelity harder. For this reason we will stick, whenever possible, to the non-annealed version of $F_\beta(t)$.

Fig. 3.1 shows the role of the correlations between k-th neighbours in the Spectral Form Factor obtained numerically. Fig. 3.1 (a) suggests that the contributions for bigger k, i.e. furthest apart neighbors, have a minimum in $F^{(k)}(t)$ at shorter times, and shows more oscillations. It is reasonable that the dip time is smaller since the energy difference $s_n^{(k)}$ is larger which implies that the time to explore all $\mathscr{H}$ is smaller. Moreover, the contribution to the fidelity at very short times is bigger the closer the neighbors are. Fig. 3.1 (b) points out that as the temperature is lowered, i.e., β is increased, the contributions of large k vanish, this happens because the factor $e^{-\beta s_n^{(k)}}$ gets smaller as we increase k, i.e. the contribution of the k-th neighbor in the thermal mixture decreases with the range k. This also explains why the dip time increases as we increase β, the relevant contributions are those with smaller k, which have a minimum later. From this plot, we can also see that the bigger the value of β, the better the approximation only considering nearest neighbors $F^{(1)}(t)$. This is reasonable since as we lower the temperature of the system, the levels correlate only with their closest neighbors.

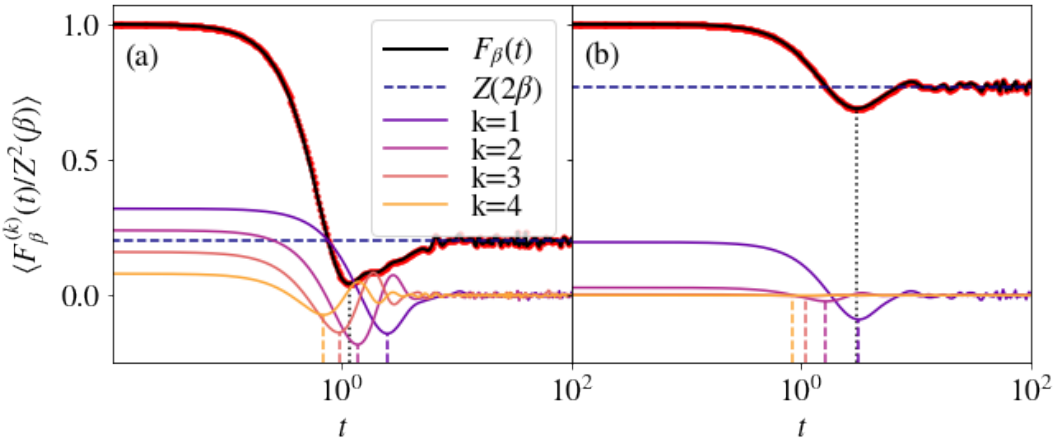

FIGURE 3.1: Contributions to the (non-annealed) Fidelity $F_\beta(t)$ from different neighbor distances k for (a) $\beta = 0$ and (b) $\beta = 2$. The dimension of the Hilbert space is $N = 5$ to distinguish better each contribution. The red circles represent the Fidelity computed numerically. The dashed lines represent the dip time of each $F_\beta^{(k)}(t)$ while the dotted line represents the dip time of $F_\beta(t)$. The results were averaged over $N_{\text{av}} = 300$ realizations. Code here.

The distribution of nearest-neighbor level spacing in RMT $s_n^{(1)} = s$ is well-known, recall §1.3.2. The k-th neighbors level spacing distributions ($k > 1$) are nonetheless, much more cumbersome [51, 88, 89] and do not have, to the best of our knowledge, closed expressions like (1.44) and (1.45). For this reason we are particularly interested in studying how much of the chaotic features of the Spectral Form Factor arise from $F^{(1)}(t)$. Since the level spacing distribution is universal, i.e. it does not depend on the eigenvalue E_n, we can take $s_n^{(1)} \to s$. Neglecting the correlations further from nearest neighbors in the large N limit, the sum may be reexpressed as an integral

over the density of states, which yields

$$\begin{aligned}\langle F_t^{(1)}\rangle &= \frac{1}{\langle Z^2(\beta)\rangle}\left(\langle Z(2\beta)\rangle + F_\beta^{(1)}(t)\right)\\ &= \frac{1}{\langle Z^2(\beta)\rangle}\left(\langle Z(2\beta)\rangle + 2\int dE\rho(E)e^{-2\beta E}\int ds\mathcal{P}(s)\cos(st)e^{-\beta s}\right)\\ &= \frac{\langle Z(2\beta)\rangle}{\langle Z^2(\beta)\rangle}\left(1+2\int ds\mathcal{P}(s)\cos(st)e^{-\beta s}\right). \end{aligned} \tag{3.21}$$

The second term in the brackets is independent of $Z(\beta)$ and therefore, since the spacing distribution is universal, it is also universal. We denote the integral as $R(\beta,t)$ and using $\mathcal{P}(s)$ for the GUE (1.45) we find that[3]

$$R(\beta,t) = 2\int_0^\infty ds\cos(st)e^{-\beta s}\mathcal{P}(s) \tag{3.22}$$

$$= -\beta + \frac{e^{-\pi t(2i\beta+t)/16}}{8}\left(e^{\beta^2\pi/16}(8+\pi(\beta-it)^2)\mathrm{erfc}\left(\frac{\sqrt{\pi}(\beta-it)}{4}\right)\right. \tag{3.23}$$

$$\left. + e^{\beta\pi(\beta+4it)/16}(8+\pi(\beta+it)^2)\mathrm{erfc}\left(\frac{\sqrt{\pi}(\beta+it)}{4}\right)\right),$$

where $\mathrm{erfc}(z)$ is the complementary error function

$$\mathrm{erfc}(z) = 1-\mathrm{erf}(z) = 1-\frac{2}{\sqrt{\pi}}\int_0^z e^{-t^2}dt. \tag{3.24}$$

Expression (3.23) may allow us to find an analytical expression for the dip time of $F_\beta^{(1)}(t)$ but one should first simplify it further.

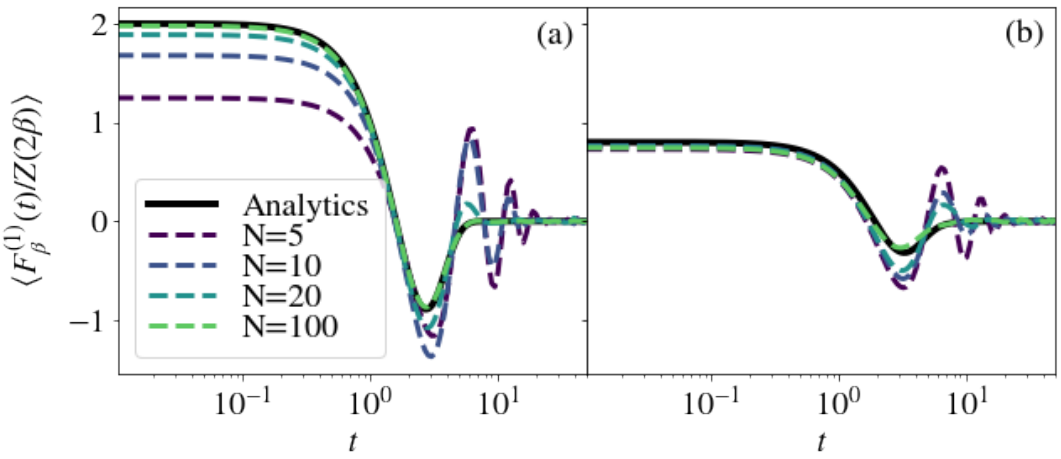

FIGURE 3.2: Comparison between the analytic expression for the nearest neighbor contribution to the SFF and the (unfolded, non-annealed) numerical results $\left\langle F_\beta^{(1)}(t)/Z(2\beta)\right\rangle$ in the GUE obtained for different system sizes at (a) $\beta = 0$ and (b) $\beta = 1$. All of the results were averaged over $N_{\mathrm{av}} = 1000$ realizations. Code here.

[3] Code here.

In Fig. 3.2 the numerical value of $F_\beta^{(1)}(t)/Z(2\beta)$ is compared to the analytical results for different dimensions of the matrices. The behavior with N is studied to check if the continuum description works nicely and if so, how big does the dimension of $\mathscr{H}$ should be. The plot shows that as we increase N we get closer and closer to the analytical formula and the oscillations seen for small N vanish, leaving us with only one dip and a plateau. For $N = 100$ the fit to the analytical expression is very good[4]. To obtain agreement between the numerics and the analytics the spectrum needs to be unfolded. This is needed because, otherwise, the step $s_n^{(1)} \to s$ is not justified since s_n depends on the Local Density of States. Comparing Fig. 3.2 (a) and (b) we see that for finite temperature the results at the beginning match the analytics, regardless of the dimension of the matrices. However, at later times the results diverge and we see some oscillations at small N that we do not see in the analytics or for larger values of N.

In conclusion, we can use the contribution to the SFF from the nearest-neighbors in energy only, $F_\beta^{(1)}(t)$, as a signature for quantum chaotic behaviour in the SFF, i.e. the ramp. However, the dip time obtained from it will overestimate the real value, because the longer-range correlations, $F_\beta^{(k)}(t)$ for $k > 1$, have a dip time before $F_\beta^{(1)}(t)$. Nonetheless, at low temperatures, the nearest-neighbor correlation accounts for the majority of the ramp in the SFF, thus giving a reliable estimate for the dip time. An analytical expression for the nearest-neighbor contribution to the SFF can be found (3.23) and the unfolded numerics show a good agreement to it at large N.

3.2 Decay of the Spectral Form Factor for the GUE

3.2.1 Relation with Maldacena's bound

For short times, the SFF is known to decay with a Gaussian shape, as Ne^{-t^2}. For an intermediate time, the envelope is a power law. We look at how well it can be fit to a decaying exponential $\sim e^{-\eta t}$ at intermediate times, that is, after the initial Gaussian decay and before the first dip. A fitting procedure for the survival probability $\tilde{g}(\beta/2, 2t) \equiv F_{\beta/2}(2t) = \frac{g(\beta/2,2t)}{Z^2(\beta)}$ is developed following:

1. We choose a beginning point t_0 and a final point t_f. These are chosen as the first inflection points of $\tilde{g}$ and $\ln \tilde{g}$ respectively, and define a fitting window.

2. Within this window, we look if the function is best fit by a Gaussian or by a decaying exponential. In the range we will fit, we take a considerable number of points to start the fit, e.g. $N_{\text{fits}} = 50$. Let's assume one of them is located at time $\tilde{t}$, then we fit the window

$$\left(\tilde{g}(\frac{\beta}{2}, 2\tilde{t}) - \alpha|\tilde{g}(\frac{\beta}{2}, 2\tilde{t}) - \min(\tilde{g}(\frac{\beta}{2}, 2t)|, \tilde{g}(\frac{\beta}{2}, 2\tilde{t}) + \alpha|\tilde{g}(\frac{\beta}{2}, 2\tilde{t}) - \min(\tilde{g}(\frac{\beta}{2}, 2t)|\right),$$

   where $\alpha < 1$ is some parameter that determines how wide our window is.

[4] Although we did not show it in the same plot the agreement for $N = 50$ is already pretty good with the exception of some small oscillations at $\beta = 1$.

3. Within that range, we then take only[5] the values of η fitted for which $\ln \tilde{g}$ better fits a linear function $-\eta t + b$ than a quadratic function $-at^2 + b'$.

Averaging over all values fulfilling the above conditions, we find the fit shown in Fig. 3.3.

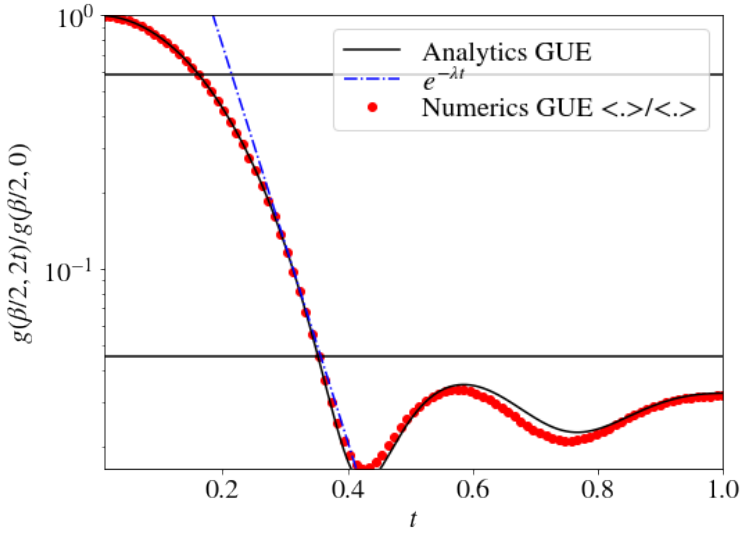

FIGURE 3.3: Fitting strategy of $\tilde{g}(\beta/2, 2t)$ for the GUE. The plot is done for $\beta = 0.1$ and $N = 10$. Code here.

This procedure can be repeated for various temperatures and the decay exponent η can be plotted as a function of β. For the GUE, Fig. 3.4 is obtained. This figure shows that the values of η are bounded and get very close to Maldacena's bound on the Lyapunov exponent $\lambda \leq \frac{2\pi}{\beta}$.

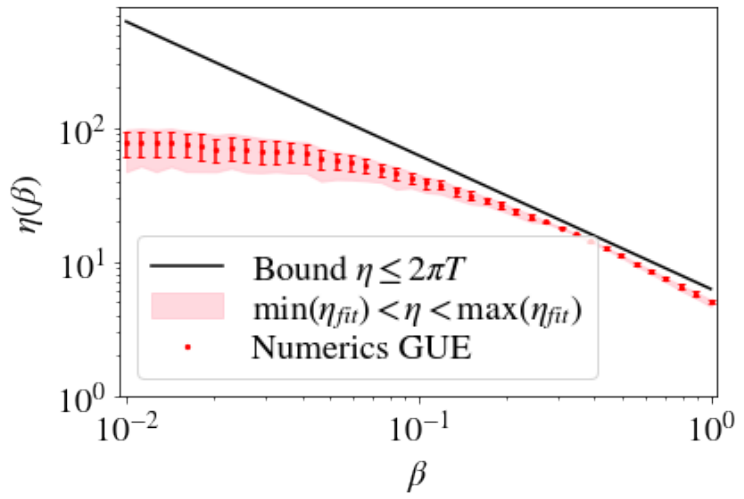

FIGURE 3.4: η exponent as a function of β for GUE with $N = 30$. Code here.

[5]Since the quadratic fit can also be a straight line if the center of the parabola is very far from the fitted region we will also take the values of η for which the errors in the fits are smaller than some very small cutoff.

If a similar fitting procedure is applied to $g(\beta,t)$ the exponent does not get close to that bound at all. It gets close to the bound $\eta \leq \frac{\pi}{2\beta}$ instead, and the same features can be seen for this alternative bound. Also extending the plot to larger values of β the exponent gets further away from the bound. The bound for $g(\beta,t)$ is obtained just by observing that the quantity

$$g\left(\frac{\beta}{2},2t\right) = \sum_{m,n} e^{-(\frac{\beta}{2}+2it)E_n} e^{-(\frac{\beta}{2}-2it)E_m}, \tag{3.25}$$

is analytic on the stripe $-\frac{\beta}{4} \leq \tau \leq \frac{\beta}{4}$ as the regularized OTOC in Maldacena's argument. While the usual spectral form factor

$$g(\beta,t) = \sum_{m,n} e^{-(\beta+it)E_n} e^{-(\beta-it)E_m}, \tag{3.26}$$

is analytic on $-\beta \leq \tau \leq \beta$. Therefore, one can easily extend Maldacena's bound to quantities analytic on the stripe $-\frac{\beta}{a} \leq \tau \leq \frac{\beta}{a}$ obtaining $\lambda \leq \frac{a\pi}{2\beta}$ which for $a = 1$ gives the bound on the standard SFF $\eta \leq \frac{\pi}{2\beta}$. From here on we will use both bounds since the difference only comes from a proportionality factor. This also implies that our results do not rely on the relation between the OTOC and the SFF derived in §3.1.1 so even if the argument used there fails, our results don't. After obtaining these results, several questions arise:

- Why are we saturating Maldacena's bound if our fitting funtion is $e^{-\eta t}$ instead of the $1 - e^{\lambda t}$ as the OTOC's behave in the Lyapunov regime?

  We tried fitting to a function of the form $1 - e^{\lambda t}$ but our data did not fit well to that function. This is related to the fact that Random Matrices do not show a Lyapunov regime as we discuss in §3.4. A possible answer to the question why does $e^{-\eta t}$ work in Maldacena's inequality (1.24) giving $\eta \leq \frac{2\pi}{\beta}$ is presented in §3.2.3.

- How much evidence do we have to introduce the fit to a decaying exponential $e^{-\eta t}$? Are we "forcing" the behavior we want to see on the quantity? This question is discussed in §3.2.2.

- Does this behavior have anything to do with chaos? We know that Maldacena's bound is related to how fast Quantum Chaos can develop, but we do not know if this is the case for our results. In fact chaos is not seen in the slope of the SFF but rather on the ramp, so is the observed phenomenon a signature of chaos?. This question is answered in §3.2.4 by observing some similar behavior in Quantum Kicked Tops. The cnclusion we draw from this section is that it is not related to chaos, so any system, regardless whether it is integrable or chaotic, can show a saturation of Maldacena's bound by appropriately choosing the dynamical quantity.

3.2.2 Relation with Bhattacharyya's bound

In [90] K. Bhattacharyya obtained a bound on how fast the decaying exponential regime can be. His arguments are based on the Mandelstam-Tamm Quantum Speed Limit, if there is a decaying exponential regime then it obeys

$$F(t) \geq e^{-2\Delta E t/\hbar}, \tag{3.27}$$

where $F(t) = |\langle\psi_0|\psi_t\rangle|^2$ is the fidelity of some pure state. We know that the Spectral Form Factor can be understood as the fidelity of a Thermo-Field Double state [63] or a Coherent Thermal State

$$g(\beta,t) = Z^2(\beta)|\langle\psi_\beta|\hat{\mathcal{U}}_t|\psi_\beta\rangle|^2 = \sum_{m,n} e^{-\beta(E_n+E_m)}e^{-it(E_n-E_m)}, \tag{3.28}$$

and actually, since the quantity with which we are working is the survival probability $g(\beta,t)/Z^2(\beta)$ it is just the fidelity between Coherent Thermal States

$$F_\beta(t) = |\langle\psi_\beta|\hat{\mathcal{U}}_t|\psi_\beta\rangle|^2 = \left|\frac{Z(\beta+it)}{Z(\beta)}\right|^2, \tag{3.29}$$

so the results obtained by Bhattacharyya directly apply to our approach. Previously to Bhattacharyya, there were already some works in which negative exponentials decays were found [91, 92]. However, these were usually valid for a much longer time window than ours or Bhattacharyya, for this reason, we will stick to his formalism. If we substitute what we found in (3.27) we find that

$$e^{-\eta t} \geq e^{-2\Delta E t/\hbar} \;\Rightarrow\; \eta \leq \frac{2\Delta E}{\hbar}. \tag{3.30}$$

This opens the question, what value of $\hbar$ should we take? Typically we work with $\hbar = 1$ but we see in Fig. 3.5 (solid blue line) that the bound is not respected. On the other side, if instead we take $\hbar$ as an effective $\hbar_{\text{eff}}$, say that we compare it with Kicked Tops which have $\hbar_{\text{eff}} = 1/S$ with the same dimension of $\mathscr{H}$ so we have $N = 2S+1$ and therefore $\hbar_{\text{eff}} = \frac{2}{N-1}$. The results of this are shown in Fig. 3.5 (solid green line).

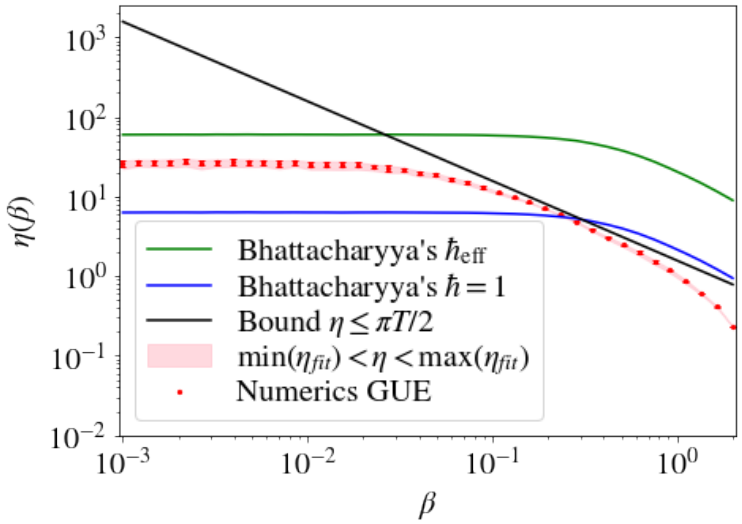

FIGURE 3.5: Decay exponent of the GUE Spectral Form Factor as a function of β. The Bhattacharyya's and Maldacena's bound are shown. In Bhatacharyya's bound $\eta \leq \frac{2\Delta E}{\hbar}$ we set $\hbar = 1$ (blue) and $\hbar_{\text{eff}} = \frac{2}{N-1}$ (green). The dimension of the matrices is $N = 20$. $\Delta E(\beta) = \left\langle \sqrt{\text{Tr}(e^{-\beta\hat{H}}\hat{H}^2) - \text{Tr}(e^{-\beta\hat{H}}\hat{H})^2} \right\rangle$ is computed numerically by averaging over the GUE ensemble. Code here.

We see that the behavior of both bounds is qualitatively similar to the behavior of the exponent in the sense that they saturate to a constant and start decaying in a similar fashion. Of course, this argument on $\hbar_{\text{eff}}$ need not be true and there may be a reason for the results with $\hbar = 1$ to fail. One possible reason for this failure is that Bhattacharyya only considered Mandelstam-Tamm bound, considering the joint Quantum Speed Limit, the results may show a different behavior.

3.2.3 A possible explanation for the saturation of the bound

The first important observation that needs to be made is that $g(\beta/2, 2(t+i\tau))$ is analytic on the same stripe of the complex plane as the OTOC $-\frac{\beta}{4} \leq \tau \leq \frac{\beta}{4}$. Furthermore we know that $F_\beta(t)$ is always smaller than 1. Therefore we can apply Maldacena's mathematical result to the survival probability. If we substitute $f \sim e^{-\eta t}$ directly in (1.24) we do not find the nice inequality $\lambda \leq \frac{2\pi}{\beta}$ but rather

$$\eta \frac{1}{e^{\eta t} - 1} \leq \frac{2\pi}{\beta}. \tag{3.31}$$

A possibility for explaining the apparent behavior $\eta \leq \frac{2\pi}{\beta}$ seen in Fig. 3.4 comes from looking at the independent term of the fit described in §3.2.1 which is approximately equal to the dimension of the Hilbert space N. So the function to which we are fitting is $f(t) = e^N e^{-\eta t}$. Typically we use matrices of at least $N \gtrsim 5$ so the prefactor e^N is large, this allows us to approximate

$$1 - f = 1 - e^N e^{-\eta t} \approx -e^N e^{-\eta t}, \tag{3.32}$$

and we can recover $\eta \leq \frac{2\pi}{\beta}$. In fact in Fig. 3.6 we see how as we increase the dimension of the Random Matrices we get closer to saturating the bound. This could be caused by the dimension N not being big enough so that we cannot make the approximation and therefore $\eta \lesssim \frac{2\pi}{\beta}$. Another observation is that as the system size is increased, η saturates to a constant at higher temperatures.

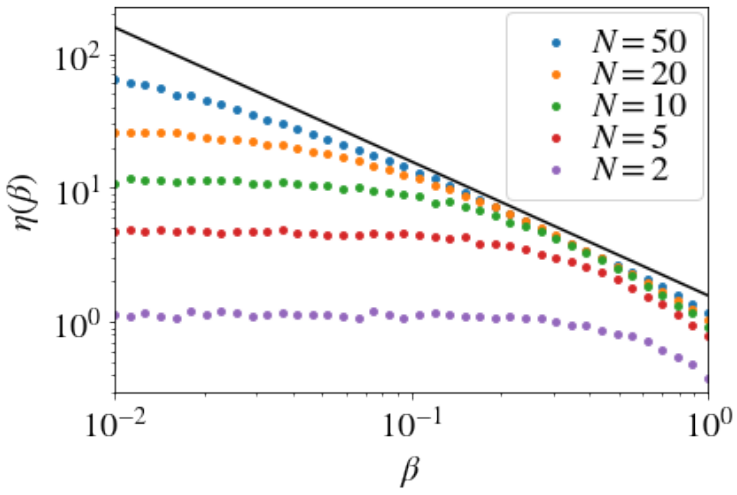

FIGURE 3.6: $\eta(\beta)$ plot for GUE with different dimensions of the Random Matrices. η is obtained from $g(\beta, t)$ and therefore the bound is $\frac{\pi}{2\beta}$. Code here.

3.2.4 Relation with the Kicked Top

This bound, while found for chaotic systems, seems not to be proper to chaotic systems only since the slope of the Spectral Form Factor does not carry information on chaos. Here we extend our study to the Kicked Top, which has the advantage of being tunable between regular and chaotic dynamics. We find that our results hold in all regimes, regardless of the integrability or non-integrability of our system.

If a similar procedure to obtain $\eta(\beta)$ is applied for the Spectral Form Factor defined for the Quantum Kicked Top in §2.4 we find the plot in Fig. 3.7, which has both GUE and Poissonian level spacing statistics. The behavior for both of them is similar to the one seen in Random Matrix Theory, this already points out that our results are not associated with any quantum chaotic feature but rather just with quantum dynamics. This could already be foreseen from the fact that we are fitting the slope of the SFF with essentially the same features for chaotic and regular phases.

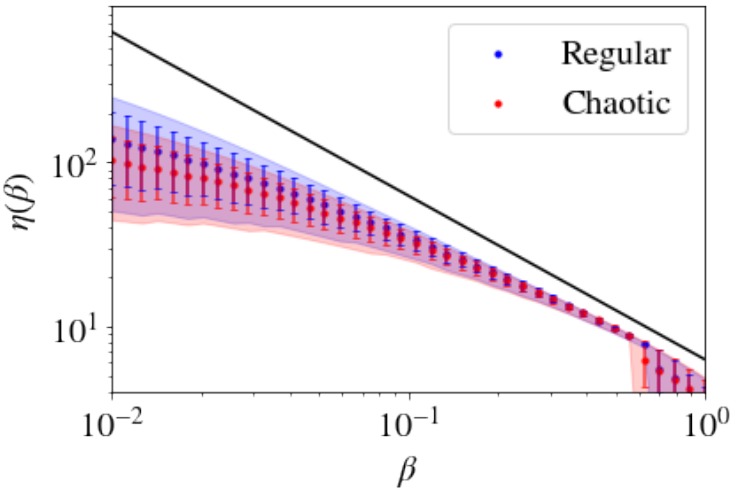

FIGURE 3.7: η exponent as a function of β for a Generalized Kicked Top with GUE statistics (red) and Poissonian statistics (blue). Both plots have $S = 50$. Code here.

To further verify the observation that the behavior seen is not chaotic in nature we compare η with the Lyapunov exponent obtained from the OTOC as in §2.1.5 and §2.2.2. The conclusion from Fig. 3.8 is that the η exponent does not carry any information related to the chaoticity of the system. It is not similar to the Lyapunov exponent and it does not change from the region with Poissonian statistics to the region with GUE statistics. Actually, if we take the η plot at a $\beta \neq 0$ the only difference is that the points fluctuate around a value lower than the one seen in Fig. 3.4. We also tried the same plot for GOE pseudo level spacing statistics or unfolding the pseudo-energies but none of those shows a clearly different behavior between the regular and chaotic phases. This leads us to conclude that η is not related to chaos, what implies that we can saturate Maldacena's bound for integrable systems by applying it to a suitable dynamical quantity.

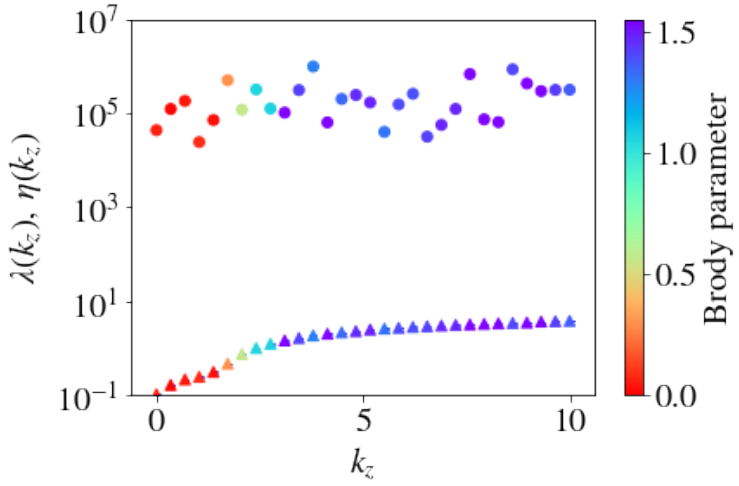

FIGURE 3.8: η (circles) and λ (triangles) as a function of k_z. The color scale represents the Brody parameter $\tilde{p}$ which characterizes the level spacing distribution $\tilde{p} \sim 0$ indicates Poissonian statistics, $\tilde{p} \sim 1$ indicates GOE statistics and $\tilde{p} \sim 1.55$ GUE statistics. Both of them are obtained for $\beta = 0$, $p_z = p_y \neq p_z$, $k_x \neq 0$. Code here.

3.3 Quantum Speed Limits in Random Matrix Theory

In this section, we will study Quantum Speed Limits in the framework of Random Matrix Theory. We introduce them in two very different contexts, we can study them directly on the Spectral Form Factor since as we know, we can understand the SFF as a fidelity between Coherent Thermal States $|\psi_\beta\rangle = Z^{-1/2}(\beta)\sum_n e^{-\beta E_n/2}|n\rangle$ or Thermofield Double States, this approach will be studied in §3.3.1. We can also compute Quantum Speed Limits in quenched dynamics [28], this will be studied in §3.3.2. The results shown in this section show some problems and need to be studied in more care since sometimes the Quantum Speed Limits are violated. For this reason, this section is still a work in progress.

3.3.1 Quantum Speed Limits on the Spectral Form Factor

The Spectral Form Factor physically is represented by the fidelity between Coherent Thermal States. This allows one to directly compute the QSL's on the survival probability. Since an analytical expression for $g(\beta, t)$ is known we can compute the derivative analytically. The three terms of the SFF are

$$F_\beta(t) = \left|\frac{Z(\beta+it)}{Z(\beta)}\right|^2 = \frac{\langle Z(2\beta)\rangle + |\langle Z(\beta+it)\rangle|^2 + g_c(\beta,t)}{\langle Z(\beta)\rangle^2}, \tag{3.33}$$
$$= \mathcal{F}_{\text{const}} + \mathcal{F}_{\text{d}} + \mathcal{F}_{\text{c}},$$

where each of the terms corresponds, respectively, to the constant, disconnected and connected parts of the survival probability. Introducing $\sigma = \beta + it$ the time derivative of the disconnected term is

$$\dot{\mathcal{F}}_{\rm d} = e^{-t^2/2}\frac{L^1_{N-1}(-\frac{\sigma^2}{2})L^1_{N-1}(-\frac{\sigma^{*2}}{2})}{\left(L^1_{N-1}(-\beta^2/2)\right)^2}\left(-t + i\sigma\frac{L^2_{N-2}(-\frac{\sigma^2}{2})}{L^1_{N-1}(-\frac{\sigma^2}{2})} - i\sigma^*\frac{L^2_{N-2}(-\frac{\sigma^{*2}}{2})}{L^1_{N-1}(-\frac{\sigma^{*2}}{2})}\right),$$

and the derivative of the connected term is given by

$$\begin{aligned}\dot{\mathcal{F}}_{\rm c} =& \frac{1}{e^{\beta^2/2}(L^1_{N-1}(-\sigma^2/2))^2}\Bigg(-tg_c \\ &- e^{\frac{\beta^2-t^2}{2}}\sum_{m,n} c_{m,n}|n-m|\left(\frac{\beta^2+t^2}{2}\right)^{|n-m|-1} tL^{|n-m|}_{\min(n,m)}\left(-\frac{\sigma^2}{2}\right)L^{|n-m|}_{\min(n,m)}\left(-\frac{\sigma^{*2}}{2}\right) \\ &- e^{\frac{\beta^2-t^2}{2}}\sum_{m,n=1} c_{m,n}\left(\frac{\beta^2+t^2}{2}\right)^{|n-m|} L^{|n-m|+1}_{\min(n,m)-1}\left(-\frac{\sigma^2}{2}\right) i\sigma L^{|n-m|}_{\min(n,m)}\left(-\frac{\sigma^{*2}}{2}\right) \\ &+ e^{\frac{\beta^2-t^2}{2}}\sum_{m,n=1} c_{m,n}\left(\frac{\beta^2+t^2}{2}\right)^{|n-m|} L^{|n-m|}_{\min(n,m)}\left(-\frac{\sigma^2}{2}\right) i\sigma^* L^{|n-m|+1}_{\min(n,m)-1}\left(-\frac{\sigma^{*2}}{2}\right)\Bigg),\end{aligned}$$

where $c_{m,n} = \min(m,n)!/\max(m,n)!$ and the last two sums start from $m,n = 1$ because $\partial_x L^\alpha_0(x) = 0$.

Fig. 3.9 shows that the numerically computed derivative agrees with the analytical expression until the ramp and the plateau where the numerical results have fluctuations and does not behave exactly as the analytics. From Fig. 3.9 it is also clear that the Quantum Speed Limits are violated, recall that the QSL on the fidelity is

$$|\dot{F}| \leq \frac{1-F}{\tau_{\rm QSL}}. \tag{3.34}$$

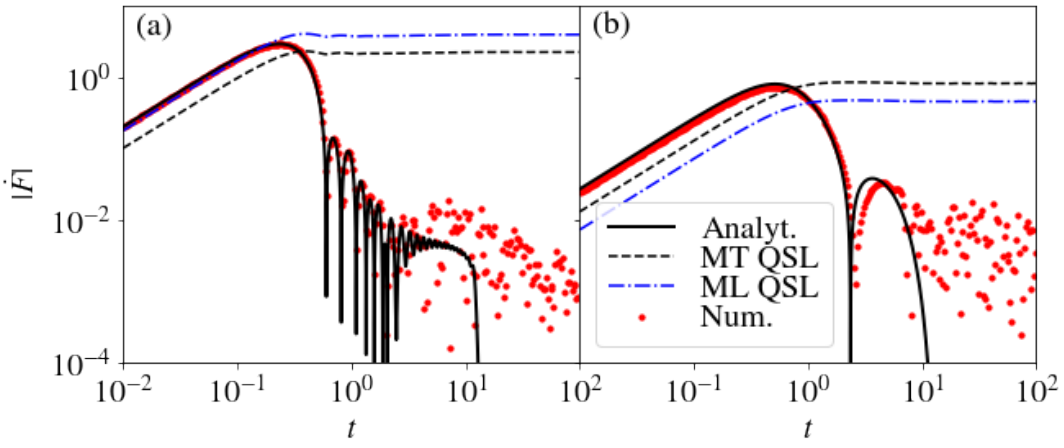

FIGURE 3.9: Quantum Speed Limits on the Fidelity for the Coherent Thermal State (SFF) for the GUE at $\beta = 0$ (a) and $\beta = 1$ (b) . Code here.

We need to use the fidelity computed numerically because F computed analytically shows problems at finite temperature due to annealing. The problem is that $F > 1$ at the beginning because the connected SFF g_c does not fully cancel $\langle Z(2\beta)\rangle$ at finite temperature and therefore $g(\beta,0) > Z^2(\beta)$. For this reason, we compute the non-annealed fidelity.

We see that the SFF computed at infinite temperature Fig. 3.9 (a) violates only the Mandelstam-Tamm bound, however this is the one that applies here since the joint QSL takes the maximum τ_{QSL} therefore the minimum $1/\tau_{\text{QSL}}$. The results at finite temperature Fig. 3.9 (b) violate both bounds. The reason for the violation is not clear yet, so work remains to be done to fix this QSL.

3.3.2 Quantum Speed Limits with quenched dynamics

In this section, QSL's for a quenched protocol are introduced [28]. The main idea is to prepare a thermal state of some Hamiltonian $\hat{H}_0$, evolve the system with the same Hamiltonian $\hat{H}_0$ until time t and evolve it back with a different Hamiltonian $\hat{H}_\tau$, note that we may as well not consider the first evolution since a thermal state will not evolve under the same Hamiltonian that generates it

$$\hat{\rho}_0 = Z^{-1}(\beta)e^{-\beta\hat{H}_0}, \qquad \hat{\rho}_t = Z^{-1}(\beta)e^{i\hat{H}_\tau t}e^{-i\hat{H}_0 t}e^{-\beta\hat{H}_0}e^{i\hat{H}_0 t}e^{-i\hat{H}_\tau t}, \tag{3.35}$$

where both $\hat{H}_0, \hat{H}_\tau$ are taken from the GUE and we average over them. In a sense, this protocol is similar to a Loschmidt echo with the exception that we do not perturb slightly $\hat{H}_0$ to obtain $\hat{H}_\tau$ but rather take both from the GUE. We compute the Uhlmann Fidelity between these two density matrices (1.98). The dynamical quantities $\Delta E, \langle E\rangle$ are computed as

$$\langle E\rangle = \left\langle \left\langle \text{Tr}\left((\hat{H}_0+\hat{H}_\tau)e^{-\beta\hat{H}_0}\right)\right\rangle_0\right\rangle_\tau, \tag{3.36}$$

$$\langle E^2\rangle = \left\langle \left\langle \text{Tr}\left((\hat{H}_0+\hat{H}_\tau)^2e^{-\beta\hat{H}_0}\right)\right\rangle_0\right\rangle_\tau, \tag{3.37}$$

$$\Delta E = \sqrt{\langle E^2\rangle - \langle E\rangle^2}, \tag{3.38}$$

$$E_0 = \left\langle \min(\text{eigvals}(H_\tau))\right\rangle_\tau, \tag{3.39}$$

where $\langle\circ\rangle_\tau$ stands for averaging over $\hat{H}_\tau$ and $\langle\circ\rangle_0$ for averaging over $\hat{H}_0$.

From Fig. 3.10 (a) we see that at $\beta = 1$ the QSL's are respected and indeed the dynamics saturates the Mandelstam-Tamm bound. This is not the case when we go to lower temperatures since in (b) the dynamics saturates the Margolus-Levitin bound but violates the Mandelstam-Tamm one, which is the one that should apply.

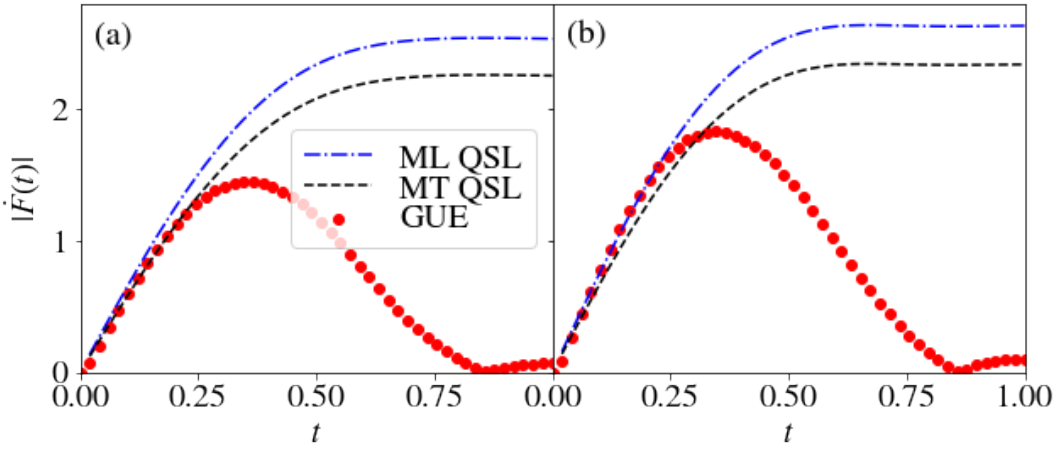

FIGURE 3.10: Speed Limits on the Uhlmann fidelity for quenched dynamics for (a) $\beta = 1$ and (b) $\beta = 5$. The dimension of the matrices is $N = 10$ and we average over $N_{\text{av}} = 100 \times 100$ Hamiltonians. Code here.

3.4 No Lyapunov regime in Random Matrix Theory

Random Matrices exhibit a problem which makes them not suitable for this work, this problem being that they do not show a Lyapunov regime. In this section, this problem will be exposed and studied. In the Lyapunov regime the OTOC is known to decay as

$$\tilde{C}(t) \propto 1 - \epsilon e^{\lambda t}, \tag{3.40}$$

for times between the dissipation time t_d and the Ehrenfest Time t_E. $t_d \ll t \ll t_E$. One should remember that the *dissipation time* is defined as that time for which the 2-point correlators saturate and the *Ehrenfest time* that time at which the OTOC saturates. The systems in which Maldacena's bound applies are those that have a big difference between these two times. To compute these time scales in Random Matrix Theory we introduce the 2 point correlator

$$B_\beta(t) = \frac{1}{Z(\beta)} \text{Tr}(e^{-\beta \hat{H}} \hat{S}_x \hat{S}_x(t)), \tag{3.41}$$

where as usual an average over $\hat{H} \in$ GUE is performed. The spin operators have spin $S = (N-1)/2$. The *dissipation time* then will be defined as the time at which the first minimum of $B_\beta(t)$ happens and the *Ehrenfest time* will be defined as the time for the first minimum of $\tilde{C}_\beta(t)$. Along with these contributions, the Spectral Form Factor is also shown in order to see in which region of the SFF the characteristic time scales of our system lay.

The results for the three quantities are plotted in Fig. 3.11. From this figure we see that at infinite temperature Fig. 3.11 (a) the dissipation time is even bigger than the Ehrenfest time. This already points out that Random Matrices are not the right framework to study the Lyapunov regime. For finite temperature like $\beta = 1$ Fig. 3.11 (b)[6] we see that the two timescales are very similar although t_E is slightly bigger

[6] In the plot it may seem like the dissipation time is on a relative maximum of B_β but we are plotting $|B_\beta|$ so that we can take the y-axis in logscale. Actually, that value has negative B_β.

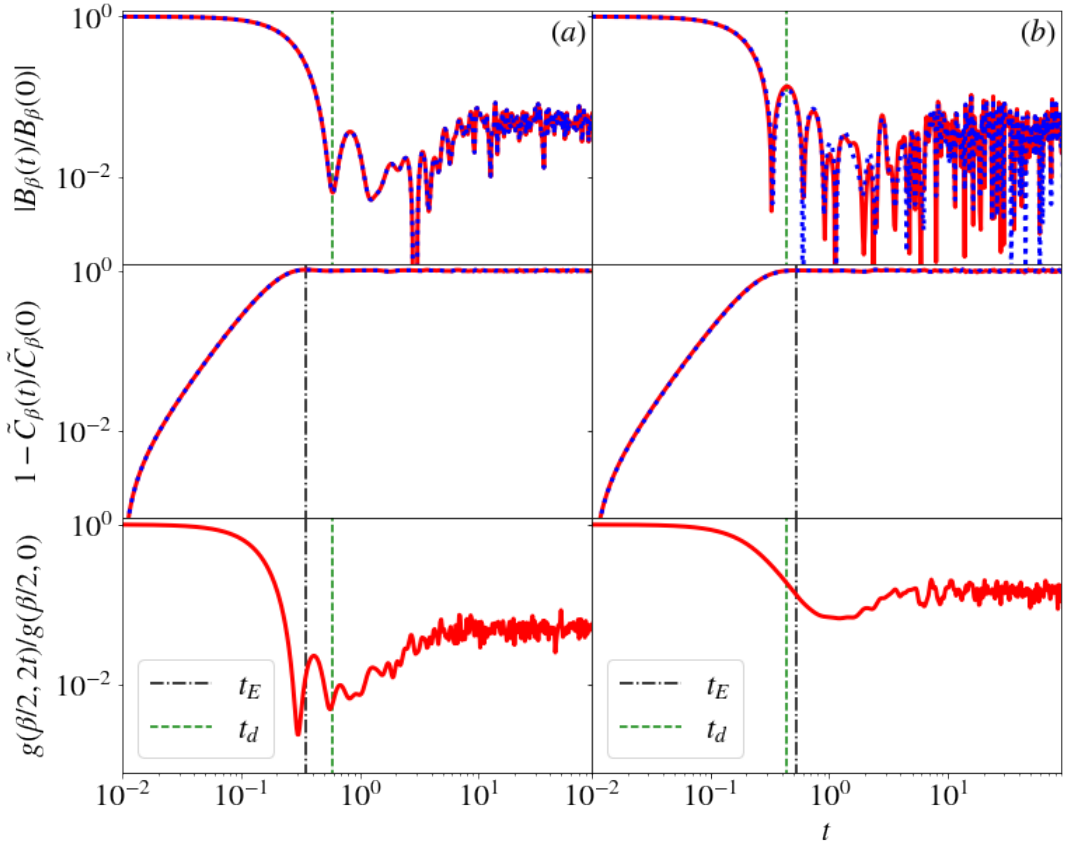

FIGURE 3.11: Time scales for the GUE with (a) $\beta = 0$ and (b) $\beta = 1$. We show a 2 point correlator $B_\beta(t) = \frac{1}{Z(\beta)}\mathrm{Tr}(e^{-\beta\hat{H}}\hat{S}_x\hat{S}_x(t))$ (upper) , the OTOC $\tilde{C}_\beta(t)$ with operators $\hat{A} = \hat{B} = \hat{S}_x$ (middle) and the Spectral Form Factor $g(\beta/2, 2t)$ (lower). The dashed blue lines are the non-annealed quantities while the solid red lines are the annealed quantities. The results are obtained for $N = 20$ and $N_{\text{av}} = 25$. Code here.

than t_d. The region between t_d and t_E is that in which we are taking the exponential fit. This justifies the selected region for some of the temperatures studied. However, the condition $t_E \gg t_d$ is not obeyed so we cannot talk about a Lyapunov regime.

The nonexistence of the Lyapunov regime in Random Matrices may also be seen from the variance of some operators. As we discussed in §1.2.2 the Lyapunov regime is also that for which the variance of some operator $\hat{G}(t)$ grows exponentially in time as

$$\mathrm{Var}(\hat{G}(t)) \propto e^{\lambda t}. \tag{3.42}$$

This variance has to be taken with respect to some state and for that, we choose $|\Psi\rangle$ to be a uniformly distributed random state and we average over many realizations. Our variance then is given by

$$\langle\langle \mathrm{Var}(\hat{G}(t))\rangle\rangle = \left\langle \left\langle \left(\langle\Psi|\hat{G}(t)^2|\Psi\rangle - \langle\Psi|\hat{G}(t)|\Psi\rangle^2 \right)^{1/2} \right\rangle_\Psi \right\rangle_{\hat{H}}. \tag{3.43}$$

The results for this variance are shown in Fig. 3.12. We see clearly that no region

admits an exponential fit, regardless of the operator chosen. The same happens when you extend the definition of the infinite temperature spin OTOC (2.35) to the evolution generated by a Random Matrix Ensemble. One can fit the first points to find a Lyapunov but this quantity is not obtained between t_d and t_E and therefore does not have the properties of a Lyapunov exponent and it overestimates the value by a lot.

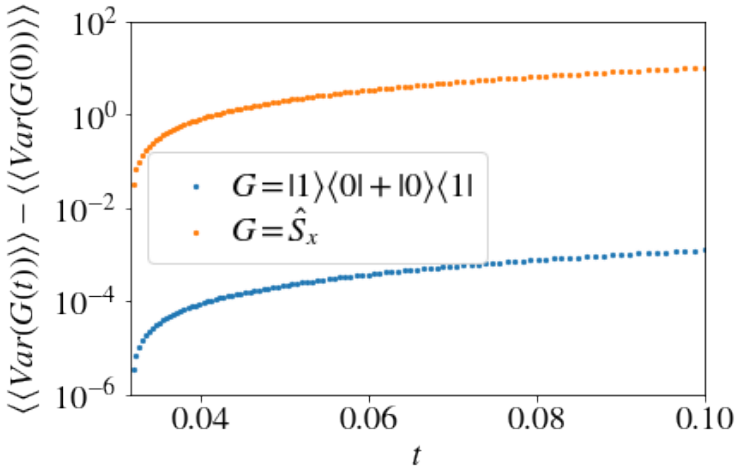

FIGURE 3.12: Variance of the $\hat{S}_x$ and $|1\rangle\langle 0| + |0\rangle\langle 1|$ operators as a function of time. The results are obtained for $N = 30$ and for $N_{\text{av}} = 100 \times 100$ realizations. Code here.

As we have argued, there is no Lyapunov regime to be found in Random Matrix Ensembles. In a sense, RMT is *too chaotic* to show a Lyapunov exponent since OTOC's saturate essentially at the same rate as 2 point functions.

3.5 Comparison between Quantum Speed Limits and Maldacena's bound

However, even if there is not a well-defined Lyapunov regime in RMT we can make an important observation. This is in part thanks to our first finding that the bound might not only appear in chaotic systems. Maldacena's inequality (1.24) and the Quantum Speed Limit on Fidelity (1.102) are very similar

$$\frac{|\dot{f}|}{1-f} \leq \frac{2\pi}{\beta}, \qquad \frac{|\dot{F}|}{1-F} \leq \frac{1}{\tau_{\text{QSL}}}. \tag{3.44}$$

In fact, if we choose our OTOC to be the fidelity OTOC (1.16) the right-hand side of both inequalities is the same and we can directly compare their left-hand side and see which of the two bounds is tighter. This procedure allows us to bound the fidelity OTOC for any time, not just in the Lyapunov regime. There is however, one problem when working with the annealed version of the quantities here. As is shown in Fig. 3.13 the annealed version of $\langle \hat{H} \rangle$ keeps decreasing[7] and does not

[7] Note that the quantity plotted is $-\langle \hat{H} \rangle$.

saturate to a fixed value[8]. This makes the selection of a ground state energy for the annealed $\langle \hat{H} \rangle$ difficult. For this reason we decided to stick to the non-annealed version, which saturates clearly to E_0 as we take $\beta \to \infty$. Another observation is that as we increase N the ground state energy gets closer to the value obtained from the semicircle law $E_0 = -\sqrt{2N}$. However even if the fit to that law was already good for $N = 50$, recall §1.3.3, the estimation for E_0 is still a bit off for $N = 50$, this is reasonable since the deviations from the semicircle law are more important around the tail of the distribution, which determines the ground state energy, used for the QSL estimate.

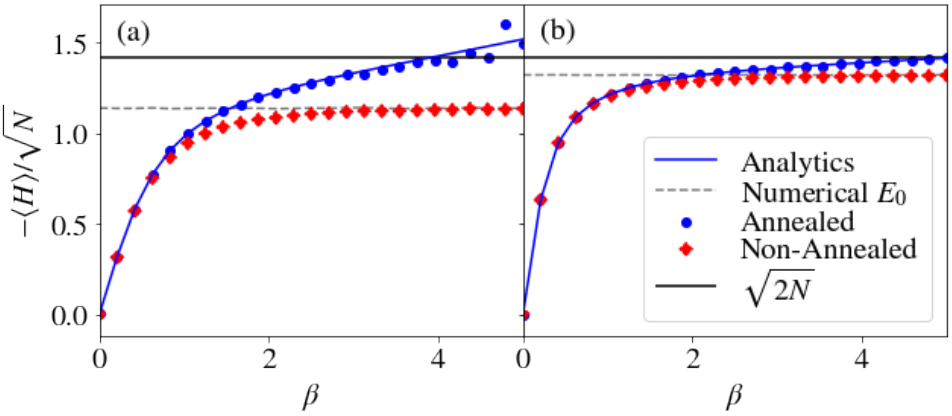

FIGURE 3.13: Average energy (annealed and non-annealed) as a function of β for the GUE with (a) $N = 10$ and (b) $N = 50$. The numerical ground state energy E_0 and the analytical value from the semicircle law $-\sqrt{2N}$ are also shown. Code here.

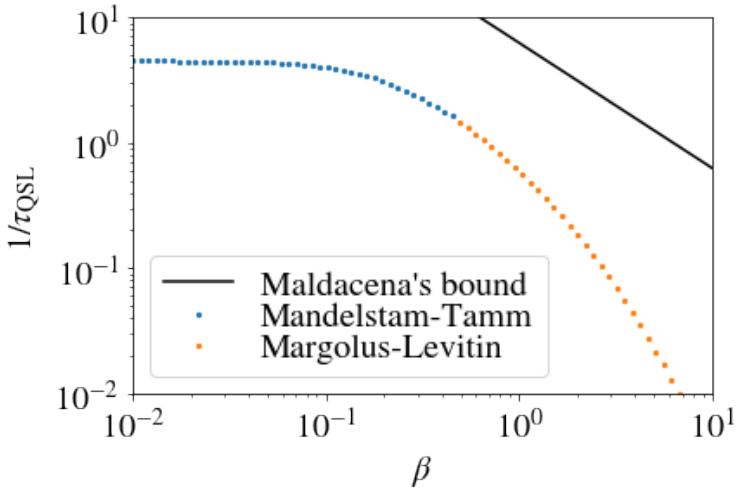

FIGURE 3.14: Comparison between the Quantum Speed Limits and the Maldacena's bound for the GUE. The dimension of the Hilbert space is $N = 100$ and the results are averaged over $N_{av} = 1000$ realizations. Code here.

[8]One may think that for $N = 50$ this does not happen but indeed it still happens, only the slope is smaller so the problem to find E_0 is essentially the same.

Fig. 3.14 shows $1/\tau_{\text{QSL}}$ obtained numerically for the GUE ensemble along with Maldacena's bound $\frac{2\pi}{\beta}$. The Speed Limit is computed for orthogonal states, that is to say, $\mathcal{L}(\rho_0, \rho_t) = \pi/2$. The plot suggests that Quantum Speed Limits set a tighter bound on $|\dot{f}|/(1-f)$ for the fidelity OTOC than the universal bound proposed by Maldacena for the Gaussian Unitary Ensemble. This is reasonable since Quantum Speed Limits are purely system-dependent and do not show universal behaviour. It is also observed that Mandelstam-Tamm holds for the high temperature regime and around $\beta \sim 1$ the crossover to Margolus-Levitin happens.

Several questions arise from these results:

- Can we find a similar bound for a more general class of OTOC's, not just the fidelity OTOC?
- If we computed QSL's for the Sachdev-Ye-Kitaev (SYK) model, which is known to saturate Maldacena's bound on the Lyapunov at low temperatures, would they also saturate this bound?

Both of these questions open up new directions of research, which could in turn give a more complete answer to the question which originated the work, to which extent can we understand Maldacena's bound as a Quantum Speed Limit? This question was only partially answered due to the difficulties encountered in the realization of the work, however these difficulties lead us to find unexpected interesting behaviour in quantities like the Spectral Form Factor. The main path of the work would continue choosing a suitable model in which we can work, by suitable we mean that it shows a Lyapunov exponent for any temperature and QSL's can be computed. One of the possible models that fulfills these properties is the SYK model.

Chapter 4

Conclusions

4.1 Main results

The main goal of the project was to find a relation between Maldacena's bound on the Lyapunov exponent $\lambda \leq \frac{2\pi}{\beta}$ and the fundamental limit on the evolution of quantum systems, Quantum Speed Limits. What we could do in this direction of work was limited by the systems and frameworks we used. First of all for the Quantum Kicked Top one can define an infinite temperature Lyapunov exponent but one cannot extend that definition to finite temperature since the Hamiltonian is time dependent and therefore we do not have a clear definition for the Boltzmann factors (§2.1.5). So we cannot test Maldacena's bound in that class of systems since one needs a notion of temperature. The problems arising with the Quantum Kicked Top made us switch the framework to Random Matrix Theory, where thermal factors can be defined without any problem. The problem with Random Matrix Theory is that it does not show a Lyapunov regime because the time scales at which two point correlators saturate are similar to those at which OTOC's saturate (§3.4) in a sense, Random Matrices are too chaotic. For this reason, we cannot test Maldacena's bound on the Lyapunov exponent using RMT. What we did is to take the more general expression (1.24) and compare it with the Quantum Speed Limit on the Fidelity OTOC This showed that the Quantum Speed Limits set a tighter bound on the Fidelity OTOC than the universal bound by Maldacena (§3.5).

Even though the main goal of the project was only partially accomplished, we found some interesting features for the Spectral Form Factor. We studied how the correlations between different neighbours contribute to the total SFF (§3.1.2), essentially the further the neighbors, the sooner their contribution to the dip. Also the effect of finite temperature is to remove the correlations between neighbors further apart. We also found an analytical expression for the contribution to the Spectral Form Factor from nearest neighbors to which our unfolded numerics fit well in the large N limit. This will be useful for future research providing a possible analytical expression for quantities such as the dip time which would be reliable in the low temperature regime.

The most striking feature we found is that the intermediate-time exponential decay of the Spectral Form Factor $g(\beta/2, 2t)$ saturates Maldacena's bound (§3.2.1). This result was unexpected for many reasons. First of all, the initial decay of the SFF is not a chaotic feature, and we showed by comparing our results with the SFF for the Kicked Top that this feature is indeed not chaotic (§3.2.4). Secondly, the fitted function was not the one used for the Lyapunov regime and did not simplify as neatly when substituted in (1.24). We discussed a possible solution for this in §3.2.3,

where we saw that for bigger N the exponent got closer and closer to the bound. These results suggest that Maldacena's bound applies not only on chaotic systems but also in systems which are totally regular, e.g. a Kicked Top with Poissonian spacing statistics.

Apart from these results, we also derived a Margolus-Levitin QSL for Floquet systems, which allowed us to propose an extension of all the discussed QSL's to the Quantum Kicked Top (§2.3). We computed QSL's for Random Matrix Theory (§3.3) in two different set-ups, the first one directly on the SFF using the fact that we can express the SFF as a fidelity of Thermal Coherent States, and the second one with quenched dynamics in a setup which reminds us of the Loschmidt echo. We also extended the infinite Temperature Lyapunov exponent on the Kicked Top to generalized Kicked Tops with any Level Spacing statistics (§2.2.2).

4.2 Experimental realization

4.2.1 Physical many-body systems

The systems discussed throughout this work are a bit far from reality. The Kicked Top has a physical meaning, however, it is difficult to imagine a physical system with a large spin which is subject to a sequence of nonlinear delta kicks. For RMT the problem is even larger because we do not really have any physical system, we just know that if the system is chaotic the results should match an average over a Random Matrix Ensemble respecting the symmetries of the system. Furthermore, in recent years there has been a growing interest in many-body quantum chaos, for this reason we here describe some many-body models in the literature in which one could witness quantum chaotic behavior.

A nice many-body realization of Kicked Tops is to relate them to Ising spin chains [93]. The main idea is to consider a system with $2S$ qubits and substitute the spin operators for

$$\hat{S}^{x,y,z} = \frac{1}{2}\sum_{j=1}^{2S} \sigma_j^{x,y,z}, \tag{4.1}$$

where $\sigma_j^{x,y,z}$ are the Pauli matrices in the j-th qubit. With this approach, one finds that the free evolution term is analogous to the magnetic field term in the Ising Hamiltonian, while the nonlinear kicks correspond to interactions between the spins. One great feature of this approach is that it allows for an analytical solution of the Kicked Top for small system sizes.

Many of the many-body models recently proposed in the literature, like for example, the SYK model, lack the tunability shown by the Kicked Top. The two models studied in [17, 18] show this property. The one in [17] is called the **Fermi-Hubbard model with an impurity**, the main idea is to consider a bath composed of spin-polarized fermions which can move freely on a 1-D lattice with N_s sites, on top of that bath we consider a single distinguishable impurity which can occupy any site. The Hamiltonian of the system is

$$\hat{H} = \hat{H}_I + \hat{H}_B + \hat{H}_{IB}, \tag{4.2}$$

where the Hamiltonian of the impurity is

$$\hat{H}_I = -J_I \sum_{j=1}^{N_s-1} (\hat{a}_{j+1}^\dagger \hat{a}_j + \hat{a}_j^\dagger \hat{a}_{j+1}) + \sum_{j=1}^{N_s} V(j) \hat{a}_j^\dagger \hat{a}_j, \tag{4.3}$$

while the bath's Hamiltonian is

$$\hat{H}_B = -J_B \sum_{j=1}^{N_s-1} (\hat{b}_{j+1}^\dagger \hat{b}_j + \hat{b}_j^\dagger \hat{b}_{j+1}) + \sum_{j=1}^{N_s} V(j) \hat{b}_j^\dagger \hat{b}_j + W_{BB} \sum_{j=1}^{N_s-1} \hat{b}_{j+1}^\dagger \hat{b}_{j+1} \hat{b}_j^\dagger \hat{b}_j, \tag{4.4}$$

and the impurity-bath interaction Hamiltonian is

$$\hat{H}_{IB} = W_{IB} \sum_{j=1}^{N_s} \hat{a}_j^\dagger \hat{a}_j \hat{b}_j^\dagger \hat{b}_j. \tag{4.5}$$

The operators $\hat{a}_j$, $\hat{a}_j^\dagger$ are the annihilation and creation operators of the impurity in site j and $\hat{b}_j$, $\hat{b}_j^\dagger$ are the annihilation and creation operators of bath particles. J_I and J_B are, respectively, the hopping strengths of the impurity and bath particles. $V(j)$ is a very small external potential which depends on the site j thus breaking any possible geometrical symmetry. W_{BB} is the strength of the Fermi-Hubbard interaction between bath particles and W_{IB} is the strength of the interaction between the impurity and the bath particles. The model is integrable for $W_{BB} \to 0$ and chaotic, with nearly GOE spacing statistics, for $W_{BB} = 1$.

Another interesting model is the one discussed in [18] where the authors study the transition between integrability and Many-Body Quantum Chaos. The model is inspired on the Kronig-Penney model for a solid. The Hamiltonian for the system is

$$\hat{H} = \epsilon_1 \left(-\sum_{j=1}^{N_p} \frac{\partial^2}{\partial x_j^2} + \sum_{j=1}^{N_p} \sum_{k=1}^{N_w-1} \delta\left(x_i - \frac{\pi k}{N_w}\right) + \sum_{\langle j,k \rangle} \delta(x_j - x_k) \right), \tag{4.6}$$

where ϵ_1 sets the unit of energy for the system, N_p stands for the number of particles, N_w stands for the number of wells in the potential, $x_j \in [0, \pi]$ is the position of the j-th particle and $\delta(x)$ is Dirac's delta function. The main idea is that we are considering N_w wells of total length L with N_p bosonic particles interacting via contact interactions. One can change the onset of quantum chaos in this model, changing the number of particles N_p and the number of wells in the system N_w.

4.2.2 Possible experimental implementation of our results

Understanding the Spectral Form factor as a fidelity (or Survival Probability) between Coherent Thermal States or ThermoField Double States can make it experimentally accessible since the fidelity is a quantity with a clear physical meaning. However, the preparation of these special states can be hard from a experimental perspective. The survival probability can be experimentally measured using interferometric techniques [94]. Also Spectral Form factors can be studied using Quantum Simulators [95] using a randomized-measurement protocol. If any of the experimental implementations of SFF-related quantities found the same saturation of

the decay exponent at short times of the SFF, this would prove our numerical results and shed some light on the possible reasons for this saturation.

4.3 Future work

Since the relation between the Maldacena's bound and QSL's is yet not very clear, the main direction of work should be in this way. The main thing to do then is to pick another system in which we see a Lyapunov regime for any temperature, and compute the QSL's for that system. Among the possible systems to consider, we have the Sachdev-Ye-Kitaev (SYK) model [31, 96, 97] which is known to saturate Maldacena's bound at low temperatures. A natural question arises, if we compare the Quantum Speed Limits with the Maldacena's inequality, as in Fig. 3.14, does the QSL saturate Maldacena's bound? This line of research would involve analytical and numerical solutions to the SYK model, which connects via the AdS-CFT correspondence to Black Hole physics.

Another possible line of work is to consider a Kicked Top in an Open Quantum System setting. This way one could define a temperature for the system and study if the Lyapunov exponent of such a system gets close to the Maldacena's bound. In such a system we would have also a Lyapunov exponent for every temperature and a Quantum Speed Limit which we could compare. This line of research would introduce us in the field of *dissipative quantum chaos*.

Further topics we encountered during this work and that could be interesting to study in any of our settings include local OTOC's which could serve as a microscope in a mixed quantum phase space to tell where chaos is present [98]. Also the Double Quantum Kicked Top [99, 100], a system in which one considers a free evolution forwards in time and another one backwards in time, shows fractality in their pseudo-energy spectrum. Does this fractal-nature of the pseudo-spectrum translate to any interesting features in any other quantities?

Appendix A

Proofs of the bound on the Lyapunov exponent

A.1 Maldacena, Shenker, and Stanford's proof

Proof. First of all, we can map the half strip to the unit circle by the transformation

$$z = \frac{1 - \sinh(\frac{2\pi}{\beta}(t + i\tau))}{1 + \sinh(\frac{2\pi}{\beta}(t + i\tau))}. \tag{A.1}$$

To check that the transformation indeed maps the half-stripe to the unit circle we plot it in Fig. A.1. We check that no point in the complex plane is mapped to a point with a radius bigger than 1 so our map indeed gets us to the unit disk.

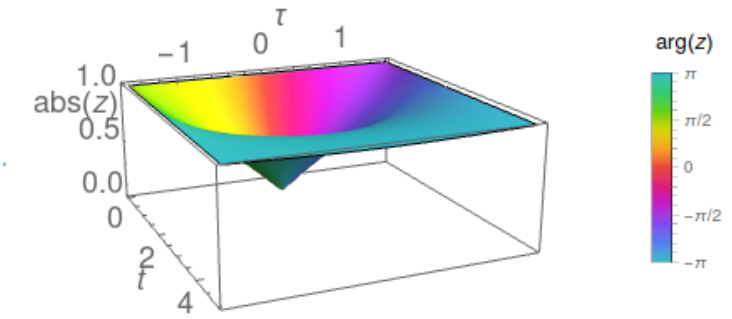

FIGURE A.1: Plot of the map from the half-stripe to the unit disk in (A.1). The height of the plot represents the absolute value of z while the color represents the phase of the complex number. The values of τ go from $-\frac{\pi}{2}$ to $\frac{\pi}{2}$. Code here.

Since the function always has an absolute value smaller than one it is mapping the unit disk onto itself. Such a function is known to obey the *Schwarz-Pick theorem* which ensures that

$$\frac{|df|}{1 - |f(z)|^2} \leq \frac{|dz|}{1 - |z|^2}. \tag{A.2}$$

Let us look at the case in which $\tau = 0$. By some simple algebra, one can prove that the right-hand side of the inequality is given by

$$\frac{|dz|}{1-|z|^2} = \frac{\cancel{(1+\sinh\frac{2\pi t}{\beta})^2}}{4\sinh\frac{2\pi t}{\beta}} \frac{2\cosh\frac{2\pi t}{\beta}}{\cancel{(1+\sinh\frac{2\pi t}{\beta})^2}} \frac{2\pi}{\beta} dt = \frac{1}{2}\frac{2\pi}{\beta}\coth\frac{2\pi t}{\beta} dt. \tag{A.3}$$

With this result and making use of the fact that $f(t)$ is real, we can re-express the Schwarz-Pick theorem (A.2) as

$$\frac{|df|}{1-f} \leq \frac{1+f}{2}\frac{2\pi}{\beta}\coth\frac{2\pi t}{\beta} dt \leq \frac{2\pi}{\beta}\coth\frac{2\pi t}{\beta} dt. \tag{A.4}$$

Now let us approximate the hyperbolic cotangent at long times $2\pi t \gg \beta$ by

$$\coth x = \frac{e^x + e^{-x}}{e^x - e^{-x}} = \frac{1}{1-e^{-2x}} + \frac{1}{e^{2x}-1} \sim 1 + \mathcal{O}(e^{-2x}), \tag{A.5}$$

so we find that

$$\frac{1}{1-f}\left|\frac{df}{dt}\right| \leq \frac{2\pi}{\beta} + \mathcal{O}(e^{-4\pi t/\beta}), \tag{A.6}$$

as we wanted to prove. □

Now all that is left to prove is that indeed our OTOC $f(t) = \tilde{C}(t)/\tilde{C}_d$ satisfies conditions 1 and 2. The first condition is way easier to prove, it is enough to consider the analytical continuation of the OTOC to complex times and we obtain

$$\tilde{C}(\beta, t+i\tau) = \frac{\mathrm{Tr}(\hat{A}(t)e^{-(\frac{\beta}{4}-\tau)\hat{H}}\hat{B}(0)e^{-(\frac{\beta}{4}+\tau)\hat{H}}\hat{A}(t)e^{-(\frac{\beta}{4}-\tau)\hat{H}}\hat{B}(0)e^{-(\frac{\beta}{4}+\tau)\hat{H}})}{Z(\beta)}. \tag{A.7}$$

Recall that a function of a complex variable $f(z)$ is analytic in z_0 if it admits a Taylor expansion around that point. We need to ask the function then to be finite and for that, the terms with real exponentials should remain with a negative exponent, otherwise, the sum may blow up and diverge, so we need

$$\frac{\beta}{4} - \tau \geq 0, \quad \frac{\beta}{4} + \tau \geq 0 \rightarrow -\frac{\beta}{4} \leq \tau \leq \frac{\beta}{4}. \tag{A.8}$$

The proof of $|f(t+i\tau)| \leq 1$ is more involved. In [6] the authors take the following strategy. First show that $|f(t+i\tau)| \leq 1$ in the boundaries of the stripe and then by using the *Phragmén-Lindelöf* principle argue that the function has to be bounded on the whole half stripe. For brevity we introduce $\hat{y} = e^{-\beta\hat{H}/4}/\sqrt[4]{Z}$. Let us first consider the edges of the half-strip $|\tau| = \beta/4$, here

$$\tilde{C}\left(t - i\frac{\beta}{4}\right) = \mathrm{Tr}\left(\hat{y}^2\hat{B}(0)\hat{A}(t)\hat{y}^2\hat{B}(0)\hat{A}(t)\right). \tag{A.9}$$

This expression may be understood as the inner product $\langle w, v\rangle = \mathrm{Tr}(w^\dagger v)$ between the "vectors" $v = \hat{y}\hat{B}(0)\hat{A}(t)\hat{y}$ and $w = \hat{y}\hat{A}(t)\hat{B}(0)\hat{y}$. Then by the Cauchy-Schwarz inequality $|\langle w, v\rangle| \leq \sqrt{\langle w, w\rangle\langle v, v\rangle}$ since $\langle v, v\rangle = \langle w, w\rangle$ and both are equal to

$\mathrm{Tr}(\hat{y}^2\hat{A}(t)\hat{B}(0)\hat{y}^2\hat{B}(0)\hat{A}(t))$ we obtain

$$\left|\tilde{C}\left(t-i\frac{\beta}{4}\right)\right| \leq \mathrm{Tr}(\hat{y}^2\hat{A}(t)\hat{B}(0)\hat{y}^2\hat{B}(0)\hat{A}(t)). \tag{A.10}$$

One should note that the last expression is in standard time ordering. In a chaotic system, we expect the OTOC to factorize at long times to $\tilde{C}_d$. This means that after a t_0 the following inequality holds $\forall\ t \geq t_0$

$$\mathrm{Tr}(\hat{y}^2\hat{A}(t)\hat{B}(0)\hat{y}^2\hat{B}(0)\hat{A}(t)) \leq \mathrm{Tr}(\hat{y}^2\hat{A}(t)\hat{y}^2\hat{A}(t))\mathrm{Tr}(\hat{y}^2\hat{B}(0)\hat{y}^2\hat{B}(0)) + \varepsilon, \tag{A.11}$$

where ε accounts explicitly for possible errors of the factorization, the exact value of ε will depend on t_0 in general, for explicit examples we refer the reader to Sect. 4.3 of [6]. We have then shown that $|\tilde{C}(t+i\tau)| \leq \tilde{C}_d + \varepsilon$ after some reference time t_0 therefore defining the function $f(t)$ as

$$f(t) = \frac{\tilde{C}(t+t_0)}{\tilde{C}_d + \varepsilon}, \tag{A.12}$$

we are sure that $|f| \leq 1$ in the boundaries $\tau = \pm\beta/4$.

Now let us study the third boundary $t = 0$. The main idea is the same as before with the only difference that now we have two possible sources of errors. The first one is the failure of the factorization of the time-ordered term, which is the same as ε defined above. The second source comes from $\tilde{C}$ not being time ordered, this is due to the onset of scrambling so, as long as we choose t_0 in a way that the error ε is bigger than the effect of scrambling the first error is the most important one and we can use the same argument to say that $|f| \leq 1$ in this boundary.

Finally to use the Phragmén-Lindelöf principle we need to show that f is bounded by some constant K in the interior $|f(z)| \leq K$. Introducing $\xi = \frac{4\tau}{\beta}$ we can rewrite (A.7) as

$$\tilde{C}(t+i\tau) = \mathrm{Tr}(\hat{y}^{1+\xi}\hat{A}(t)\hat{y}^{1-\xi}\hat{B}(0)\hat{y}^{1+\xi}\hat{A}(t)\hat{y}^{1-\xi}\hat{B}(0)), \tag{A.13}$$

and therefore

$$|\tilde{C}(t+i\tau)| \leq \mathrm{Tr}(\hat{y}^{1+\xi}\hat{B}(0)\hat{y}^{1-\xi}\hat{A}(t)\hat{y}^{1+\xi}\hat{A}(t)\hat{y}^{1-\xi}\hat{B}(0)). \tag{A.14}$$

Since the correlator is time-ordered at times longer than t_0 is known to saturate to

$$\sim \mathrm{Tr}(\hat{y}^{1+\xi}\hat{B}\hat{y}^{3-\xi}\hat{B})\mathrm{Tr}(\hat{y}^{1+\xi}\hat{A}\hat{y}^{3-\xi}\hat{A}). \tag{A.15}$$

Therefore one obtains that $|\tilde{C}|$ is bounded by

$$|\tilde{C}(t+i\tau)| \leq \mathrm{Tr}(\hat{y}\hat{B}\hat{y}^2\hat{B})\mathrm{Tr}(\hat{y}\hat{A}\hat{y}^2\hat{A}). \tag{A.16}$$

Which is not $\tilde{C}_d$ but is finite and therefore we have proven $|f| \leq K$ and the Phragmén-Lindelöf follows assuring that $|f| \leq 1$.

There is one issue with this proof, any system has Poincaré recurrences, by which at very long times the system goes back to the original state. The argument based on t_0 will fail when considering these recurrences since (A.11) will break at this recurrence time. The authors suggest that to address this problem one should limit the region with a fourth boundary at some time $t_{\max}$ such that $t_E \ll t_{\max} \ll t_{\mathrm{rec}}$.

A.2 Tsuji, Shitara, and Ueda's proof

The factorization condition *for all time after* t_0 is a too strong condition since the Lyapunov regime only happens up to the finite Ehrenfest time, also the issues with Poincaré recurrences are not taken into account with enough care in Maldacena's proof. For this reason, an alternative derivation of the bound is desirable. This alternative derivation was proposed by Tsuji, Shitara, and Ueda in [32].

The regularization that we introduce in the OTOC is not unique, in fact, another common regularization is to split the Boltzmann factor in 2, which gives

$$C_0(t) = \frac{1}{2}\left(\mathrm{Tr}(\hat{y}^2\hat{A}(t)\hat{B}(0)\hat{y}^2\hat{A}(t)\hat{B}(0)) + \mathrm{Tr}(\hat{y}^2\hat{B}(0)\hat{A}(t)\hat{y}^2\hat{B}(0)\hat{A}(t))\right), \tag{A.17}$$

which comes from regularizing the OTOC splitting the squared commutator in two as $\sim \mathrm{Tr}([\hat{A}(t),\hat{B}(0)]e^{-\beta\hat{H}/2}[\hat{A}(t),\hat{B}(0)]e^{-\beta\hat{H}/2})$. One can define a one-parameter family of OTOC's as

$$\begin{aligned} C_\gamma(t) = \frac{1}{2}\Bigg(&\mathrm{Tr}(\hat{y}^{2(1-\gamma)}\hat{A}(t)\hat{y}^{2\gamma}\hat{B}(0)\hat{y}^{2(1-\gamma)}\hat{A}(t)\hat{y}^{2\gamma}\hat{B}(0)) \\ &+\mathrm{Tr}(\hat{y}^{2(1-\gamma)}\hat{B}(0)\hat{y}^{2\gamma}\hat{A}(t)\hat{y}^{2(1-\gamma)}\hat{B}(0)\hat{y}^{2\gamma}\hat{A}(t))\Bigg), \end{aligned} \tag{A.18}$$

where $0 \leq \gamma \leq 1$. This function has the property of being symmetrical around $\gamma = 1/2$, i.e. $C_\gamma(t) = C_{1-\gamma}(t)$. For $\gamma = 0, 1$ we recover C_0 and for $\gamma = 1/2$ we recover the usual regularized OTOC as defined in Def. 6. The same authors found a fluctuation dissipation theorem for OTOCs [101] and $C_\gamma(t)$ is related to the fluctuation part of it.

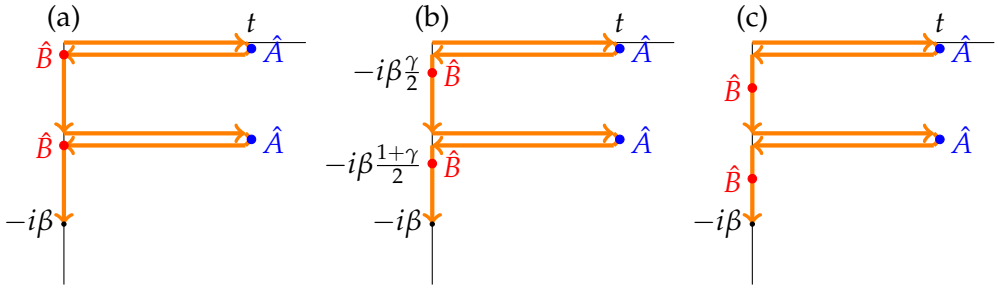

FIGURE A.2: Path on the complex time plane for (a) $C_0(t)$, (b) $C_\gamma(t)$ and (c) $\tilde{C}(t) = C_{1/2}(t)$.

Theorem 2. *If our one-parameter family of OTOCs $C_\gamma(t)$ has a uniform*[1] *asymptotic expansion of the form*[2]

$$C_\gamma(t) = c_0(\gamma) - \varepsilon c_1(\gamma)e^{\lambda(\gamma)t} + \mathcal{O}(\varepsilon^2), \tag{A.19}$$

where the terms appearing obey $c_1(\gamma) \geq 0$, $\lambda(\gamma) > 0$ and $c_1(\gamma)$ is non-zero for at least one value of γ. Then the following properties hold:

[1] Here by uniform we mean that the speed at which the expansion converges does not depend on t or γ. That is to say $C_\gamma(t)$ converges to $c_0(\gamma)$ as $\varepsilon \to 0$ uniformly in all the domain of t, γ. Also $(C_\gamma(t) - c_0(\gamma))/\varepsilon$ converges to $-c_1(\gamma)e^{\lambda(\gamma)t}$ as $\varepsilon \to 0$ uniformly in all of the domain.

[2] We are also assuming that ε is independent of $\hbar$. This is the case for large N theories but not for semiclassical approximations where ε is $\hbar^2$, in that case one should take the asymptotic expansion in ε at a fixed value of $\hbar$.

1. *The exponent $\lambda(\gamma) = \lambda$ is independent of γ. This is, the value of the Lyapunov does not depend on the regularization chosen.*

2. *The coefficient $c_1(\gamma)$ has the expression*

$$c_1(\gamma) = \tilde{c}_1 \cos\left((1-2\gamma)\frac{\beta\lambda}{4}\right), \tag{A.20}$$

where $\tilde{c}_1 > 0$.

3. *The exponent λ satisfies the inequality*

$$\lambda \leq \frac{2\pi}{\beta\hbar}. \tag{A.21}$$

Proof. We can move the dependence on γ from the Boltzmann factors to the operators thus obtaining

$$\begin{aligned} C_\gamma(t) = &\frac{1}{2}\mathrm{Tr}\left\{\hat{y}\hat{A}\left(t - i\left(\gamma-\frac{1}{2}\right)\frac{\beta\hbar}{2}\right)\hat{y}\hat{B}(0)\hat{y}\hat{A}\left(t - i\left(\gamma-\frac{1}{2}\right)\frac{\beta\hbar}{2}\right)\hat{y}\hat{B}(0)\right\} \\ &+\frac{1}{2}\mathrm{Tr}\left\{\hat{y}\hat{A}\left(t + i\left(\gamma-\frac{1}{2}\right)\frac{\beta\hbar}{2}\right)\hat{y}\hat{B}(0)\hat{y}\hat{A}\left(t + i\left(\gamma-\frac{1}{2}\right)\frac{\beta\hbar}{2}\right)\hat{y}\hat{B}(0)\right\}, \quad \text{(A.22)} \\ = &\frac{1}{2}\left(\tilde{C}\left(t - i\left(\gamma-\frac{1}{2}\right)\frac{\beta\hbar}{2}\right) + \tilde{C}\left(t + i\left(\gamma-\frac{1}{2}\right)\frac{\beta\hbar}{2}\right)\right). \quad \text{(A.23)} \end{aligned}$$

So we see that we can express any of the possible regularizations of the OTOC in terms of the usual regularized OTOC $\tilde{C}(t)$. For brevity we can define $z = t + i\left(\gamma - \frac{1}{2}\right)\frac{\beta\hbar}{2}$ and therefore

$$C_\gamma(t) = \frac{1}{2}\left(\tilde{C}(z) + \tilde{C}(z^*)\right). \tag{A.24}$$

We know that at $\gamma = \frac{1}{2}$ in the Lyapunov regime the OTOC decays as

$$C_{1/2}(t) = \tilde{C}(t) = c_0 - \varepsilon\tilde{c}_1 e^{\lambda t} + \mathcal{O}(\varepsilon^2). \tag{A.25}$$

From Maldacena's argument we know that the OTOC is analytic in a half strip, this means that it is infinitely differentiable anywhere on that strip so we can write (A.24) as

$$\begin{aligned} C_\gamma(t) &= \frac{1}{2}\exp\left\{-i\frac{\beta\hbar}{2}\left(\gamma-\frac{1}{2}\right)\partial_t\right\}\tilde{C}(t) + \frac{1}{2}\exp\left\{i\frac{\beta\hbar}{2}\left(\gamma-\frac{1}{2}\right)\partial_t\right\}\tilde{C}(t) \quad \text{(A.26)} \\ &= \cos\left\{\frac{\beta\hbar}{2}\left(\gamma-\frac{1}{2}\right)\partial_t\right\}\tilde{C}(t), \quad \text{(A.27)} \end{aligned}$$

where we know that the action of an operator $\exp(q\partial_t)$ on a function of time is to shift time by a quantity q .

Since $\tilde{C}(z)$ is holomorphic in the half-strip any time derivative of $\tilde{C}(t)$ has a uniform asymptotic expansion in the same time window as $\tilde{C}(t)$. This means that we can exchange the limit $\varepsilon \to 0$ and the time derivative thus obtaining

$$C_\gamma(t) = c_0 - \varepsilon \tilde{c}_1 \cos \frac{(1-2\gamma)\beta\hbar\lambda}{4} e^{\lambda t} + \mathcal{O}(\varepsilon^2), \tag{A.28}$$

and with this we have proven statements 1. and 2. of the theorem. To prove statement 3. we can use the fact that $c_1(\gamma) \geq 0$ and so we need that

$$\cos \frac{(1-2\gamma)\beta\hbar\lambda}{4} \geq 0, \tag{A.29}$$

this implies that

$$(1-2\gamma)\frac{\beta\hbar\lambda}{4} \leq \frac{\beta\hbar\lambda}{4} \leq \frac{\pi}{2} \Rightarrow \lambda \leq \frac{2\pi}{\beta\hbar}. \tag{A.30}$$

□

Appendix B

Quantum Speed Limits in Phase Space

B.1 Key concepts on Wigner's Formalism

For any density matrix $\hat{\rho}$ representing a quantum state its **Wigner Function** can be defined as

$$W(x,p) \coloneqq \frac{1}{\pi\hbar}\int_{-\infty}^{\infty}\langle x+y|\hat{\rho}|x-y\rangle\, e^{-2ipy/\hbar}dy. \tag{B.1}$$

$W(x,p)$ is a quasi-probability distribution, since it is normalized and has the right marginals, i.e. $\int_\Gamma dxdpW(x,p) = 1$, $\int dxW(x,p) = |\tilde{\psi}(p)|^2$ and $\int dpW(x,p) = |\psi(x)|^2$. However it can take negative values and therefore it is not a proper joint probability distribution. For any operator $\hat{G}$ the **Wigner transformation** is defined as

$$G(x,p) \coloneqq \int_{-\infty}^{\infty} dy e^{ipy/\hbar}\left\langle x-\frac{y}{2}\middle|\,\hat{G}\,\middle|x+\frac{y}{2}\right\rangle. \tag{B.2}$$

The Wigner-transformed operator allows writing expectation values as

$$\langle\hat{G}\rangle = \mathrm{Tr}(\hat{\rho}\hat{G}) = \int_\Gamma dxdpW(x,p)G(x,p). \tag{B.3}$$

Taking $\hat{G} = \hat{\rho}_0$ the fidelity for a pure state can be written as as

$$F(t) = \mathrm{Tr}(\hat{\rho}_0\hat{\rho}_t) = \int_\Gamma d^2\Gamma W_0(x,p)W_t(x,p), \tag{B.4}$$

where $d^2\Gamma = 2\pi\hbar dxdp$. The product of Wigner Distributions is given by the *Moyal product*, defined as

$$A(x,p)\star B(x,p) \coloneqq A(x,p)\exp\left[\frac{i\hbar}{2}(\overleftarrow{\partial}_x\vec{\partial}_p - \overleftarrow{\partial}_p\vec{\partial}_x)\right]B(x,p), \tag{B.5}$$

where $\overleftarrow{\partial}_x$ represents the derivative acting on the function on the left and $\vec{\partial}_x$ the derivative acting on the function on the right. The evolution of the Wigner function can be written, analogously to the Heisenberg equation, in terms of the *Moyal bracket* $\{\{\ ,\ \}\}$ which is a nothing but a commutator with Moyal products

$$\frac{\partial W_t}{\partial t} = \{\{H,W_t\}\} = -\frac{i}{\hbar}\left(H(x,p)\star W_t(x,p) - W_t(x,p)\star H(x,p)\right). \tag{B.6}$$

B.2 Bound on the fidelity derivative

The derivative of the fidelity is given by

$$\dot{F}(t) = \int d^2\Gamma W_0 \partial_t W_t = \int d^2\Gamma W_0 \{\{H, W_t\}\}, \tag{B.7}$$

integrating by parts we can write

$$\dot{F}(t) = \int d^2\Gamma W_0 \partial_t W_t = \text{Boundary terms}\Big|_{\partial\Gamma} - \int d^2\Gamma \partial_t W_0 W_t = -\int d^2\Gamma \{\{H, W_0\}\} W_t,$$

where we are assuming that the Wigner functions vanish at infinity. We can write the modulus of the time derivative of the fidelity as

$$|\dot{F}(t)| = \sqrt{\iint d^2\Gamma d^2\Gamma' W_t^2 \{\{H, W_0\}\}^2}. \tag{B.8}$$

For two vectors on a Hilbert space $|u\rangle, |v\rangle \in \mathscr{H}$ the Cauchy-Schwarz inequality states that

$$|\langle u|v\rangle|^2 \leq \langle u|u\rangle \langle v|v\rangle, \tag{B.9}$$

by using this relation the modulus of the fidelity derivative is bounded by

$$|\dot{F}(t)| \leq \sqrt{\underbrace{\int d^2\Gamma W_t^2}_{\leq 1} \int d^2\Gamma' \{\{H, W_0\}\}^2} \leq \sqrt{\int d^2\Gamma' \{\{H, W_0\}\}^2} := \nu_\Gamma. \tag{B.10}$$

Which is exactly (1.103), as we wanted to prove.

Appendix C

Exact results for the Gaussian Unitary Ensemble

C.1 Derivation of the Average Partition Function

In this section we will follow App. C of [63]. The analytically continued partition function reads

$$Z(\beta + it) = \sum_n e^{-(\beta+it)E_n}. \tag{C.1}$$

This expression can be rewritten as an integral by

$$Z(\sigma) = \int \mathrm{d}E e^{-\sigma E} \sum_n \delta(E - E_n), \tag{C.2}$$

where $\sum_n \delta(E - E_n)$ is the Density of states. When we average over the GUE ensemble the density of states is given exactly by [51]

$$\langle \rho(E) \rangle = \sum_{j=0}^{N-1} \varphi_j^2(E), \tag{C.3}$$

where $\varphi_j(E)$ are the Harmonic oscillator eigenfunctions

$$\varphi_j(E) = \frac{e^{-E^2/2}}{\sqrt{2^j j! \sqrt{\pi}}} \mathcal{H}_j(E), \tag{C.4}$$

and $\mathcal{H}_j(E)$ are the Hermite polynomials, as we already discussed in 3.1. We will refer to the coefficient as $c_j = (2^j j! \sqrt{\pi})^{-1/2}$. Here the $\varphi_j(E)$ play the role of orthonormal polynomials for the GUE ensemble.

C.1.1 Some useful integrals

First we introduce some integrals and evaluate them since they will prove to be useful later on in the discussion. These integrals are

$$\mathcal{I}_n(\sigma) := \int_{-\infty}^{\infty} \mathrm{d}E e^{-\sigma E - E^2} \mathcal{H}_n(E), \tag{C.5}$$

$$\mathcal{I}_{nm}(\sigma) := \int_{-\infty}^{\infty} \mathrm{d}E e^{-\sigma E - E^2} \mathcal{H}_n(E) \mathcal{H}_m(E). \tag{C.6}$$

To evaluate them we need the identity

$$\int \mathrm{d}E e^{-E^2} \mathcal{H}_n(E) f(E) = \int \mathrm{d}E e^{-E^2} \partial_E^n f(E), \tag{C.7}$$

which comes from the definition of Hermite polynomials

$$e^{-E^2} \mathcal{H}_n(E) = (-\partial_E)^n e^{-E^2}, \tag{C.8}$$

after n integrations by parts that move the derivative to act on $f(E)$, not on the Gaussian. Note that here we are assuming that the integrands decay sufficiently fast at the boundary so that we can neglect the boundary terms. To evaluate $\mathcal{I}_n(\sigma)$ we choose $f(E) = e^{-\sigma E}$, therefore we find

$$\int_{-\infty}^{\infty} \mathrm{d}E e^{-E^2} \mathcal{H}_n(E) e^{-\sigma E} = \int \mathrm{d}E e^{-E^2} \partial_E^n f(E) \tag{C.9}$$

$$= (-\sigma)^n \int_{-\infty}^{\infty} e^{-E^2 - \sigma E - \frac{\sigma^2}{4}} e^{\frac{\sigma^2}{4}}, \tag{C.10}$$

$$\mathcal{I}_n(E) = e^{\sigma^2/4} (-\sigma)^n \sqrt{\pi}, \tag{C.11}$$

in the second line we just completed the square, introduce the new variable $u = E + \frac{\sigma}{2}$ and integrated over that obtaining the factor $\sqrt{\pi}$.

To evaluate the second integral we choose $f_m(E) = e^{-\sigma E} \mathcal{H}_m(E)$. The derivatives now are

$$\partial_E^n f_m(E) = \sum_{k=0}^{n} \binom{n}{k} (-\sigma)^k e^{-\sigma E} \partial_E^{n-k} \mathcal{H}_m(E). \tag{C.12}$$

The derivatives of Hermite polynomials obey $\partial_x \mathcal{H}_n(x) = 2n H_{n-1}(x)$ so the derivative of our Hermite polynomial gives us

$$\partial_E^{n-k} \mathcal{H}_m(E) = 2^{n-k} \frac{m!}{(m+k-n)!} \mathcal{H}_{m+k-n}(E). \tag{C.13}$$

When introducing this expression in the integral we find

$$\mathcal{I}_{nm} = \sum_{k=0}^{n} \binom{n}{k} (-\sigma)^k 2^{n-k} \frac{m!}{(m+k-n)!} \int \mathrm{d}E e^{-E^2} e^{-\sigma E} \mathcal{H}_{m+k-n}(E), \tag{C.14}$$

one should note that the integral is just $\mathcal{I}_{m+k-n}(E)$ so we have

$$\mathcal{I}_{nm}(E) = e^{\sigma^2/4} (-\sigma)^{m-n} 2^n \sqrt{\pi} m! \sum_{k=0}^{n} \frac{(-\sigma)^{2k} n!}{2^k (m+k-n)! k! (n-k)!}, \tag{C.15}$$

$$= e^{\sigma^2/4} (-\sigma)^{m-n} 2^n \sqrt{\pi} n! L_n^{m-n} \left(-\frac{\sigma^2}{2} \right). \tag{C.16}$$

When we look at the diagonal we set $m = n$ so we find

$$\mathcal{I}_{nn}(E) = e^{\sigma^2/4} 2^n \sqrt{\pi} n! \sum_{k=0} \binom{n}{k} \frac{(-\sigma)^{2k}}{2^k k!} = e^{\sigma^2/4} \sqrt{\pi} 2^n n! L_n \left(-\frac{\sigma^2}{2} \right), \tag{C.17}$$

where we used the closed form of the Laguerre polynomials

$$L_n(x) = \sum_{k=0}^{n} \binom{n}{k} \frac{(-x)^k}{k!}.$$

C.1.2 Averaged analytically continued partition function for the GUE

The integral we want to compute to obtain $\langle Z(\sigma)\rangle$ is

$$\langle Z(\sigma)\rangle = \sum_{j=0}^{N-1} c_j^2 \int \mathrm{d}E e^{-\sigma E} e^{-E^2} \mathcal{H}_j^2(E) = \sum_{j=0}^{N-1} c_j^2 \mathcal{I}_{jj}(E), \tag{C.18}$$

the prefactors cancel out and we find that

$$\langle Z(\sigma)\rangle = e^{\sigma^2/4} \sum_{j=0}^{N-1} L_j\left(-\frac{\sigma^2}{2}\right) = e^{\sigma^2/4} L_{N-1}^1\left(-\frac{\sigma^2}{2}\right), \tag{C.19}$$

where we used the property of generalized Laguerre polynomials

$$L_n^{\alpha+1}(x) = \sum_{j=0}^{n} L_j^{\alpha}(x). \tag{C.20}$$

C.2 Derivation of the Connected Spectral Form Factor

Expanding the expression of the connected Spectral Form Factor we find [28]

$$g_c(\sigma) = -\sum_{n=0}^{N-1}\sum_{n=0}^{N-1} \int \mathrm{d}E\mathrm{d}E' \varphi_n(E)\varphi_m(E) e^{-\sigma E} \varphi_m(E')\varphi_n(E') e^{-\sigma^* E'}, \tag{C.21}$$

$$= -\sum_{n,m=0}^{N-1} \frac{\mathcal{I}_{nm}(\sigma)\mathcal{I}_{mn}(\sigma^*)}{2^n n! \pi 2^m m!}. \tag{C.22}$$

We have to be careful in the expression used before because we will take $n \leq m$ so the role played by n with be played by $\min(n,m)$ and the role played by $n-m$ will be played by $|n-m|$. With this the correct expression for $\mathcal{I}_{nm}(\sigma)$ is slightly modified from (C.16) and reads

$$\mathcal{I}_{n,m}(\sigma) = \sqrt{\pi} e^{\sigma^2/4} (-\sigma)^{|m-n|} 2^{\min(n,m)} \min(n,m)! L_{\min(n,m)}^{|m-n|}\left(-\frac{\sigma^2}{2}\right). \tag{C.23}$$

Then substituting this in (C.22) and $\mathcal{I}_{nm}(\sigma)\mathcal{I}_{mn}(\sigma^*) = |\mathcal{I}_{nm}(\sigma)|^2$ we find equation (3.9) of the main text.

Bibliography

[1] L. Mandelstam and I. Tamm, "The Uncertainty Relation Between Energy and Time in Non-relativistic Quantum Mechanics," en, in *Selected Papers*, I. E. Tamm, B. M. Bolotovskii, V. Y. Frenkel, and R. Peierls, Eds., Berlin, Heidelberg: Springer, 1991, pp. 115–123, ISBN: 978-3-642-74626-0. DOI: 10.1007/978-3-642-74626-0_8.

[2] N. Margolus and L. B. Levitin, "The maximum speed of dynamical evolution," en, *Physica D: Nonlinear Phenomena*, Proceedings of the Fourth Workshop on Physics and Consumption, vol. 120, no. 1, pp. 188–195, Sep. 1998, ISSN: 0167-2789. DOI: 10.1016/S0167-2789(98)00054-2.

[3] S. Deffner and S. Campbell, "Quantum speed limits: From Heisenberg's uncertainty principle to optimal quantum control," en, *J. Phys. A: Math. Theor.*, vol. 50, no. 45, p. 453 001, Oct. 2017, ISSN: 1751-8121. DOI: 10.1088/1751-8121/aa86c6.

[4] M. M. Taddei, B. M. Escher, L. Davidovich, and R. L. de Matos Filho, "Quantum Speed Limit for Physical Processes," *Phys. Rev. Lett.*, vol. 110, no. 5, p. 050 402, Jan. 2013. DOI: 10.1103/PhysRevLett.110.050402.

[5] A. del Campo, I. L. Egusquiza, M. B. Plenio, and S. F. Huelga, "Quantum Speed Limits in Open System Dynamics," *Phys. Rev. Lett.*, vol. 110, no. 5, p. 050 403, Jan. 2013. DOI: 10.1103/PhysRevLett.110.050403.

[6] J. Maldacena, S. H. Shenker, and D. Stanford, "A bound on chaos," en, *J. High Energ. Phys.*, vol. 2016, no. 8, p. 106, Aug. 2016, ISSN: 1029-8479. DOI: 10.1007/JHEP08(2016)106. arXiv: 1503.01409.

[7] B. Shanahan, A. Chenu, N. Margolus, and A. del Campo, "Quantum Speed Limits across the Quantum-to-Classical Transition," *Phys. Rev. Lett.*, vol. 120, no. 7, p. 070 401, Feb. 2018. DOI: 10.1103/PhysRevLett.120.070401.

[8] M. Okuyama and M. Ohzeki, "Quantum Speed Limit is Not Quantum," *Phys. Rev. Lett.*, vol. 120, no. 7, p. 070 402, Feb. 2018. DOI: 10.1103/PhysRevLett.120.070402.

[9] S. H. Strogatz, *Nonlinear Dynamics and Chaos: With Applications to Physics, Biology, Chemistry and Engineering*, en. Westview, 2000.

[10] M. A. Porter, "An Introduction to Quantum Chaos," *arXiv:nlin/0107039*, Aug. 2001. arXiv: nlin/0107039.

[11] M. Berry, "Quantum chaology, not quantum chaos," en, *Phys. Scr.*, vol. 40, no. 3, pp. 335–336, Sep. 1989, ISSN: 1402-4896. DOI: 10.1088/0031-8949/40/3/013.

[12] J. M. G. Gómez, K. Kar, V. K. B. Kota, R. A. Molina, A. Relaño, and J. Retamosa, "Many-body quantum chaos: Recent developments and applications to nuclei," en, *Physics Reports*, vol. 499, no. 4, pp. 103–226, Mar. 2011, ISSN: 0370-1573. DOI: 10.1016/j.physrep.2010.11.003.

[13] B. Bertini, P. Kos, and T. Prosen, "Exact Spectral Form Factor in a Minimal Model of Many-Body Quantum Chaos," *Phys. Rev. Lett.*, vol. 121, no. 26, p. 264 101, Dec. 2018. DOI: 10.1103/PhysRevLett.121.264101.

[14] P. Kos, M. Ljubotina, and T. Prosen, "Many-Body Quantum Chaos: Analytic Connection to Random Matrix Theory," *Phys. Rev. X*, vol. 8, no. 2, p. 021 062, Jun. 2018. DOI: 10.1103/PhysRevX.8.021062.

[15] A. Chan, A. De Luca, and J. T. Chalker, "Solution of a Minimal Model for Many-Body Quantum Chaos," *Phys. Rev. X*, vol. 8, no. 4, p. 041 019, Nov. 2018. DOI: 10.1103/PhysRevX.8.041019.

[16] A. J. Friedman, A. Chan, A. De Luca, and J. T. Chalker, "Spectral Statistics and Many-Body Quantum Chaos with Conserved Charge," *Phys. Rev. Lett.*, vol. 123, no. 21, p. 210 603, Nov. 2019. DOI: 10.1103/PhysRevLett.123.210603.

[17] M. Kourehpaz, S. Donsa, F. Lackner, J. Burgdörfer, and I. Březinová, "Tuning canonical typicality by quantum chaos," *arXiv:2103.05974*, Mar. 2021. arXiv: 2103.05974.

[18] T. Fogarty, M. Á. García-March, L. F. Santos, and N. L. Harshman, "Probing the edge between integrability and quantum chaos in interacting few-atom systems," *Quantum*, vol. 5, p. 486, Jun. 2021, ISSN: 2521-327X. DOI: 10.22331/q-2021-06-29-486. arXiv: 2104.12934.

[19] S. Wimberger, "Nonlinear Hamiltonian Systems," en, in *Nonlinear Dynamics and Quantum Chaos: An Introduction*, ser. Graduate Texts in Physics, S. Wimberger, Ed., Cham: Springer International Publishing, 2014, pp. 21–102, ISBN: 978-3-319-06343-0. DOI: 10.1007/978-3-319-06343-0_3.

[20] A. N. Kolmogorov, "A new metric invariant of transitive dynamical systems and automorphisms of Lebesgue spaces," *Trudy Matematicheskogo Instituta imeni VA Steklova*, vol. 169, pp. 94–98, 1985.

[21] A. N. Kolmogorov, "Entropy per unit time as a metric invariant of automorphisms," in *Dokl. Akad. Nauk SSSR*, vol. 124, 1959, pp. 754–755.

[22] Y. G. Sinai, "On the notion of entropy of a dynamical system," in *Doklady of Russian Academy of Sciences*, vol. 124, 1959, pp. 768–771.

[23] Y. Sinai, "Kolmogorov-Sinai entropy," en, *Scholarpedia*, vol. 4, no. 3, p. 2034, Mar. 2009, ISSN: 1941-6016. DOI: 10.4249/scholarpedia.2034.

[24] J. R. Dorfman, *An Introduction to Chaos in Nonequilibrium Statistical Mechanics*, ser. Cambridge Lecture Notes in Physics. Cambridge: Cambridge University Press, 1999, ISBN: 978-0-521-65589-7. DOI: 10.1017/CBO9780511628870.

[25] E. Brézin and S. Hikami, "Spectral form factor in a random matrix theory," *Phys. Rev. E*, vol. 55, no. 4, pp. 4067–4083, Apr. 1997. DOI: 10.1103/PhysRevE.55.4067.

[26] S. Heusler, S. Müller, P. Braun, and F. Haake, "Universal spectral form factor for chaotic dynamics," en, *J. Phys. A: Math. Gen.*, vol. 37, no. 3, pp. L31–L37, Jan. 2004, ISSN: 0305-4470. DOI: 10.1088/0305-4470/37/3/L02.

[27] R. E. Prange, "The Spectral Form Factor Is Not Self-Averaging," *Phys. Rev. Lett.*, vol. 78, no. 12, pp. 2280–2283, Mar. 1997. DOI: 10.1103/PhysRevLett.78.2280.

[28] A. Chenu, J. Molina-Vilaplana, and A. del Campo, "Work Statistics, Loschmidt Echo and Information Scrambling in Chaotic Quantum Systems," en-GB, *Quantum*, vol. 3, p. 127, Mar. 2019. DOI: 10.22331/q-2019-03-04-127.

[29] A. I. Larkin and Y. N. Ovchinnikov, "Quasiclassical Method in the Theory of Superconductivity," *Soviet Journal of Experimental and Theoretical Physics*, vol. 28, p. 1200, Jun. 1969, ISSN: 1063-7761.

[30] W. H. Miller, S. D. Schwartz, and J. W. Tromp, "Quantum mechanical rate constants for bimolecular reactions," *J. Chem. Phys.*, vol. 79, no. 10, pp. 4889–4898, Nov. 1983, ISSN: 0021-9606. DOI: 10.1063/1.445581.

[31] B. Kobrin, Z. Yang, G. D. Kahanamoku-Meyer, C. T. Olund, J. E. Moore, D. Stanford, and N. Y. Yao, "Many-Body Chaos in the Sachdev-Ye-Kitaev Model," *Phys. Rev. Lett.*, vol. 126, no. 3, p. 030 602, Jan. 2021. DOI: 10.1103/PhysRevLett.126.030602.

[32] N. Tsuji, T. Shitara, and M. Ueda, "Bound on the exponential growth rate of out-of-time-ordered correlators," *Phys. Rev. E*, vol. 98, no. 1, p. 012 216, Jul. 2018. DOI: 10.1103/PhysRevE.98.012216.

[33] A. Kitaev, *"Hidden Correlations in the Hawking Radiation and Thermal Noise," talk given at Fundamental Physics Prize Symposium, Nov. 10, 2014.*

[34] R. J. Lewis-Swan, A. Safavi-Naini, J. J. Bollinger, and A. M. Rey, "Unifying scrambling, thermalization and entanglement through measurement of fidelity out-of-time-order correlators in the Dicke model," en, *Nat Commun*, vol. 10, no. 1, p. 1581, Apr. 2019, ISSN: 2041-1723. DOI: 10.1038/s41467-019-09436-y.

[35] J. Loschmidt, *Über den Zustand des Wärmegleichgewichtes eines Systems von Körpern mit Rücksicht auf die Schwerkraft. 2 2*, German. Wien, 1876.

[36] E. L. Hahn, "Spin Echoes," *Phys. Rev.*, vol. 80, no. 4, pp. 580–594, Nov. 1950. DOI: 10.1103/PhysRev.80.580.

[37] W.-K. Rhim, A. Pines, and J. S. Waugh, "Time-Reversal Experiments in Dipolar-Coupled Spin Systems," *Phys. Rev. B*, vol. 3, no. 3, pp. 684–696, Feb. 1971. DOI: 10.1103/PhysRevB.3.684.

[38] A. Peres, "Stability of quantum motion in chaotic and regular systems," *Phys. Rev. A*, vol. 30, no. 4, pp. 1610–1615, Oct. 1984. DOI: 10.1103/PhysRevA.30.1610.

[39] R. A. Jalabert and H. M. Pastawski, "Environment-independent decoherence rate in classically chaotic systems," en, *Phys. Rev. Lett.*, vol. 86, no. 12, pp. 2490–2493, Mar. 2001, ISSN: 0031-9007, 1079-7114. DOI: 10.1103/PhysRevLett.86.2490. arXiv: cond-mat/0010094.

[40] A. Chenu, I. L. Egusquiza, J. Molina-Vilaplana, and A. del Campo, "Quantum work statistics, Loschmidt echo and information scrambling," en, *Sci Rep*, vol. 8, no. 1, p. 12 634, Dec. 2018, ISSN: 2045-2322. DOI: 10.1038/s41598-018-30982-w.

[41] A. Goussev, R. A. Jalabert, H. M. Pastawski, and D. A. Wisniacki, "Loschmidt echo," en, *Scholarpedia*, vol. 7, no. 8, p. 11 687, Aug. 2012, ISSN: 1941-6016. DOI: 10.4249/scholarpedia.11687.

[42] Y. Sekino and L. Susskind, "Fast scramblers," en, *J. High Energy Phys.*, vol. 2008, no. 10, pp. 065–065, Oct. 2008, ISSN: 1126-6708. DOI: 10.1088/1126-6708/2008/10/065.

[43] D. N. Page, "Average Entropy of a Subsystem," *Phys. Rev. Lett.*, vol. 71, no. 9, pp. 1291–1294, Aug. 1993, ISSN: 0031-9007. DOI: 10.1103/PhysRevLett.71.1291. arXiv: gr-qc/9305007.

[44] P. Hayden and J. Preskill, "Black holes as mirrors: Quantum information in random subsystems," en, *J. High Energy Phys.*, vol. 2007, no. 09, pp. 120–120, Sep. 2007, ISSN: 1126-6708. DOI: 10.1088/1126-6708/2007/09/120.

[45] N. Lashkari, D. Stanford, M. Hastings, T. Osborne, and P. Hayden, "Towards the fast scrambling conjecture," en, *J. High Energ. Phys.*, vol. 2013, no. 4, p. 22, Apr. 2013, ISSN: 1029-8479. DOI: 10.1007/JHEP04(2013)022.

[46] S. H. Shenker and D. Stanford, "Black holes and the butterfly effect," *J. High Energ. Phys.*, vol. 2014, no. 3, p. 67, Mar. 2014, ISSN: 1029-8479. DOI: 10.1007/JHEP03(2014)067. arXiv: 1306.0622.

[47] C. Pierre, "Random matrices and Riemann hypothesis," *arXiv:1109.5586 [math]*, Sep. 2011. arXiv: 1109.5586 [math].

[48] E. Wigner and P. Dirac, "On the statistical distribution of the widths and spacings of nuclear resonance levels," 1951. DOI: 10.1017/S0305004100027237.

[49] H.-J. Stöckmann and J. Stein, "'"Quantum" chaos in billiards studied by microwave absorption," *Phys. Rev. Lett.*, vol. 64, no. 19, pp. 2215–2218, May 1990. DOI: 10.1103/PhysRevLett.64.2215.

[50] H.-J. Stöckmann, *Quantum Chaos: An Introduction*. Cambridge: Cambridge University Press, 1999, ISBN: 978-0-521-02715-1. DOI: 10.1017/CBO9780511524622.

[51] M. L. Mehta, *Random Matrices*, en. Elsevier / Academic Press, 2004, ISBN: 978-0-12-088409-4.

[52] S. Wimberger, "Aspects of Quantum Chaos," en, in *Nonlinear Dynamics and Quantum Chaos: An Introduction*, ser. Graduate Texts in Physics, S. Wimberger, Ed., Cham: Springer International Publishing, 2014, pp. 103–202, ISBN: 978-3-319-06343-0. DOI: 10.1007/978-3-319-06343-0_4.

[53] O. Bohigas, M. J. Giannoni, and C. Schmit, "Characterization of Chaotic Quantum Spectra and Universality of Level Fluctuation Laws," *Phys. Rev. Lett.*, vol. 52, no. 1, pp. 1–4, Jan. 1984. DOI: 10.1103/PhysRevLett.52.1.

[54] T. A. Brody, J. Flores, J. B. French, P. A. Mello, A. Pandey, and S. S. M. Wong, "Random-matrix physics: Spectrum and strength fluctuations," *Rev. Mod. Phys.*, vol. 53, no. 3, pp. 385–479, Jul. 1981. DOI: 10.1103/RevModPhys.53.385.

[55] J. v. Neumann, "Beweis des Ergodensatzes und desH-Theorems in der neuen Mechanik," de, *Z. Physik*, vol. 57, no. 1, pp. 30–70, Jan. 1929, ISSN: 0044-3328. DOI: 10.1007/BF01339852.

[56] M. A. Jafarizadeh, N. Fouladi, H. Sabri, and B. R. Maleki, "Investigation of Level Statistics by Generalized Brody Distribution and Maximum Likelihood Estimation Method," *arXiv:1210.4751 [nucl-th, physics:physics]*, Oct. 2012. arXiv: 1210.4751 [nucl-th, physics:physics].

[57] F. Haake, *Quantum Signatures of Chaos*, en. Springer Berlin Heidelberg, Oct. 2010, ISBN: 978-3-642-10259-2.

[58] E. P. Wigner, "Results and theory of resonance absorption," in *Conference on Neutron Physics by Time-of-Flight*, 1956, pp. 1–2.

[59] V. Oganesyan and D. A. Huse, "Localization of interacting fermions at high temperature," *Phys. Rev. B*, vol. 75, no. 15, p. 155 111, Apr. 2007. DOI: 10.1103/PhysRevB.75.155111.

[60] Y. Y. Atas, E. Bogomolny, O. Giraud, and G. Roux, "The distribution of the ratio of consecutive level spacings in random matrix ensembles," *Phys. Rev. Lett.*, vol. 110, no. 8, p. 084 101, Feb. 2013, ISSN: 0031-9007, 1079-7114. DOI: 10.1103/PhysRevLett.110.084101. arXiv: 1212.5611.

[61] G. Muga, R. S. Mayato, and I. Egusquiza, Eds., *Time in Quantum Mechanics*, en, Second, ser. Lecture Notes in Physics. Berlin Heidelberg: Springer-Verlag, 2008, ISBN: 978-3-540-73472-7. DOI: 10.1007/978-3-540-73473-4.

[62] L. B. Levitin and T. Toffoli, "Fundamental Limit on the Rate of Quantum Dynamics: The Unified Bound Is Tight," *Phys. Rev. Lett.*, vol. 103, no. 16, p. 160 502, Oct. 2009. DOI: 10.1103/PhysRevLett.103.160502.

[63] A. del Campo, J. Molina-Vilaplana, and J. Sonner, "Scrambling the spectral form factor: Unitarity constraints and exact results," *Phys. Rev. D*, vol. 95, no. 12, p. 126 008, Jun. 2017. DOI: 10.1103/PhysRevD.95.126008.

[64] J. Uffink, "The rate of evolution of a quantum state," *American Journal of Physics*, vol. 61, no. 10, pp. 935–936, Oct. 1993, ISSN: 0002-9505. DOI: 10.1119/1.17368.

[65] A. Uhlmann, "The "transition probability" in the state space of a $_*$-algebra," en, *Reports on Mathematical Physics*, vol. 9, no. 2, pp. 273–279, Apr. 1976, ISSN: 0034-4877. DOI: 10.1016/0034-4877(76)90060-4.

[66] W. K. Wootters, "Statistical distance and Hilbert space," *Phys. Rev. D*, vol. 23, no. 2, pp. 357–362, Jan. 1981. DOI: 10.1103/PhysRevD.23.357.

[67] F. Haake and D. L. Shepelyansky, "The Kicked Rotator as a Limit of the Kicked Top," en, *EPL*, vol. 5, no. 8, pp. 671–676, Apr. 1988, ISSN: 0295-5075. DOI: 10.1209/0295-5075/5/8/001.

[68] F. Haake, M. Kuś, and R. Scharf, "Classical and quantum chaos for a kicked top," en, *Z. Physik B - Condensed Matter*, vol. 65, no. 3, pp. 381–395, Sep. 1987, ISSN: 1431-584X. DOI: 10.1007/BF01303727.

[69] M. Kuś, R. Scharf, and F. Haake, "Symmetry versus degree of level repulsion for kicked quantum systems," en, *Z. Physik B - Condensed Matter*, vol. 66, no. 1, pp. 129–134, Mar. 1987, ISSN: 1431-584X. DOI: 10.1007/BF01312770.

[70] R. Scharf, B. Dietz, M. Kuś, F. Haake, and M. V. Berry, "Kramers Degeneracy and Quartic Level Repulsion," en, *EPL*, vol. 5, no. 5, pp. 383–389, Mar. 1988, ISSN: 0295-5075. DOI: 10.1209/0295-5075/5/5/001.

[71] F. Waldner, D. R. Barberis, and H. Yamazaki, "Route to chaos by irregular periods: Simulations of parallel pumping in ferromagnets," *Phys. Rev. A*, vol. 31, no. 1, pp. 420–431, Jan. 1985. DOI: 10.1103/PhysRevA.31.420.

[72] S. Chaudhury, A. Smith, B. E. Anderson, S. Ghose, and P. S. Jessen, "Quantum signatures of chaos in a kicked top," en, *Nature*, vol. 461, no. 7265, pp. 768–771, Oct. 2009, ISSN: 1476-4687. DOI: 10.1038/nature08396.

[73] J. H. Shirley, "Solution of the Schr\"odinger Equation with a Hamiltonian Periodic in Time," *Phys. Rev.*, vol. 138, no. 4B, B979–B987, May 1965. DOI: 10.1103/PhysRev.138.B979.

[74] Y. B. Zel'Dovich, "The quasienergy of a quantum-mechanical system subjected to a periodic action," *Soviet Physics JETP*, vol. 24, no. 5, pp. 1006–1008, 1967.

[75] K. Szczygielski, "On the Floquet analysis of commutative periodic Lindbladians in finite dimension," en, *Linear Algebra and its Applications*, vol. 609, pp. 176–202, Jan. 2021, ISSN: 0024-3795. DOI: 10.1016/j.laa.2020.09.005.

[76] A. Juan-Delgado and A. Chenu, "First Law of Quantum Thermodynamics in a Driven Open Two-Level System," *arXiv:2104.10691 [quant-ph]*, Aug. 2021. arXiv: 2104.10691 [quant-ph].

[77] R. J. Glauber and F. Haake, "Superradiant pulses and directed angular momentum states," *Phys. Rev. A*, vol. 13, no. 1, pp. 357–366, Jan. 1976. DOI: 10.1103/PhysRevA.13.357.

[78] A. Perelomov, "Coherent States for the Rotation Group of Three-Dimensional Space," en, in *Generalized Coherent States and Their Applications*, ser. Texts and Monographs in Physics, A. Perelomov, Ed., Berlin, Heidelberg: Springer, 1986, pp. 54–66, ISBN: 978-3-642-61629-7. DOI: 10.1007/978-3-642-61629-7_5.

[79] R. F. Fox and T. C. Elston, "Chaos and a quantum-classical correspondence in the kicked top," en, *Phys. Rev. E*, vol. 50, no. 4, pp. 2553–2563, Oct. 1994, ISSN: 1063-651X, 1095-3787. DOI: 10.1103/PhysRevE.50.2553.

[80] V. Constantoudis and N. Theodorakopoulos, "Lyapunov exponent, stretching numbers, and islands of stability of the kicked top," *Phys. Rev. E*, vol. 56, no. 5, pp. 5189–5194, Nov. 1997. DOI: 10.1103/PhysRevE.56.5189.

[81] C. Yin and A. Lucas, "Quantum operator growth bounds for kicked tops and semiclassical spin chains," *Phys. Rev. A*, vol. 103, no. 4, p. 042 414, Apr. 2021. DOI: 10.1103/PhysRevA.103.042414.

[82] E. B. Rozenbaum, S. Ganeshan, and V. Galitski, "Lyapunov Exponent and Out-of-Time-Ordered Correlator's Growth Rate in a Chaotic System," en, *Phys. Rev. Lett.*, vol. 118, no. 8, p. 086 801, Feb. 2017, ISSN: 0031-9007, 1079-7114. DOI: 10.1103/PhysRevLett.118.086801.

[83] L. Sá, P. Ribeiro, and T. Prosen, "Complex Spacing Ratios: A Signature of Dissipative Quantum Chaos," *Phys. Rev. X*, vol. 10, no. 2, p. 021 019, Apr. 2020. DOI: 10.1103/PhysRevX.10.021019.

[84] F. Haake, "Random-Matrix Theory," en, in *Quantum Signatures of Chaos*, F. Haake, Ed., Berlin, Heidelberg: Springer, 2010, pp. 61–143, ISBN: 978-3-642-05428-0. DOI: 10.1007/978-3-642-05428-0_4.

[85] L. Zhang, V. Khemani, and D. A. Huse, "A Floquet model for the many-body localization transition," *Phys. Rev. B*, vol. 94, no. 22, p. 224 202, Dec. 2016. DOI: 10.1103/PhysRevB.94.224202.

[86] A. Flack, B. Bertini, and T. Prosen, "Statistics of the spectral form factor in the self-dual kicked Ising model," *Phys. Rev. Research*, vol. 2, no. 4, p. 043 403, Dec. 2020. DOI: 10.1103/PhysRevResearch.2.043403.

[87] J. Li, T. Prosen, and A. Chan, "Spectral statistics of non-Hermitian matrices and dissipative quantum chaos," *arXiv:2103.05001 [cond-mat, physics:hep-th, physics:nlin, physics:quant-ph]*, Mar. 2021. arXiv: 2103.05001 [cond-mat, physics:hep-th, physics:nlin, physics:quant-ph].

[88] M. L. Mehta and J. Des Cloizeaux, "The probabilities for several consecutive eigenvalues of a random matrix," *Indian J. Pure Appl. Math*, vol. 3, no. 2, pp. 329–351, 1972.

[89] S. C. L. Srivastava, A. Lakshminarayan, S. Tomsovic, and A. Bäcker, "Ordered level spacing probability densities," en, *J. Phys. A: Math. Theor.*, vol. 52, no. 2, p. 025 101, Dec. 2018, ISSN: 1751-8121. DOI: 10.1088/1751-8121/aaefa4.

[90] K. Bhattacharyya, "Quantum decay and the Mandelstam-Tamm-energy inequality," en, *J. Phys. A: Math. Gen.*, vol. 16, no. 13, pp. 2993–2996, Sep. 1983, ISSN: 0305-4470. DOI: 10.1088/0305-4470/16/13/021.

[91] L. Fonda, G. C. Ghirardi, and A. Rimini, "Decay theory of unstable quantum systems," en, *Rep. Prog. Phys.*, vol. 41, no. 4, pp. 587–631, Apr. 1978, ISSN: 0034-4885. DOI: 10.1088/0034-4885/41/4/003.

[92] C. B. Chiu, E. C. G. Sudarshan, and B. Misra, "Time evolution of unstable quantum states and a resolution of Zeno's paradox," *Phys. Rev. D*, vol. 16, no. 2, pp. 520–529, Jul. 1977. DOI: 10.1103/PhysRevD.16.520.

[93] S. PG, V. Madhok, and A. Lakshminarayan, "Out-of-time-ordered correlators and the Loschmidt echo in the quantum kicked top: How low can we go?" *arXiv:2011.04641 [quant-ph]*, Nov. 2020. arXiv: 2011.04641 [quant-ph].

[94] M. Cetina, M. Jag, R. S. Lous, I. Fritsche, J. T. M. Walraven, R. Grimm, J. Levinsen, M. M. Parish, R. Schmidt, M. Knap, and E. Demler, "Ultrafast many-body interferometry of impurities coupled to a Fermi sea," en, *Science*, vol. 354, no. 6308, pp. 96–99, Oct. 2016, ISSN: 0036-8075, 1095-9203. DOI: 10.1126/science.aaf5134.

[95] L. K. Joshi, A. Elben, A. Vikram, B. Vermersch, V. Galitski, and P. Zoller, "Probing many-body quantum chaos with quantum simulators," Jun. 2021. arXiv: 2106.15530.

[96] A. Kitaev, "A simple model of quantum holography," in *KITP Strings Seminar and Entanglement*, vol. 12, 2015, p. 26.

[97] S. Sachdev and J. Ye, "Gapless spin-fluid ground state in a random quantum Heisenberg magnet," *Phys. Rev. Lett.*, vol. 70, no. 21, pp. 3339–3342, May 1993. DOI: 10.1103/PhysRevLett.70.3339.

[98] Z. Wang, J. Feng, and B. Wu, "Microscope for Quantum Dynamics with Planck Cell Resolution," *arXiv:2101.09971 [quant-ph]*, Jan. 2021. arXiv: 2101.09971 [quant-ph].

[99] J. Wang and J. Gong, "Butterfly Floquet Spectrum in Driven SU(2) Systems," *arXiv:0906.2259*, Jun. 2009. DOI: 10.1103/PhysRevLett.102.244102. arXiv: 0906.2259.

[100] J. N. Bandyopadhyay, J. Wang, and J. Gong, "Generating a Fractal Butterfly Floquet Spectrum in a Class of Driven SU(2) Systems: Eigenstate Statistics," *Phys. Rev. E*, vol. 81, no. 6, p. 066 212, Jun. 2010, ISSN: 1539-3755, 1550-2376. DOI: 10.1103/PhysRevE.81.066212. arXiv: 0910.4423.

[101] N. Tsuji, T. Shitara, and M. Ueda, "Out-of-time-order fluctuation-dissipation theorem," *Phys. Rev. E*, vol. 97, no. 1, p. 012 101, Jan. 2018. DOI: 10.1103/PhysRevE.97.012101.